

**Investigation of Charge Carriers in Nanocrystal-Based  
Aerogels and the Influence of Micro- and Nanostructuring**

Von der Naturwissenschaftlichen Fakultät der  
Gottfried Wilhelm Leibniz Universität Hannover

zur Erlangung des Grades

**Doktor der Naturwissenschaften (Dr. rer. nat.)**

genehmigte Dissertation

von

**Pascal Rusch, M. Sc.**

2022

---

Referent: Prof. Dr. rer. nat. Nadja-Carola Bigall  
Korreferent: Prof. Dr. rer. nat. Denis Gebauer  
weiterer Korreferent Prof. Dr. rer. nat. Liberato Manna  
Tag der Promotion: 26.09.2022

## Abstract

The transformation of intricate nanocrystals (NCs) available through colloidal chemical synthesis into branched network structures (referred to as gels) presents a promising pathway to macroscopic solids exhibiting properties of their NC building blocks. In this work, the possibilities to influence these properties at various stages during the gel synthesis sequence will be explored and expanded on. Additionally, the nanoscopic (opto-)electronic properties of networks build up from semiconducting, photoluminescent (PL) NCs will be investigated to gather insights into the electronic structure of such networks and the dynamics of excited charge carriers therein.

In chapter 5 the investigation of gel networks based on CdSe/CdS dot/rod NC building blocks is shown. The PL properties of such structures are analysed in regards to their temperature and time dependent emission (down to 4 K). It is shown that at cryogenic temperature the emission splits into two discernible processes correlating to dark and bright exciton states. While this observation is comparable to the results obtained for individual NCs, at all temperatures gel networks exhibit a longer PL decay most likely caused by increased electron delocalization. The investigation also includes a look at differently sized CdSe cores used for synthesis of the CdSe/CdS dot/rod building blocks. It is found that the combination of different core sizes and therefore different emission color building blocks allows for straight-forward color tuning of the final networks.

The modification of NC-based gels with thin metal oxide shells is shown in chapter 6. Importantly, NC-based aerogels can be influenced not only at the point of NC building block synthesis but also after the gel formation (post-gelation). In this work, the application of wet-chemical methods based on colloidal seeded-growth processes to a NC-based gel network substrate is presented. This results in uniform, thin shells over the whole of the gel network. The approach can be shown to work on different gel substrates (semiconducting and noble metal) and different shell materials (silica and titania) with only minor modifications. The mechanical stability which is one of the common problems in the applicability of NC-based gels is considerably improved by this shell reinforcement.

Building on these developed processes the optical properties of modified CdSe/CdS dot/rod gels are investigated in chapter 7. The silica modification of either the individual NC building blocks before gel assembly or the continuous gel after assembly yield two comparable systems only differing in one crucial point. In gels based on silica modified building blocks, these NC building blocks are isolated and thereby decoupled in the final gel network. For a modification after the gel assembly the building blocks are connected first and therefore coupled in the final gel. The crucial influence on charge carrier dynamics in such networks is shown by time-resolved PL spectroscopy and supported by theoretical calculations. Driving this process further, by incorporation of ZnS at the tip of the CdSe/CdS dot/rod building blocks using a cation exchange procedure a large bandgap material of variable length is introduced to the connecting point of the building blocks. Through the length of the ZnS segment separating the CdSe/CdS building blocks the interaction between these building blocks can not simply be coupled and decoupled but even influenced in its strength as also shown by optical spectroscopy.

Keywords: Nanocrystal-based Aerogels, Semiconductor Nanocrystals, Time-resolved photoluminescence spectroscopy

## Kurzzusammenfassung

Die Transformation von komplexen Nanokristallen (NC), hergestellt durch kolloid-chemische Synthese, in verzweigte Netzwerkstrukturen (Gele genannt) repräsentiert einen vielversprechenden Weg zu makroskopischen Feststoffen, die die Eigenschaften ihrer NC Baueinheiten zeigen. In dieser Arbeit werden Möglichkeiten untersucht und erweitert, die Eigenschaften dieser Netzwerke an verschiedenen Punkten ihrer Herstellung zu beeinflussen. Zudem werden die (opto-)elektronischen Eigenschaften von Netzwerken basierend auf halbleitenden, lumineszenten NC untersucht, um ein tieferes Verständnis der elektronischen Struktur dieser Netzwerke und der Vorgänge der angeregten Ladungsträger zu generieren.

Die Untersuchung von Gelnetzwerken aus stäbchenförmigen CdSe/CdS NC-baueinheiten ist in Kapitel 5 beschrieben. Die Photolumineszenz-(PL-)Eigenschaften dieser Strukturen werden temperaturabhängig (bis zu 4K) in Hinblick auf ihre zeitaufgelöste Emission untersucht. Dabei wird gezeigt, dass im kryogenen Bereich zwei Prozesse zur Emission beitragen, die sich hellen und dunklen Excitonen zuordnen lassen, ein von einzelnen NC bekanntes Verhalten. Die PL-lebenszeit ist allerdings bei allen Temperaturen in Netzwerkstrukturen länger, vermutlich aufgrund einer stärkeren Delokalisierung der angeregten Elektronen. Zusätzlich ist die Untersuchung von Netzwerken, bei denen die Bausteine auf unterschiedlichen Größen an CdSe Quantenpunkten in den CdSe/CdS Stäbchen basieren, gezeigt. Aus unterschiedlichen Größen resultieren unterschiedliche PL-Farben und ein unkomplizierter Weg zur Farbeinstellung in diesen Netzwerkstrukturen wird aufgezeigt.

Die Modifikation von Nanokristallgelen mit dünnen Metalloxidschalen wird in Kapitel 6 gezeigt. NC-basierte Aerogele können nicht nur über die gezielte Synthese der Baueinheiten beeinflusst werden, sondern auch nach der Netzwerkbildung (post-Gelierung). In diesem Abschnitt wird die Adaption bekannter nasschemischer Prozesse zur Anwendung an Nanokristallgelen als Substrat beschrieben. Dabei werden Gelnetzwerke vollständig mit einer einheitlichen, dünnen Schale ummantelt. Dieser Prozess kann auf verschiedene Substrate (Gele aus Halbleiter oder Edelmetall NC) und für verschiedenen Schalenmaterialien (Siliziumdioxid und Titandioxid) mit minimalen Änderungen angepasst werden. Die mechanische Stabilität, eine bedeutende Hürde in der Anwendbarkeit von Nanokristallgelen, wird durch die Verstärkung mit einer solchen Schale deutlich erhöht.

Darauf aufbauend werden die PL Eigenschaften modifizierter Netzwerke aus CdSe/CdS Stäbchen in Kapitel 7 untersucht. Die Modifikation mit einer Silikatschale wird entweder an einzelnen kolloiden Nanokristallbaueinheiten vor der Netzwerkbildung oder an dem bereits verbundenen Netzwerk durchgeführt. Werden zuerst die Baueinheiten mit einer Silikatschale umschlossen, so sind diese im finalen Netzwerk isoliert bzw. entkoppelt voneinander, während Baueinheiten, die zuerst in ein Netzwerk überführt werden, auch nach dem Wachstum der Silikatschale miteinander kontaktiert bzw. gekoppelt sind. Der entscheidende Einfluss dieser Verbindung auf die Ladungsträgervorgänge wird durch zeitaufgelöste PL-spektroskopie gezeigt und von theoretischen Berechnungen unterstützt. Dieser Ansatz wird durch den gezielten Einbau von ZnS an die Spitzen der CdSe/CdS Stäbchen weiter verfolgt. Durch einen Kationenaustauschprozess ist es möglich, verschiedene Mengen ZnS (ein Material mit großer Bandlücke) so in die Baueinheiten einzubringen, dass es sich im Netzwerk an den Kontaktpunkten befindet. Über die Länge dieser ZnS Abschnitte zwischen den CdSe/CdS Einheiten, können die Einheiten nicht nur gekoppelt und entkoppelt werden, sondern die Stärke der Wechselwirkung zwischen den Baueinheiten, welche sich in den optischen Eigenschaften widerspiegelt, gesteuert werden.

Schlagworte: Nanokristall-basierte Aerogele, Halbleiternanokristalle, zeitaufgelöste Photolumineszenzspektroskopie

## Preface

The research presented in this thesis was conducted during my time working under the supervision of Prof. Nadja C. Bigall at the Institute of Physical Chemistry and Electrochemistry of the Leibniz Universität Hannover between 2017 and 2022. The research included in this thesis has been published in four original articles of which I am first author. There are further 16 articles that have been published in this time where I am a co-author or (shared) first author which are not included in this thesis, but are listed in the appendix (section 9.1).

In the following, the contributions of all individual authors of the articles included in this thesis are detailed. The first article, *Temperature and Composition Dependent Optical Properties of CdSe/CdS Dot/Rod-Based Aerogel Networks*, as presented in section 5.2, was written by me. I have synthesized the samples and performed the optical and structural characterization. I thank D. Pluta for his assistance during the temperature-dependent spectroscopy; Dr. F. Lübkeermann, Dr. D. Zámbo and Prof. D. Dorfs for their valuable input to the discussion of the results; Prof. N. C. Bigall for supervision and helpful comments during discussion of the results and writing of the manuscript.

The second article, *Versatile Route to Core-Shell Reinforced Network Nanostructures*, as presented in section 6.2, was written by me. I have performed the synthesis and optical characterization of the samples, as well as structural characterization via bright field transmission electron microscopy (BF-TEM). I thank F. Niemeyer, who worked on his bachelor thesis under my supervision, and D. Pluta, who did a research internship under my supervision, for their helpful first experiments; B. Schremmer, Dr. F. Lübkeermann and M. Rosebrock for the structural characterization via scanning electron microscopy (SEM); Dr. F. Lübkeermann furthermore for energy dispersive x-ray analysis scanning electron microscopy (STEM-EDX); Dr. M. Schäfer for argon physisorption measurements; Dr. M. Jahns for assistance in the mechanical characterization; Prof. P. Behrens and Prof. N. C. Bigall for the valuable discussions and help during result interpretation and manuscript writing.

The third article, *Nanocrystal Aerogels with Coupled or Decoupled Building Blocks*, as presented in section 7.2, was written by me. I have performed the synthesis and optical characterization of the samples as well as the structural investigation via TEM. I thank B. Schremmer for the SEM

measurements; Dr. C. Strelow of the Universität Hamburg for theoretical calculations; Prof. D. Dorfs, Prof. A. Mews of the Universität Hamburg and Prof. N. C. Bigall for their valuable input during result interpretation and manuscript writing.

The fourth article, *Influencing the Coupling Between Network Building Blocks in CdSe/CdS Dot/Rod Aerogels by Partial Cation Exchange*, as presented in section 7.3, was written by me. I have performed the synthesis and optical characterization of the samples as well as the structural investigation via TEM. I thank J. G. Eckert for the SEM measurements; H. Borg for XPS measurements; Dr. F. Lübke, Prof. D. Dorfs and Prof. N. C. Bigall for their advice and their valuable input during interpretation and manuscript writing.

## Acknowledgements

First and foremost I want to thank my supervisor, Prof. Dr. Nadja C. Bigall, for her support directly with the discussions and advice, helping me to steadily improve. And for giving me not only the opportunity to work on the topics of this thesis but also the trust and freedom to follow my ideas.

I also want to thank Prof. Dr. Denis Gebauer and Prof. Dr. Liberato Manna for reviewing this thesis as co-referees and Prof. Dr. Peter Behrens for agreeing to serve as chair of the examination board.

I want to also thank all the colleagues I worked with in my time in the *Function Nanostructures* group for the enthusiasm, the pleasant work environment and their discussions and advice as well. I would like to thank Dr. Dominik Hinrichs, Dr. Torben Kodanek, Dr. Suraj Naskar, Jan F. Miethe, Patrick Adel, Dr. Franziska Lübke and Dr. Axel Freytag for introducing me into the world of nanochemistry, our lab and the group. I would like to thank the colleagues I have shared most of the PhD time with, Björn Schremmer, Max Niemeyer, Patrick Bessel, Daniel Kranz, Rasmus Himstedt, Anja Schlosser, Dennis Müller and Marina Rosebrock for their help in and out of the lab. And I would also like to thank the next generation of PhD students, Denis Pluta, Jakob Schlenkrich, Rebecca Graf, Christoph Wesemann, J. Gerrit Eckert, Sven Getschmann, Lars Klepzig and Andre Niebur for bringing in new ideas and keeping the flame going. Especially, I want to thank Dr. Franziska Lübke and Dr. Dániel Zámbo for their time whenever I needed help or someone to discuss ideas and results with.

I want to also thank Björn Schremmer, Marina Rosebrock, Denis Pluta, Jakob Schlenkrich and Dr. Franziska Lübke for their time at the SEM (or TEM). Likewise I want to thank Dr. Fritz Schulze-Wischeler for the introduction into the TEM and the help during measurements. I would like to thank the students, I worked with during their Bachelors and Master Thesis or Internship, for their interest and willingness to learn, their hard work and the good time, Moritz Kügler, Denis Pluta, Sven Getschmann, Björn Gastmann, Luisa Steingrube, Kornelius Rautmann, Astita Dubey, Sebastian Schermer and Fabian Niemeyer. I also want to specially thank Dr. Franziska Lübke and Christoph Wesemann for proof-reading this thesis. I would like to thank my cooperation partners for their time and help in my works, Dr. Mandy

## Acknowledgements

---

Jahns, Dr. Malte Schäfer and Prof. Peter Behrens (Institut for Inorganic Chemistry) and Dr. Christian Strelow and Prof. Alf Mews (Institute for Physical Chemistry, Universität Hamburg). But I also want to thank all the others I collaborated with for the good cooperation, challenging measurements (sometimes more and sometimes less) and allowing me an insight into other subjects to learn from, Dr. Dominik Göbel, Dr. Isabel Ramirez y Medina and Yannik Appiarius (Universität Bremen), Dr. Yuiping Liu (Institute of Solid-State Physics), Abdelrahim Alahmad (Institute of Technical Chemistry) and Dr. Ina Strauß and Felix Rieck genannt Best (Institute of Physical Chemistry and Electrochemistry).

Additionally, I want to thank my friends. I want to thank the *Pub-Quiz Crew*, Franzi, Dawid, Mandy, Björn, Jan, Max, Lars, Rasmus and Patrick, for the joyful evenings over the last years. I also want to thank Basti, Jan, Max, Philip and Daniel with whom I have started this journey in 2011 for the time spent together learning, working, drinking, hiking, BBQing and much more. Likewise, I want to thank Alex, Florian and Philippe for our time spend together, lending me an ear when I was down and offering an outside view. I want to also thank Magrit Meyer for supporting me and teaching me a lot of what I know, apart from chemistry. Finally, but most importantly I want to thank my parents, Evelyn und Manfred, without you I would never have made it this far. I cannot bring to words how much support and encouragement I have gotten from you or how much this means to me.

# Contents

Abstract . . . . .	iii
Kurzzusammenfassung . . . . .	iv
Preface . . . . .	v
Acknowledgements . . . . .	vii
<b>1 Introduction</b>	<b>1</b>
<b>2 Nanometer-sized Materials: On the border between Molecules and Bulk</b>	<b>5</b>
2.1 Optical Properties of Semiconducting Nanocrystals . . . . .	5
2.2 Optical Properties of Metal Nanocrystals . . . . .	8
2.3 Synthesis of Nanometer-sized Materials . . . . .	10
<b>3 Network Structures: Putting the Pieces Together</b>	<b>19</b>
3.1 Network Formation . . . . .	19
3.2 Preparation of Aerogels . . . . .	23
3.3 Nanocrystal-Based Network Structures . . . . .	25
<b>4 Bibliography</b>	<b>31</b>
<b>5 Optical Properties of Nanocrystal-Based Aerogel Networks</b>	<b>55</b>
5.1 Summary . . . . .	55
5.2 Temperature and Composition Dependent Optical Properties of CdSe/CdS Dot/Rod- Based Aerogel Networks . . . . .	57

## CONTENTS

---

<b>6</b>	<b>Post-Gelation Approach for Structuring Nanocrystal-Based Aerogels</b>	<b>69</b>
6.1	Summary . . . . .	69
6.2	Versatile Route to Core-Shell Reinforced Network Nanostructures . . . . .	70
<b>7</b>	<b>Influencing Charge Carriers in Nanocrystal Aerogels</b>	<b>81</b>
7.1	Summary . . . . .	81
7.2	Nanocrystal Aerogels with Coupled and Decoupled Building Blocks . . . . .	83
7.3	Influencing the Coupling Between Network Building Blocks in CdSe/CdS Dot/Rod Aerogels by Partial Cation Exchange . . . . .	91
<b>8</b>	<b>Summary</b>	<b>103</b>
<b>9</b>	<b>Outlook</b>	<b>105</b>
	<b>Appendix</b>	<b>xi</b>
9.1	List of Publications . . . . .	xi
9.2	Conference Contributions . . . . .	xv
9.3	Curriculum Vitae . . . . .	xvii

# 1 Introduction

The connection between a materials composition and its properties is intuitive for everyone. Simply using ones eye and evaluating the optical properties it is apparent: Different substances have different colors. This relation gets more complex when applied to the structure of a material. Still, with minor effort it is understandable that e.g. an amorphous material looks different from a crystalline one. However, when looking at materials with nanoscale dimensions, another influence will appear in the form of the size of the material. This interaction between material properties and size emerges at the nanoscale when the sizes are in the range of or much lower than the wavelength of light. The fact that two particles exhibit different optical and electronic properties even though they are equal in composition and structure simply due to different sizes is unimaginable in the macroscopic world we all live in, and therefore fascinating for laypersons and experts alike. In essence, semiconducting materials like the ones used throughout this work exhibit a dependence of the individual particle size to the band gap if the size is below the so-called *Bohr-Exciton-Radius*.<sup>[1]</sup> But also other materials, like metals showing a *localized surface plasmon resonance*<sup>[2]</sup> or magnetic materials showing superparamagnetism,<sup>[3]</sup> behave differently when produced with nanoscopic dimensions compared to their macroscopic counterparts. All procedures explored to synthesize such nanoscopic materials can be broadly classified into two categories, the *top-down* and *bottom-up* approach. In case of the former a macroscopic material is divided into smaller particles to the desired size, prominent examples include ball-milling<sup>[4, 5]</sup> and laser ablation.<sup>[6, 7]</sup> The latter approach is based on building the nanomaterials from single molecules or atoms for example by wet-chemical synthesis. While *top-down* methods allow for larger scale production, the structures usually show more defects compared to materials produced by *bottom-up* methods.<sup>[8]</sup> As crystal defects are a major point

influencing the optical and electronic properties, in the study of semiconducting, photoluminescent nanocrystals like in this work a *bottom-up* approach is preferred. This is also based on the refined ability to control the wet-chemical synthesis - a key being the introduction of the *hot-injection* synthesis[9] - via solvents, temperature, ligands, additives, precursors and more.[10, 11] The methods developed for nanocrystal synthesis including facetation control, heterostructure formation and bandgap engineering grow ever more complex and intricate with the aim of yielding particles, tailor made to have the exact desired properties. At the same time, applications in form of a colloidal solution, as usually generated by the synthesis, can be limited or not desirable. In consequence, methods to immobilize these nanocrystals under retention of their so desired properties have to be developed. One such method, promising to introduce nanoscale materials into the macroscopic world, is the assembly of porous network structures, commonly called gels.[12] While a more traditional approach to gels is their synthesis along the *sol-gel* route, they can also be assembled from previously and separately produced building blocks, in this case nanocrystals. As the building blocks of a gel network only attach to each other at small contact patches, the high surface-to-volume ratio of the nanoscale building blocks as well as their size dependent properties can be retained in the resulting macroscopic solid. In the advancing investigation of aerogel networks build up from nanocrystals, it is not only possible to retain properties from building block to network, but new properties can emerge caused by the assembly and connection of the building blocks. This has been observed in case of CdSe/CdS dot/rod nanocrystals. The band structure of these nanocrystals, in which a high offset between the CdSe and the CdS valence band exists but the positions of both respective conduction bands are very similar, is responsible for unique optical properties once they are assembled into a network. When assembling such heterostructured building blocks into an aerogel the band structure of the generated connected network leads to a delocalization of the electron throughout this network as the electrons are not strongly confined to the CdSe due to the small conduction band offset. This model was first proposed when observing an elongation of photoluminescence lifetime in these structures by time-resolved photoluminescence spectroscopy.[13] This thesis aims to further investigate this phenomenon and also to find colloidal synthetic pathways to influence the structure of such networks and thereby their optical properties.

---

To gain insight into the processes during excitation of the charge carriers inside such networks time-resolved optical measurements are performed at varying temperatures between room temperature and 4K. With the same aim networks are assembled from CdSe/CdS dot/rod heterostructured nanocrystals using different sizes of CdSe quantum dots (which therefore have different band gaps) and optically investigated. These in-depth time and temperature resolved spectroscopic investigations on aerogel networks based on different CdSe/CdS dot/rod building blocks as well as mixtures thereof are presented in chapter 5.

The most common approach to influence and direct the properties of nanocrystal-based aerogel networks is the finely tuned synthesis of the nanocrystal building blocks. This allows for shape- and facet-controlled,[14, 15] for core-shell-structured[16] or for bandgap-engineered building blocks.[13, 17] In this approach the separation of building block synthesis and network assembly are utilized to control the network properties via their building blocks before even assembling them. However, it should also be possible to take influence on the network once it is generated. One of the most used methods of nanocrystal modification is the growth of oxide shells (usually silica)[18–24] to stabilize and protect the nanocrystals in unfavourable surroundings of e.g. high or low pH or high ionic strength[21], as well as reduce their cytotoxicity[25, 26]. In an endeavour to show the potential to adapt methods developed for nanocrystal modification in colloidal dispersion to a NC-based gel substrate, the growth of thin metal oxide shells grown on a nanocrystal gel network after its assembly (*post-gelation*) is investigated in chapter 6. A gel network as substrate presents certain limitations on the available synthesis conditions, e.g. mixing, temperature and reaction medium. Nonetheless, successful methods to modify semiconductor and noble metal NC-based aerogels with silica and titania shells are developed and shown to significantly increase the mechanical stability of the gel networks.

Combining the investigation of the building block interaction within a gel network and the new synthetic approaches of network modification after gelation, it is possible to use the sequence of synthesis steps to control the network structure. Namely, by first performing a silica shell modification on CdSe/CdS dot/rod building blocks and then assembling these into gel networks, a network structure is generated in which the individual CdSe/CdS building blocks are embedded into a silica gel matrix separated from each other. By switching the order of operations, it is also possible to first connect CdSe/CdS building blocks into a gel network and

then surround this connected network with a silica shell. This results in two compositionally comparably but structurally different gel networks, one with decoupled (isolated) and one with coupled (connected) building blocks. Between these two digital states the existence of intermittent structures is thinkable. Therefore, a shallow tunable barrier between the nanocrystal building blocks is needed. The development of cation exchange as a powerful tool in nanocrystal modification allows the introduction of ZnS (a large bandgap material compared to CdSe and CdS) to the tips of CdSe/CdS dot/rod nanocrystals. By this modification it is possible to generate building blocks with controlled lengths of a large bandgap material at the attachment points in the later network presenting the envisioned tunable barrier between the building blocks. These structures, the aforementioned completely coupled and decoupled networks as well as networks with variable coupling via their controllable barrier, are investigated structurally and optically to understand the charge carrier processes within them in chapter 7.

Overall, this thesis presents advancements in the toolbox of synthetic approaches to tune NC-based networks both in the state of the nanocrystals (by modifying the building blocks in colloidal solution) before gelation and in the assembled network state after gelation. These methods are applied to first understand the charge carrier processes within such network structures and use this knowledge to control them.

## 2 Nanometer-sized Materials: On the border between Molecules and Bulk

The interest of researchers in nanometer-sized materials is founded in the unique and advantageous properties of these so-called nanoparticles. The most important characteristic being their size in the range of 1 to 100 nm.[27] The minuscule size of these particles is also the source of their properties of interest. For example but not limited to their size being in the range of biomolecules enabling interaction with cellular material.[28] Their high surface-to-volume ratio caused by the faster scaling of surface area with diminishing particle size gives rise to their high potential for catalytic applications.[29–31] Their size-dependent optical and electrical properties allow (opto-)electrical applications, but also the probing of their properties by optical spectroscopy.[32] As the spectroscopic investigation of complex nanometer-sized systems is one of the core works of this thesis their optical properties will be discussed in further detail within this chapter as well as the synthesis procedures to manufacture such nanosystems.

### 2.1 Optical Properties of Semiconducting Nanocrystals

The electronic and optical properties of semiconducting nanocrystals (NC) are determined not only by the material from which the NCs are composed of but also to a crucial degree by their size and shape. This dependency is caused by the so-called quantum confinement, graphically illustrated in figure 2.1.[33, 34]

With NCs being in the border region between single molecules and bulk solids, their properties can accordingly be described as border cases of the theories describing these two sub-

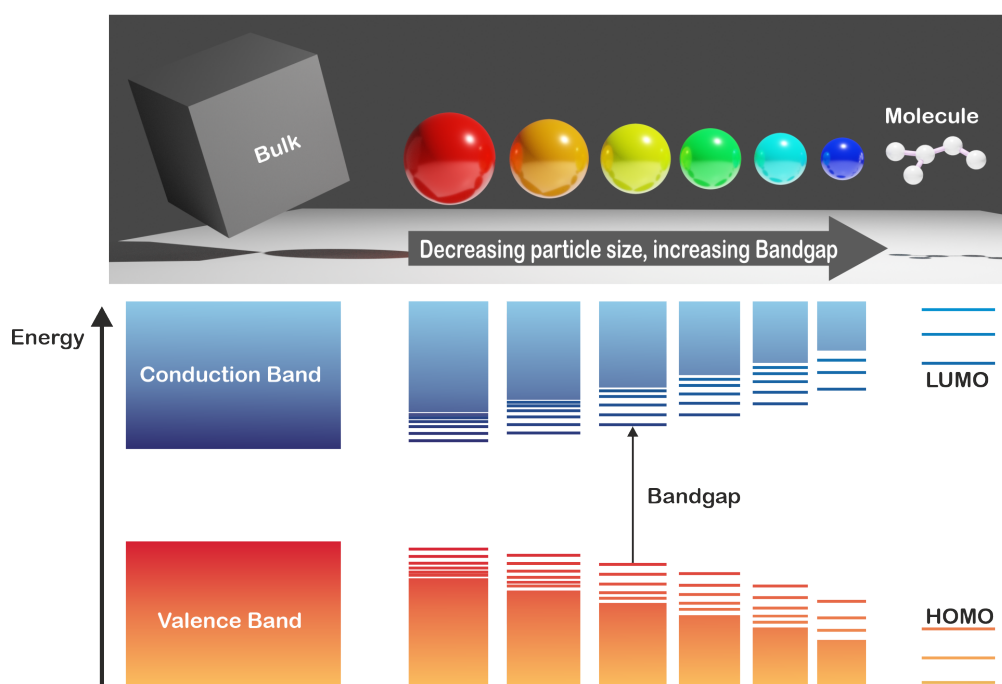


Figure 2.1: Schematic depiction of change in bandgap with changing particle size. Own representation inspired by [35]

jects. The electronic structure of single molecules can be described by the linear combination of atomic orbitals (LCAO). Linear combinations of the atomic orbitals from each atom the molecule consists of are built, forming energetically favoured binding and energetically higher anti-binding molecular orbitals. The bandgap of this structure is the energy difference between the highest occupied molecular orbital (HOMO) and the lowest unoccupied molecular orbital (LUMO). A NC can be seen as a very large molecule and molecular orbitals can likewise be built. Due to the large number of atoms, relative to a molecule, comprising a NC the resulting molecular orbitals are very similar in energy and can therefore be interpreted similar to a band structure as known from solid state physics which is dependent on the size of the NC.[34, 36] Looking from a different point of view NCs can also be interpreted as very small solids. The excitation of an electron ( $e^-$ ) from the valence into the conduction band caused by e.g. light irradiation leaves an uncompensated charge in the valence band, the so-called hole ( $h^+$ ). These two charge carriers are still bound together by their opposite charge and the resulting COULOMB attraction. Therefore, they form a quasi-particle referred to as an exciton with an average dis-

tance between the charge carriers,  $e^-$  and  $h^+$ , called the *Bohr-Exciton-Radius*. If the size of the NC is below this radius the exciton is effectively confined to a smaller space leading to the formation of energy levels comparable to the simpler model of a *particle-in-a-box* with the surface of the NC acting as potential barrier. Unlike this simple model the potential inside a crystalline material is not constant but periodically changing due to the positive atomic nuclei. To account for this the charge carriers are usually given an approximated effective mass.[37–39] The combination of the *effective-mass-approximation* and the *particle-in-a-box*, then culminates in the formula (equation 2.1) derived by BRUS[40] for the bandgap of nanocrystalline materials:

$$E_{NC}(r) = E_{Bulk} + \frac{h^2}{8r^2} \cdot \left( \frac{1}{m_c^*} + \frac{1}{m_h^*} \right) - \frac{1.8e^2}{4\pi\epsilon_r\epsilon_0 r} \quad (2.1)$$

$E_{NC}$	- nanocrystal bandgap	$r$	- nanocrystal radius
$E_{Bulk}$	- bandgap of the bulk material	$h$	- Planck constant
$m_c^*$	- effective mass of the electron	$m_h^*$	- effective mass of the hole
$e$	- charge of an electron	$\epsilon_r$	- relative permittivity of the material
$\epsilon_0$	- relative permittivity of vacuum		

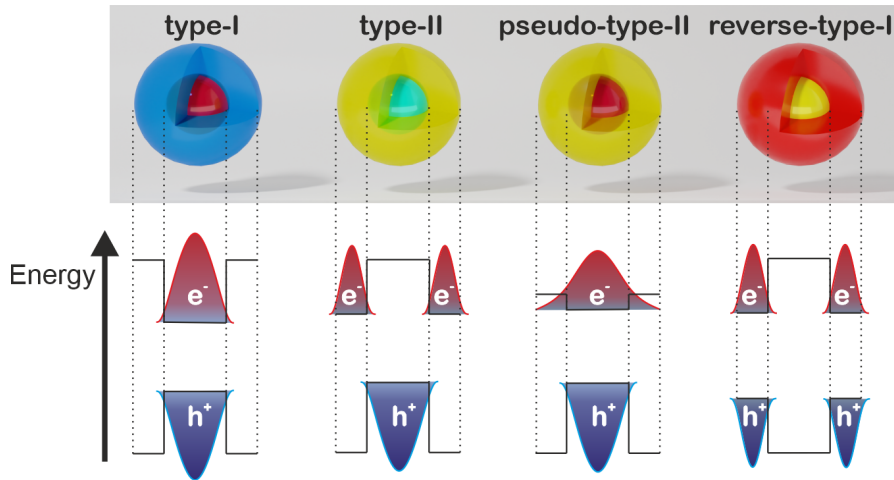


Figure 2.2: Schematic depiction of different band alignments in heterostructured semiconductor nanocrystals with resulting electron and hole wavefunction. Own representation inspired by [41]

The electronic structure of NCs can be tuned further by the introduction of heterostructures, meaning particles consisting of more than one material. For semiconducting NCs this is often realised in form of a core/shell structure. These structures allow for the combination of different band gap materials which can be aligned in different fashions as shown in

figure 2.2. Different combinations are classified as *type-I*, in which the shell material has an energetically higher conduction band and lower valence band than the core material resulting in a confinement of both charge carriers in the core, and *type-II*, in which both bands (conduction and valence) of the shell material are either energetically higher or lower compared to the core material, resulting in a spatial separation of the excited charge carriers. Typical examples for *type-I* structures are CdSe/ZnS[42, 43] or InP/ZnS[44, 45] heteroparticles. Structures like these are usually synthesised to improve the optical properties of the NCs. The large bandgap shell isolates the core from the surroundings, prohibiting non-radiative processes and saturating surface defects on the core. All of this leads to higher quantum yields. Contrary, *type-II* structures exhibiting charge carrier separation have low overlap of hole and electron wavefunctions, which usually results in long exciton lifetimes and mostly, but not necessarily poor quantum yields, as non-radiative pathways can be faster than the radiative recombination. Typical *type-II* structures include ZnSe/CdS[46–48] or CdSe/CdTe[49–51] and are used in photocatalytic or photoelectric applications for which the charge carrier separation can be beneficial. The recombination at the interface can also be exploited to generate low energy (red or near-infrared) emission from larger bandgap materials. Additionally the *quasi-type-II* and the *reverse-type-I* have also been classified. In the *reverse-type-I* the band alignment of the *type-I* structures is reversed, so that both excited charge carriers are localized in the shell. These structures, e.g. CdS/CdSe core/shell NCs, are being discussed for applications in optical emitters or photovoltaic cells,[52–55] but mostly remain a niche interest. In the *quasi-type-II* system one charge carrier is confined while the other one much less so due to a very low band offset between either the conduction or valence band of core and shell material. The most known structure of the *quasi-type-II* kind and also one of the most investigated nanostructures overall is CdSe/CdS.[56–61] However, the boundary between *type-I* and *quasi-type-II* is rather fluid depending on the respective band offsets and is subject of discussion.[62–66]

## 2.2 Optical Properties of Metal Nanocrystals

The optical properties of noble metal NCs will be discussed here only briefly as the focus of most of this work will be on networks of semiconducting nanocrystals. Noble metal nanocrystals

tals will be used in chapter 6 as alternative material to show the versatility of the developed method. These metallic NCs, like semiconducting NCs, display characteristic interactions with electromagnetic radiation though based on entirely different underlying processes. The optical properties of metallic NCs are results of a collective movement of electrons, in contrast to the excitation of single electrons in semiconducting NCs. The oscillating electromagnetic field of light moves the free charge carriers (usually electrons). With this change in charge carrier density a corresponding restoring force is generated by the COULOMB attraction between the charge carriers and the atomic nuclei. In bulk materials the resulting charge carrier density oscillations, called plasmons, are propagating and not easily excitable by light.[67] In nanocrystalline form, these plasmons are localized due to the small size and the curvature of NCs and if the frequency of the incident light matches the plasmon frequency, a resonant absorption takes place resulting in a strong absorption of the light and the typical intense colouring of noble metal NC solutions.

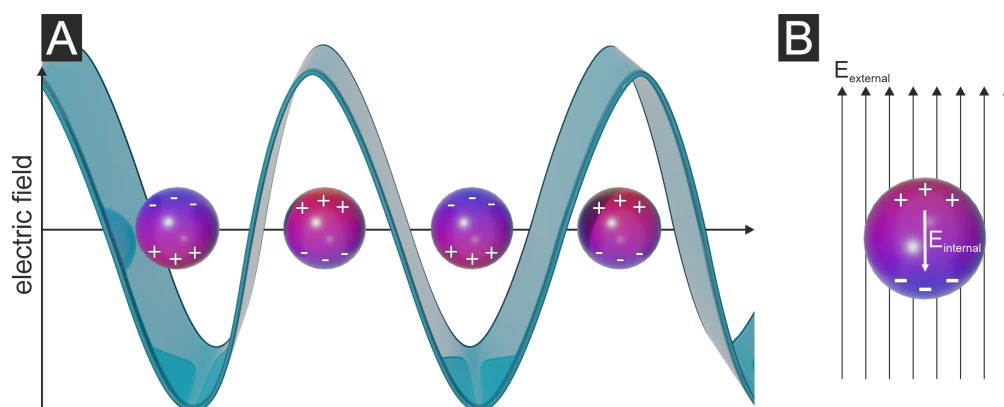


Figure 2.3: Interaction between light and nanocrystals containing free charge carriers. Schematic depiction of (A) the electric field of light inducing a shift in charge carrier density in the nanocrystals (nanocrystals not to scale) and (B) the charge carrier distribution caused by the outside electric field generating an internal electric field in the nanocrystal leading to a returning force and a charge carrier oscillation.

The theory behind this so-called *localized surface plasmon resonance* (LSPR) was outlined in 1908 by solving the MAXWELL-equation for the absorption and scattering interaction of light and small metal particles.[68] In the description of LSPRs of small metal NCs the *quasi-static* approximation is usually applied. This comprises of the assumption that the electric field acting

on the NCs is significantly smaller in size than the wavelength of the incident electromagnetic wave ( $r \leq 0.01\lambda$ ). Therefore, the electric field is assumed to be homogeneous. This is roughly applicable to particles in the size of 5 to 30 nm under visible light irradiation and can be combined with the DRUDE model to describe the charge carrier oscillations caused by displacement and restoring COULOMB attractions with the resonance and plasmon frequency given by equation 2.2 and schematically shown in figure 2.3.[67, 69]

$$\omega_{LSPR} = \sqrt{\frac{\omega_p^2}{1 + 2\epsilon_m} - \gamma^2} \text{ and } \omega_p = \sqrt{\frac{ne^2}{\epsilon_0 m_{eff}}} \quad (2.2)$$

$\omega_{LSPR}$	-	frequency of the LSPR	$\omega_p$	-	plasmon frequency
$\epsilon_m$	-	relative permittivity of the medium	$\gamma$	-	dampening factor
$n$	-	density of free charge carriers	$e$	-	elemental charge
$\epsilon_0$	-	relative permittivity of vacuum	$m_{eff}$	-	effective mass of the charge carriers

Accordingly, the plasmon frequency is only dependent on the material of the NC (in the form of free charge carrier density and dielectric constant) and its surroundings within this approximation. If the size regime of the *quasi-static* approximation is exceeded additional higher modes, e.g. quadrupoles, can be excited in the NCs and the interaction with light has to be described by the MIE theory.[68]

## 2.3 Synthesis of Nanometer-sized Materials

As mentioned earlier, two general approaches to generate particles with nanometer scale can be differentiated, *top-down* and *bottom-up*. The synthesis procedures can be attributed to these approaches by the process in which the NC is generated, either by taking a larger bulk material and reducing it in size (*top-down*), usually via physical methods like milling[4, 5] or laser ablation,[6, 7] or (*bottom-up*) building the NC up from smaller molecular or atomic building blocks. Between these the latter methods offer a more precise control over the final product regarding its monodisperse size, crystallinity and allow for the construction of complex heterostructures via controlling the nucleation process.[10, 11] These wet-chemical methods are also employed in this work to generate NCs and will be further discussed in the following section. As the particles and their assemblies are studied by spectroscopic means later – and the aforementioned

parameters (i.e. size and crystallinity) strongly influence the optical properties – a high level of control over these is desired.

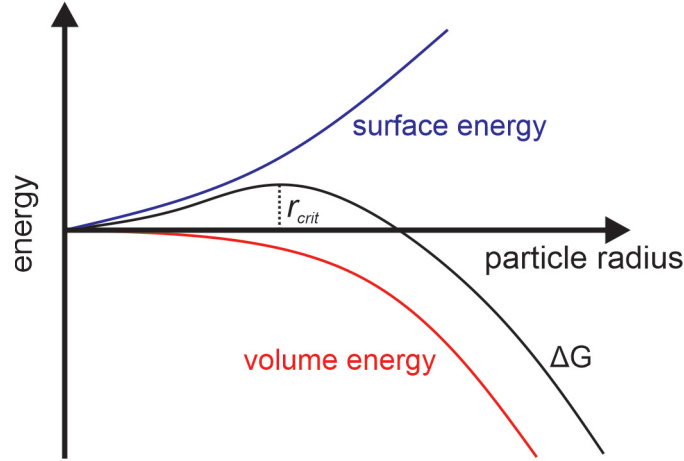


Figure 2.4: Development of surface energy, volume energy and overall free enthalpy of crystal seed nucleation. Own representation inspired by [35]

Wet-chemical methods of NC synthesis are based on the precipitation of particles from supersaturated solutions which can be divided in the processes nucleation and growth. In this regard, different forms of nucleation can be distinguished in form of primary homogeneous and heterogeneous and secondary nucleation. Secondary nucleation happens on crystalline surfaces added to the solution, while primary heterogeneous nucleation occurs on amorphous surfaces like dust or dirt. Primary homogeneous nucleation takes place without any interfaces present before the nucleation. The change in free enthalpy during nucleation is shown in figure 2.4 and given by equation 2.3 with the first term denoting the change due to the newly formed crystal volume and the second term the contribution of the newly formed interface on the crystal surface.[70]

$$\Delta G = \frac{4}{3}\pi r^3 \frac{k_B T \ln(S)}{V_m} + 4\pi r^2 \gamma \quad (2.3)$$

$\Delta G$	- free enthalpy of crystal formation	$r$	- nanocrystal radius
$k_B$	- Boltzmann constant	$T$	- temperature
$S$	- oversaturation	$V_m$	- molar volume of the bulk crystal
$\gamma$	- surface free energy per unit area		

This surface term scales with  $r^2$  and will predominate for small particles sizes. With an

increase in size however the volume term ( $\propto r^3$ ) will inevitably surpass this and nuclei above a critical radius ( $r_{crit}$ ) will decrease their energy by growing and are stable once large enough, as depicted in figure 2.4. This critical radius can be derived by setting  $\frac{\partial \Delta G}{\partial r} = 0$  resulting in equation 2.4.[70]

$$r_{crit} = \frac{2V_m\gamma}{3k_B T \ln(S)} \quad (2.4)$$

It can also be seen that the critical radius  $r_{crit}$  decreases with increasing level of supersaturation. In a solution of particle building blocks different levels of concentration can be defined. The saturation limit is given by the solubility of the building block in the given solvent. If the concentration is increased above this limit primary homogeneous nucleation is still very unlikely as the nuclei will most likely be too small and dissolve, but secondary nucleation can take place in this region as the solubility is exceeded. Only with a further increase in concentration, above a critical level of supersaturation, spontaneous primary homogeneous nucleation will take place.

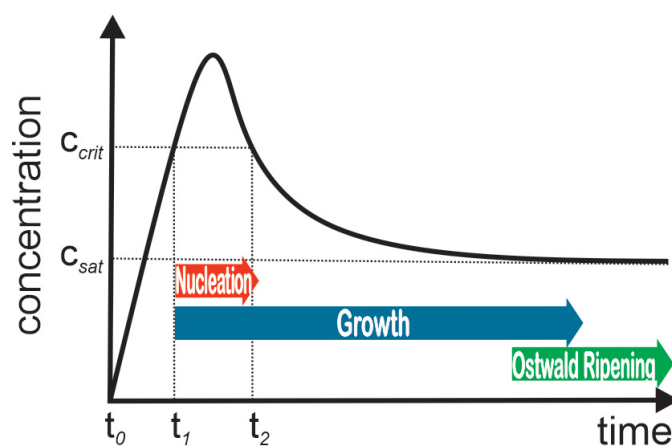


Figure 2.5: Concentration of *monomers* over time (with the saturation concentration ( $c_{sat}$ ) and the concentration necessary for spontaneous nucleation ( $c_{crit}$ ) marked and  $t_1$  and  $t_2$  marking the time the nucleation of particles starts and ends, respectively) during nanocrystal synthesis (*LaMer-Diagram*). Own representation inspired by [71]

As described, the controlled synthesis of nanometer-sized particles is based on the ability to direct particle nucleation and growth. One of the oldest universal descriptions of the nucleation theory in supersaturated solutions was provided by LAMER and DINEGAR on the example of sulfur.[71] This theory is often used to describe the processes during nanoparticle formation. As

described in this, often via the so-called *LaMer-Diagram* shown in figure 2.5, the most important task when synthesizing monodisperse nanometer-sized particles is the separation of the two phases of particle synthesis, namely nucleation and growth. In the first step ( $t_0 \rightarrow t_1$ ), before the reaction, the concentration of the monomers is low. Monomer refers to the small molecules or clusters forming the particle. When the concentration is raised it will at some point exceed the saturation limit. As discussed earlier, all systems need at least a certain amount of oversaturation before particles form. Only when the monomer concentration is raised above the limit of critical nucleation, particles will form ( $t_1$ ). New particles will continue to nucleate as long as the monomer concentration is above this limit ( $t_1 \rightarrow t_2$ ), while already formed particles will grow in size. For this reason the aim of controlled nanoparticle syntheses is to keep the nucleation phase ( $t_1 \rightarrow t_2$ ) as short as possible so the nucleation and growth phase overlap only shortly as to obtain monodisperse particles. Below the critical concentration ( $t_2$  onwards) the particles will continue to grow until the saturation concentration is reached. On much larger time scales, at concentrations around the saturation limit the process of OSTWALD ripening will influence the particle size. In this process smaller particles dissolve to facilitate the growth of larger particles. Smaller particles are unfavoured due to their higher surface curvature resulting in faster solvation. Larger particles will therefore benefit in the continuous equilibrium of dissolving and reattaching of monomers while smaller particles gradually degrade.

The earliest examples of nanoparticle synthesis are quite old, but at that point the underlying processes had not been understood yet.[72–74] After the studies mentioned earlier,[71] the organized development of nanoparticle synthesis procedures yielded ways to generate nanoparticles from various materials.[75, 76] As the contents of this thesis are focussed on semiconducting particles produced in organic media, this will also be the focus of this section, referring to further literature for information on metal,[70, 77, 78] metal oxide,[70, 79] and polymer nanoparticle[80] synthesis.

Although the synthesis of especially CdTe NCs has also been very successfully demonstrated in aqueous media,[81] the synthesis of the semiconducting NCs like the ones used in this work are usually performed in organic solvents. The diverse selection of organic media offers the ability to tune the synthesis over a wider temperature range and by the use of specific additives. The breakthrough in the field of semiconductor quantum dot (QD) synthesis has been

the introduction of the *hot-injection* synthesis.[9] This procedure is based on the decomposition of metal-organic precursors (e.g. dimethylcadmium) after the quick injection into hot high-boiling organic solvents (e.g. tri-*n*-octylphosphine oxide, TOPO). The rapid increase in concentration via the quick injection and the following rapid decrease caused by the nucleation burst of NCs constitutes the aforementioned control over size and monodispersity. The next important step has been the replacement of the toxic and pyrophoric precursors. Synthesis routes starting with CdO as starting material have been described and offer an easier to handle alternative.[82] The addition of certain organic molecules acting as complexing agents for the NC precursors and surface ligands for the resulting particle has also been investigated intensively, resulting in better control of NC shape and structure.[83–87] Building on these works a large array of NC syntheses for semiconducting materials has been outlined, for the well established II-VI semiconductors (CdTe,[9, 82, 85, 88] CdSe,[9, 82, 87] CdS,[9, 82] ZnS,[89] ZnSe,[90] HgTe[91]), as well as IV-VI (PbSe,[92] PbS[93–95]) or III-V (InP,[96] GaAs,[97, 98] GaN[99]) semiconductors.

The techniques of NC synthesis offer chemists the ability to adapt their product for an intended function. With the ever-growing advance of nanomaterials into the subjects of science as well as commercial products,[100] in turn more and more elaborate ways to tailor nanoparticles to exhibit desired properties were developed. This marked the advent of heterostructures, nanoparticles consisting of more than one compound, in the form of core-shell structures,[101, 102] janus particles,[102, 103] and other variations, e.g. core/shell/shell[102, 104] or embedded particles.[105] The consequences of formation of heterostructures to the electronic structure of the resulting NCs has been described earlier in section 2.1. In the endeavour to create heteronanostructures again the nucleation and growth need to be controlled meticulously to generate the structures as desired. Usually, the synthesis of heteronanostructures is based on a *seeded-growth* approach, first synthesising a seed NC of one material which is then used to initiate the growth of the second material onto itself. Contrary to the single material NC synthesis discussed earlier, the secondary nucleation is very much needed in this procedure and primary nucleation needs to be avoided as to generate a pure product free of homogeneously nucleated shell material. The activation energy for secondary nucleation is generally lower than the activation energy for homogeneous nucleation, allowing the control over these processes by the

reaction conditions such as monomer concentration. In the *seeded-growth* process a new solid-solid interface is generated and the growth of the second material can take place in mostly two fashions depending on this interface. The energy for this deposition process is given in equation 2.5.

$$\Delta G_{\text{seeded-growth}} = \gamma_1 - \gamma_2 + \gamma_{1,2} \quad (2.5)$$

$\Delta G_{\text{seeded-growth}}$	-	free enthalpy of nanoheterocrystal formation
$\gamma_X$	-	liquid-solid surface energy of material X
$\gamma_{1,2}$	-	solid-solid surface energy between material 1 and 2

If the liquid-solid surface energy of the second material ( $\gamma_2$ ) is favourable compared to that of the seed material ( $\gamma_1$ ) or the solid-solid surface energy of the newly formed interface ( $\gamma_{1,2}$ ) is small which is the case for good crystallographic matching of the two materials, the deposition takes place in form of a continuous uniform shell. In contrast, if the crystallographic matching is poor or the surface energy of the second material is higher than the one of the seed material ( $\gamma_2 > \gamma_1$ ) the deposition of the second material happens in an island-like domain growth. This can further be influenced by the addition of surface active molecules, ligands, which may change the surface energy of the individual materials. These mechanisms are referred to as FRANK-VAN DER MERWE and VOLMER-WEBER mode respectively.[102]

The growth of uniform core/shell NCs is very common in the field of semiconductor NCs and different types and examples[42–45, 47, 50–53, 59, 60] have been mentioned in section 2.1. Apart from these one-step reactions a shell growth can also be performed successively layer-by-layer in the *successive ionic layer adsorption and reaction (SILAR)*[106] or *colloidal atomic layer deposition (c-ALD)*[107] approaches. In these methods individual cation and anion layers of the desired shell material are grown one by one which allows for strict control over the shell thickness. Another common practice is the growth of several different shells to gradually alter the lattice constant and reduce the crystallographic mismatch between the layers, e.g. in CdSe/CdS/ZnS.[108] Additionally, the deliberate synthesis of non-uniform shells has been investigated, resulting in differently shaped heterosystems.[46, 61, 109–111] Similar to shape control in single material systems[87, 112] the deposition of asymmetric shells makes use of surfactants binding preferably to certain crystal facets or an inherent asymmetry in the seed NC due to its crystal structure and kinetic control in the reaction.[102] The heterostructure

made up of CdSe QDs which are then used in a *seeded-growth* synthesis to grow elongated CdS shells[109] (referred to as CdSe/CdS dot/rod) takes up a special spot within this thesis as it is the structure most of this work is based upon. This is a *quasi type-II* NC, meaning the hole is localized in the CdSe core (due to the large offset between the CdSe and CdS valence bands) while the electron is delocalized throughout the entire NC (due to the marginal offset between the conduction bands). As will be described later (in section 3.3), this results in unique optical properties when connecting these dot/rods into network structures.

All of the named examples deal with heteronanostructures made up of two different semiconductors. There are, naturally, also a myriad of heterostructures from different material types. Core/shell structures of metal/semiconductor hybrids have been achieved by various methods.[113–115] The same material combination in different shape, as semiconductor decorated with metal domains, has gathered large interest due to its photocatalytic properties and accordingly the formation of these structures has been investigated extensively, directing the domain size and position by different methods.[116–123] The combination of various NCs with silica in core/shell particles can be interesting for very different reasons. Often an outer silica shell is employed to facilitate water solubility and with it biocompatibility in structures such as metal oxide/silica or semiconductor/silica.[25, 26, 124] In metal/silica core/shell structures[19, 125] it can additionally serve to tune the optical properties of the particles. The general synthesis route of these structures consists of the hydrolysis of silica precursors in presence of the core NCs inside a microemulsion solvent system,[124] but methods without the need for an emulsion have also been developed.[21, 22] The broad silicon metal-organic chemistry allows for further adjustments such as the introduction of small silicon based ligand molecules improving the attachment of the shell, the additional functionalization of the silica shell or a controllable porosity of the shell.[126, 127] These core/shell modification methods will be build upon in chapter 6 to apply this nanoscale synthesis not simply to a NC dispersion but a macroscopic network of particles of hundreds of kilometers length.

Another tool for tailoring nanocrystals is cation exchange. In this method an already synthesized nanocrystal is used and the individual cations in its structure replaced.[55, 128] Nanocrystals with well-established syntheses can essentially be used as templates. The advantage of this approach lies in the ability to generate nanocrystals in materials, shapes or crystal struc-

tures that are hard and sometimes even unattainable.[129] The anion lattice ideally stays unaffected by the cation exchange as anions are larger than cations and less likely to be exchanged.[130] The cation exchange in nanocrystals is feasible only because of the small diffusion length needed in these materials. This allows the reaction to finish on reasonable time scales and at reasonable conditions as compared to cation exchanges on macroscopic scales. The mechanisms behind this cation exchange can be understood as a four step process. In a theoretical system of  $CA + B^{x+} \rightarrow BA + C^{x+}$  these steps represent dissociation of the original compound, desolvation of the introduced cation, association of the new compound and solvation of the original cation.[131]



This process is therefore influenced by the contributions of the different crystal energies (represented in the dissociation and association) and the solvation energies (represented in desolvation and solvation). Consequently, a cation exchange is preferred when the crystal energy of the target compound is favoured. This is influenced by the lattice energies but also lattice strain and surface energy. Likewise, an influence can also be exerted through the solvation energy by the choice of solvent and additional ligands to e.g. facilitate the solvation of the original cation. In cases of non-isovalent exchanges, e.g.  $Cd + 2Cu^+ \rightarrow Cd_2^+ + 2Cu$ , additional factors like entropy and reaction kinetics further influence the reaction.[131] The exchange starting from copper compounds or using copper compounds as intermediate phase is a common practice due to the high mobility of copper ions in the crystal lattice which is caused by their defect rich structures.[130] A cation exchange will start on the surface and proceed into the structure via solid-state diffusion. It has been shown that these cation exchanges can be performed shape selectively on NCs, e.g. starting at the tip in case of rod-shaped or multipod NCs.[132, 133]

The technique of selectively exchanging cations from the tip of NCs will be employed later in section 7.3 to tune the bandstructure of NC building blocks.

As will be described in the following chapter 3, NCs of all designs, materials and shapes can be employed as building blocks to constitute larger network structures whose assembly, modification and characterization are at the center of this work. The properties of such networks result as much from the synthesis of the building blocks as from the assembly process itself. Precise control over the nanoparticle synthesis in turn allows control over their properties and the properties of the network structures build up from them.

## 3 Network Structures: Putting the Pieces Together

In the following the general principles behind gel network structure formation and destabilization of colloidal nanoparticle solutions, the conversion of wet gels to their air filled counterparts and the current state-of-the-art of NC-based gel structures will be discussed.

### 3.1 Network Formation

A gel or a network structure can be produced by many different approaches. The more classically known methods are based on the sol-gel process. This procedure is typical of metal oxide gel structures like silica, titania, vanadium oxide, but can also be applied to organic and biopolymers. It starts from molecular precursor compounds, mostly metal organic or salts, which react in hydrolysis and condensation reactions to form the amorphous metal oxide network. However, there is a different route to inorganic network structures starting with the separated colloidal synthesis of NC building blocks and a second step for the formation of the network. This allows for a fine-tuning of the building block properties as well as further influencing the network.[12, 134, 135] The state-of-the-art of NC-based network structures will be further detailed later in section 3.3. First, the fundamental principles of NC network assembly will be discussed here. Generally, NCs finely dispersed in solution need to be stabilized. They are subject to gravitational forces facilitating a particle precipitation, which can be exploited for NC purification, but also BROWNIAN motion keeping the NCs moving. Due to their high surface area and surface energy there is also a thermodynamic driving force inducing aggregation of particles

into larger structures, while VAN-DER-WAALS (VdW) interactions pull the particles towards each other. VdW forces are caused by dipole interaction between particles (or molecules) which are present in all systems. These dipoles can be the permanent dipoles in polar species but also induced by random fluctuations in electron density. Interestingly, VdW interactions between nanocrystals can be estimated to act over comparably large distances (see equation 3.1) unlike the very short range interaction that VdW forces represent when looking at molecules.[136]

$$V_{VdW} \approx -\frac{A_H}{12} \frac{r}{D} \quad (3.1)$$

$V_{VdW}$  - Van-der-Waals interaction energy  
 $r$  - nanocrystal radius  
 $A_H$  - Hamaker constant  
 $D$  - distance between particle surfaces

Due to their long range and their dependence on bulk properties like refractive index and dielectric constant (which are simplified into the Hamaker constant), VdW forces are seldom modified to tune particle interactions.[134] This is amplified by the relatively large differences between dielectric properties of common solvents and inorganic NCs allowing only a low range of tunability.

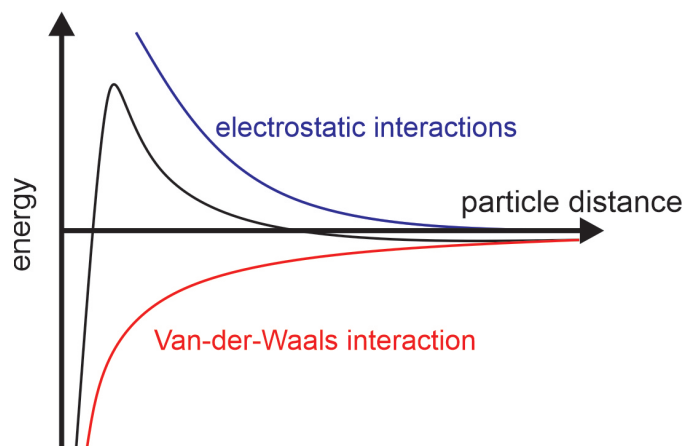


Figure 3.1: Development of the total interaction energy in case of two electrostatically stabilized nanocrystals approaching each other with contribution of the repulsive electrostatic interaction and the attractive Van-der-Waals interaction. Own representation inspired by [134]

To generate a stable NC colloid different methods can be employed to keep particles from fusing together counteracting the above mentioned attractive interactions. In polar solvents the most popular way is the use of electrostatic stabilization. Therefore, either the particle itself or

the ligands surrounding the particle are endowed with a certain charge leading to a surface charge of the particle and the formation of an electric double layer around the particles. As the particles now exhibit the same charge they will repel each other. The interaction between two equal NCs due to these electrostatic interactions can be described by equation 3.2.[134]

$$V_{elec} \approx 2\pi\epsilon_m\epsilon_0 r\phi_0^2 e^{-\frac{D}{\lambda_D}} \quad (3.2)$$

$V_{elec}$	-	electrostatic interaction energy	$\epsilon_m$	-	relative permittivity of the medium
$\epsilon_0$	-	relative permittivity of the vacuum	$r$	-	nanocrystal radius
$\phi_0$	-	surface potential	$D$	-	inter-particle distance
$\lambda_D$	-	Debye length			

The effect of these counteracting forces can be visualized using the DLVO (Derjaguin, Landau, Verwey, Overbeek) theory according to which such forces are added to generate an expression for the overall interaction in dependence on the distance between the particles. A visualization of this approach is shown in figure 3.1. It can be seen that over long distances an overall attraction between particles due to the VdW interaction exists. A particle dispersion is stabilized in a local energy minimum at certain moderate distances. For particles moving closer to each other an energy barrier by the repulsive electrostatic interactions keeps particles from aggregating. However, as this barrier can be overcome - either by sufficient energy in the system or by changing the height of the barrier - past the barrier an aggregation of the particles is energetically strongly advantageous. The strength of the energy barrier in electrostatically stabilized NCs is dependent on the medium (see equation 3.2) but also the DEBYE length which in itself is dependent on temperature directly and indirectly via the permittivity of the medium and the ionic strength (see equation 3.3).[134]

$$\lambda_D = \sqrt{\frac{\epsilon_m\epsilon_0 k_{BT}}{e^2 N_A 2I}} \quad (3.3)$$

$\lambda_D$	-	Debye length	$\epsilon_m$	-	relative permittivity of the medium
$\epsilon_0$	-	relative permittivity of the vacuum	$k_B$	-	Boltzmann constant
$T$	-	temperature	$e$	-	charge of an electron
$N_A$	-	Avogadro constant	$I$	-	ionic strength of the medium

In organic, non-polar solvents the usual strategy is the use of long chain organic surface ligands to coat the particles. These ligands then form a sterical barrier between the NCs. This strategy is common in case of most semiconductor chalcogenide NCs such as the ones used

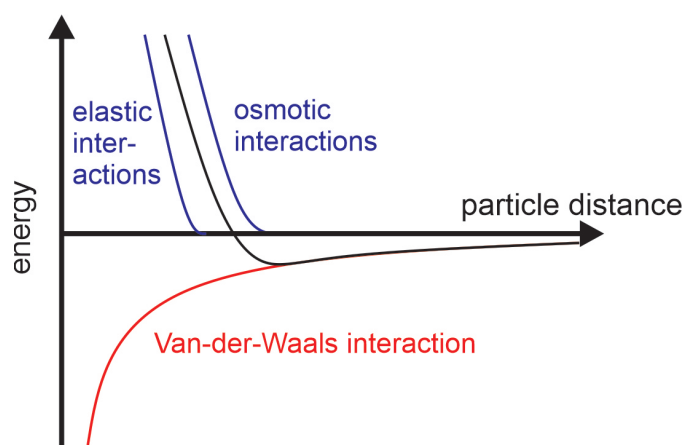


Figure 3.2: Development of the total interaction energy in case of two nanocrystals stabilized by bulky organic ligands approaching each other with contribution of the repulsive steric interaction through osmotic and elastic forces and the attractive Van-der-Waals interaction. Own representation inspired by [134]

throughout most of this work. The interaction of the ligands and the solvent is complex, but can be described to a large part by osmotic and elastic repulsive interactions when particles approach each other. Ligand shells overlapping presents an effective local ligand concentration increase in the overlapping region causing an osmotic pressure of the solvent. The solvent molecules attempting to compensate this concentration difference will separate the NCs. At even closer distances the ligands themselves are compressed into more unfavourable configurations resulting in strong repulsive forces. Again the forces acting in such systems can be summed up as depicted in figure 3.2. In this case of steric stabilization, there is no energy barrier like described for electrostatic stabilization but rather a strong and growing repulsion for particles moving closer together. There exists however an energetic minimum for the particle distances and depending on circumstances moving particles further apart than this minimum can be difficult. The forces between the particles can in this instance be controlled via the ligand and solvent interaction (e.g. be introduction of anti-solvents or change in temperature) and via the ligand coverage.[134] The controlled slow removal of ligand through various means is one of the most common gelation methods for NCs and the one used in most of the present work. The generation of network structures build up from NC building blocks represents a convenient approach to transform these NCs into macroscopic solids. This assembly necessitates the

destabilization of the NC *sol*. To maintain control over the network structure this destabilization has to be carefully managed by directing the inter-particle forces detailed above. To this day a multitude of methods adapted for the respective NC, its solvent and its surface functionalization have been demonstrated to successfully generate NC-based network structures which will be discussed in detail in section 3.3.

## 3.2 Preparation of Aerogels

To convert a solvent filled gel structure while retaining its filigree network, it can not simply be dried under ambient conditions. During drying of porous structures a meniscus is forming inside the pores causing capillary forces dependent on the pore diameter. The capillary stress arising during the drying within the small pores of the network can reach the order of 1000 bar and lead to a collapse of the network structure.[137] A collapsed network structure is commonly referred to as *Xerogel*.

There are several approaches to circumvent the problem the capillary forces pose during the drying process and retain the original structure. The most universally known being the *supercritical drying* (SCD) or *critical point drying*. In this, the solvent inside the gel is brought above its critical point to reach a supercritical state. In this state there is no difference and therefore no interface between liquid and gaseous state resulting in the elimination of the capillary forces. Due to the usually high pressures needed, this procedure is carried out in an autoclave. The SCD is also the historical method.[138] The solvents used in this case were mostly alcohols, from which metal oxide but also organic gels were dried. This *hot* SCD has the inherent problem of the high pressures and temperatures necessary to reach the critical point of e.g. methanol and ethanol (ca. 60-80 bar and 240 °C) in conjunction with the flammability of these solvents. A very important step for the safety and viability of SCD has been the introduction of *cold* SCD comprising of an additional solvent exchange step to liquid carbon dioxide.[139] The CO<sub>2</sub> can then be supercritically extracted as its critical point is accessible at relatively moderate conditions. In practice this is generally done by transferring a lyogel in a suitable solvent into an autoclave which is then pressurized and filled with liquid CO<sub>2</sub>. The original solvent is separated and the temperature of the container is increased until above the critical point of CO<sub>2</sub> (ca.

74 bar and 31 °C). The pressure inside the container is then carefully vented under isothermal conditions (see also the phase diagram in figure 3.3 for illustration of the process).[137] The network structures produced by this procedures are usually named *aerogels*.

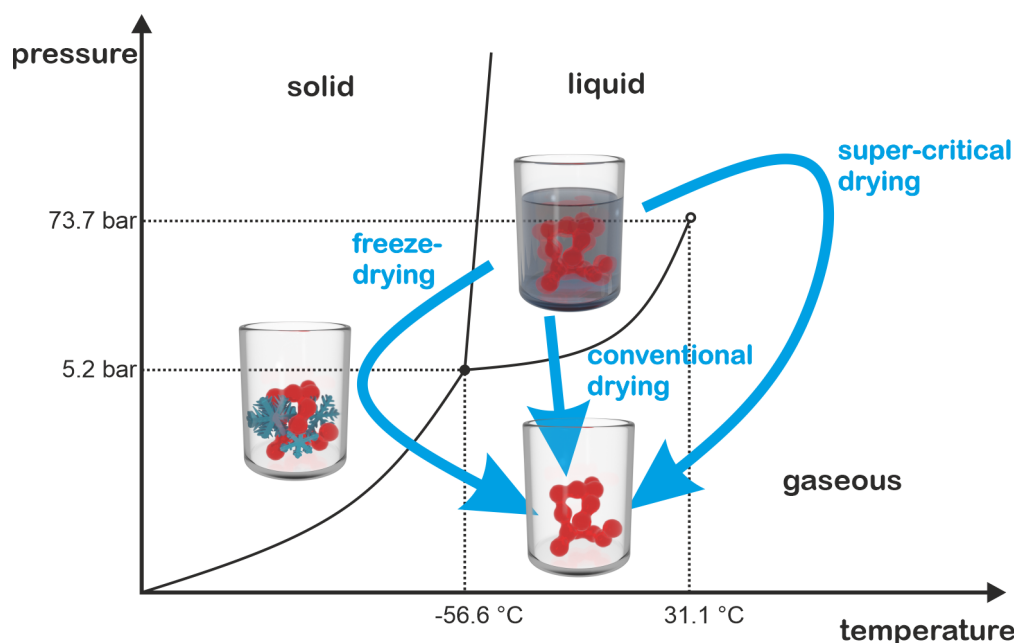


Figure 3.3: Phase diagram of CO<sub>2</sub> with arrows describing the course of different drying techniques. Own representation inspired by [12]

A second procedure avoiding the gas-liquid interface and resulting capillary forces is the *freeze-drying*. Here, the solvent is first frozen solid and sublimated at low pressure afterwards to extract it from inside the network. The pressure needs to be low to allow the vapour pressure of the frozen solvent to drive the extraction of the solvent from the gel.[137] This method was described for silica gels, but yielded relatively poor results due to cracks in the dried gel triggered by the crystallization of the solvent.[140] In the field of NC-based gels the simultaneous network formation and freezing of the solvent has shown promising results.[141, 142] These gels can be referred to as *cryoaerogels* or *cryogels*.

The third option to obtain porous dried network structures is to actually perform conventional solvent evaporation or *ambient pressure drying* (APD). In this technique the occurrence of a meniscus and the resulting capillary forces is tolerated and other precautions are taken to ensure the network can withstand the stress exacted on it. The two important points are the

choice of solvent, as the capillary stress depends on the surface tension of the solvent and the network reinforcement. The stress acting on the network can be greatly reduced by employing low surface tension solvents (e.g. acetone) plus the strength of the network can be increased by surface modification with methyl groups preventing further condensation of the network during drying.[143–146]

Often gels are further reinforced by cross-linking with organic molecules forming organic-inorganic hybrid gels.[147] These gels are then sometimes called *aerogel-like xerogels*. It has to be noted at this point that the definitions of *aerogel*, *xerogel* and others are blurred and used in different meanings in literature also because they do not refer to a materials property, but the process that has been used to create it. All of the methods for APD have been limited to *classical* sol-gel networks and not yet found applicability in the NC-based gels.

Out of the three ways detailed here, the supercritical drying is until today the preferred method to reliably produce NC-based aerogels and it is the one employed for all dried porous network materials discussed in this thesis.

### 3.3 Nanocrystal-Based Network Structures

The assembly of colloidal nanocrystal building blocks into larger interconnected network structures has first been described on the example of CdS colloids.[148, 149] The gelation was induced by the slow partial oxidation of the thiolate surface ligands on the particles accidentally or intentionally induced by atmospheric oxygen or addition of hydrogen peroxide, leading to a gentle destabilisation of the colloid and a bridging between the particles via sulfur-sulfur bonds. In reference to similarities to the sol-gel process these networks are often called gels, in which case the colloidal nanoparticle dispersion is the sol. After the first experiments with wet nanocrystal-based gels[148] the first report of successful drying to obtain NC-based aerogels introduced this new material class on the example of CdS.[150] The number of available materials for nanoparticle-based aerogels was soon expanded to PbS, CdSe and ZnS, in this case using tetranitromethane as oxidizer for ligand removal.[151, 152] While these materials displayed the quantum confinement inherent to their NC building blocks in their absorption the emission was usually lost or drastically diminished in the resulting aerogel due to surface etching and

resulting trapping effects. This was overcome by the use of more complex structures, namely CdSe/ZnS core/shell nanocrystals, allowing the production of highly fluorescent NC-based network structures.[17] The repertoire of materials was further extended to CdTe, introducing high intensity light irradiation as gelation inducer. The light initiates photocatalytic decomposition of the ligands of the NCs similar to the earlier described chemical oxidizers.[153] Similar techniques have more recently yielded Ni<sub>2</sub>P[154] and InP[155] NC-based network structures. With the report of noble metal nanocrystal-based networks the range of materials was broadened even further. In this instance gels from aqueous Au, Ag, and Pt nanoparticles, but also mixtures thereof have been prepared by either oxidation (H<sub>2</sub>O<sub>2</sub>) or change in solvent polarity (by addition of ethanol). Also, the favourable effects of mixing different nanoparticle (Au and Ag or Pt and Ag) building blocks on network formation and stability have been mentioned in this work.[156] Other methods based on ligand removal employ propylene oxide as oxidizer for the assembly of ceria (CeO<sub>2</sub>) NCs,[157] the reductive removal of surface ligands on Pt nanocubes by hydrazine,[15] and the non-oxidizing ligand removal by trivalent cations, demonstrated on different cadmium chalcogenide nanostructures.[158] The development of new network assembly methods continues to bring forward ever new pathways to NC-based networks. The use of tetrazoles as nanoparticle ligand allows for the network formation by addition of metal ions that form complexes with the tetrazole effectively *glueing* the particles together. In turn these networks can therefore reversibly formed this way and dissolved by addition of a stronger complexing agent.[159, 160] With the introduction of the so-called *all-inorganic* nanoparticles,[161] in which small inorganic atoms and complexes are employed as ligands, also gave access to a new route of gel formation based similarly on a complexation mechanism.[162, 163] The electrochemical gelation of nanoparticles has also been reported either by an electrochemical stripping of the ligands[164] or by *in situ* generated crosslinking metal ions.[165, 166]

A completely different way based not on chemical interactions, but on physical forces to assemble NCs into porous network structures is the cryoaerogelation. In this case the colloidal building block solution is rapidly frozen by immersion in liquid nitrogen. The NCs are not incorporated in the ice crystals and accumulate in the remaining space where they are pressed together to form lamellar network structures.[141, 167] In a similar manner, networks were generated by sublimation of organic crystals decorated with nanoparticle building blocks.[168]

Another method of network formation by physical forces is the combination of two NC building blocks which have each been modified with specific surface ligands to have opposing surface charges, e.g. aminothiols and thiocarboxylic acids resulting in positive and negative surface charge respectively. When mixed together the two differently modified building blocks attract each other and the network is formed.[169, 170] In some cases also simple heating of the colloidal building block solution can lead to gelation. Heat influences the stability of solutions in many ways, e.g. by influencing the equilibrium of bound and free ligands on the NC surface and especially in aqueous solutions changing the dielectric constant of the medium. These effects have been used to assemble Au-titania[171], antimony-doped tin oxide[172], and recently with  $\text{Cu}_3\text{N}$  NC networks[173] the first nitride NC-based gel. Another different method is the centrifugation assisted gelation in which the colloidal building block solutions are exposed to low-force centrifugation which in certain cases is enough to cause concentration of particles and particle aggregation into network structures in the bottom part of the container. This was demonstrated for  $\text{InTaO}_4$ . [174]

As already mentioned in case of nanoparticles not only composition, but also size and shape play a defining role in their resulting properties. Accordingly, the influence of different NC shapes as network building blocks has been investigated, demonstrating higher resulting porosities and increased resistance to mechanical stress for anisotropic building blocks (rods and branched NCs).[175] Also hollow noble metal NC building blocks have been assembled into gels.[176–178] More recent interesting uses of shape-controlled building blocks employ CdSe-based nanoplatelets[14] (2D nanostructures with the thickness of only a few monolayers) or Pt nanocubes.[15] In both instances the resulting networks only exhibit certain crystallographic facets, making these structures interesting for site selective catalytic reactions.[15] A different work is focused on the use of CdSe/CdS dot/rod nanostructures as network building blocks.[13] The elongated, rod-shaped building blocks show a tendency to assemble tip-to-tip. Furthermore, these semiconducting building blocks offer interesting electronic properties with the excited hole highly confined in the CdSe core while the excited electron is much more delocalized as depicted in figure 3.4. The interconnected network shows highly increased fluorescence lifetime which was attributed to the mobility of the excited electron inside the network.[13] The CdSe/CdS dot/rod NC-based networks will be used for further studies on NC-

based network modification in chapter 6 as well as on the highly interesting (opto-)electronic behaviour in chapter 5 and 7.

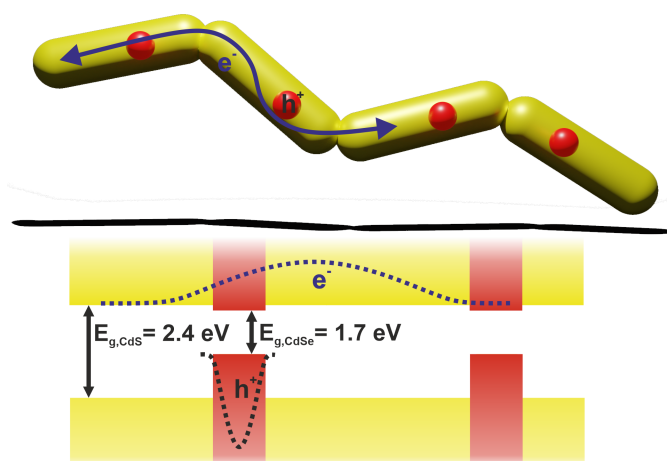


Figure 3.4: Schematic depiction of a network of connected CdSe/CdS dot/rod nanocrystals and of the band structure of two connected dot/rods with electron and hole wave functions

Apart from tuning the individual building blocks, the network itself can also be tuned. By means of cation exchange, mentioned earlier and commonly employed in NC chemistry but much less on the level of NC-based gels, the composition of the network can be tuned after the fact. This allows access to gel networks of materials which beforehand could not be gelled due to their instability to common gelation conditions.[179, 180] The electrochemical deposition of a surface layer onto preformed noble metal NC-based networks has been reported.[181] In this thesis, the modification of continuous NC-based gels by wet-chemical methods will be described in chapter 6. A different approach is the concurrent gelation of more than one component, especially the combination of noble metal NCs and semiconducting NCs in one network has gathered some interest because of the effective charge separation on excitation between the two components.[182–184] Other works also show energy transfer within a network of two semiconducting NCs with different bandgaps.[160] Very recently the potential to tune the network homogeneity in two component gels by the gelation kinetics has been demonstrated.[185] This technique has earlier been used in single component gels to tune the network density influencing bandstructure and opacity of the final gel.[186, 187] While all these works focus on adjusting the networks on the nano- to microscale, the reported fabrication of laterally resolved

NC-based gels by inkjet printing showcases the macroscopic shaping of these structures.[188] Overall, NC-based networks can be influenced before and even after gelation on all size scales from individual atoms in the NCs crystal structure up to the macroscopic shape of the monolith.[135]

The high surface area of these porous network structures makes them interesting subjects for interface-driven applications. These include photocatalysis by NC-based aerogel fragments in solution[189], by monolithic aerogels in a gas-phase flow reactor[190] and electrocatalysis[191]. In the area of electrocatalysis a lot of work was done on composition tuning of the noble metal catalytic network structures. One of the key advantages of NC-based aerogels in this context is their resistance to thermal aggregation and their self-support, meaning no detachment from a support material is possible.[178, 191–194] The high porosity of NC-based aerogels also lead to studies on their application in thermoelectrics.[195, 196] Due to their high surface area and the potential to finely tune the electronic structure of their building blocks the photoelectrochemical properties of NC-based gels have gathered some interest,[158, 197, 198] leading to proof-of-concepts of NC-based aerogel photoelectrochemical sensing.[142, 199]

In summary, the assembly of isolated, colloidally stable NC building blocks enables the separation of the building block formation and the network formation similar to the principles of nanoparticle synthesis. Beyond this, the network itself also presents a point to further influence the properties via control of the structure. This in turn allows for the precise tuning of the individual building blocks and the network itself to suit certain applications or the principle investigation of NC-based network properties.



## 4 Bibliography

- (1) H. WELLER, “Quantized Semiconductor Particles: A novel state of matter for materials science”, *Adv. Mater.*, 1993, **5**, 88–95, DOI: 10.1002/adma.19930050204.
- (2) K. L. KELLY, E. CORONADO, L. L. ZHAO and G. C. SCHATZ, “The Optical Properties of Metal Nanoparticles: The Influence of Size, Shape, and Dielectric Environment”, *J. Phys. Chem B*, 2003, **107**, 668–677, DOI: 10.1021/jp026731y.
- (3) S. BEDANTA and W. KLEEMANN, “Supermagnetism”, *J. Phys. D: Appl. Phys.*, 2009, **42**, DOI: 10.1088/0022-3727/42/1/013001.
- (4) T. TSUZUKI and P. G. McCORMICK, “Mechanochemical synthesis of nanoparticles”, *J. Mater. Sci.*, 2004, **39**, 5143–5146, DOI: 10.1023/B:JMSC.0000039199.56155.f9.
- (5) S. AMIRKHANLOU, M. KETABCHI and N. PARVIN, “Nanocrystalline/nanoparticle ZnO synthesized by high energy ball milling process”, *Mater. Lett.*, 2012, **86**, 122–124, DOI: 10.1016/j.matlet.2012.07.041.
- (6) G. W. YANG, “Laser ablation in liquids: Applications in the synthesis of nanocrystals”, *Prog. Mater. Sci.*, 2007, **52**, 648–698, DOI: 10.1016/j.pmatsci.2006.10.016.
- (7) H. NASER, M. A. ALGHOUL, M. K. HOSSAIN, N. ASIM, M. F. ABDULLAH, M. S. ALI, F. G. ALZUBI and N. AMIN, “The role of laser ablation technique parameters in synthesis of nanoparticles from different target types”, *J. Nanoparticle Res.*, 2019, **21**, DOI: 10.1007/s11051-019-4690-3.
- (8) J. ECKERT, J. HOLZER, C. KRILL and W. JOHNSON, “Structural and thermodynamic properties of nanocrystalline fcc metals prepared by mechanical attrition”, *Journal of Materials Research*, 1992, **7**, 1751–1761, DOI: 10.1557/JMR.1992.1751.

- (9) C. B. MURRAY, D. J. NORRIS and M. G. BAWENDI, "Synthesis and characterization of nearly monodisperse CdE (E = sulfur, selenium, tellurium) semiconductor nanocrystallites", *J. Am. Chem. Soc.*, 1993, **115**, 8706–8715, DOI: 10.1021/ja00072a025.
- (10) C. B. MURRAY, C. R. KAGAN and M. G. BAWENDI, "Synthesis and Characterization of Monodisperse Nanocrystals and Close-Packed Nanocrystal Assemblies", *Annu. Rev. of Mater. Sci.*, 2000, **30**, 545–610, DOI: 10.1146/annurev.matsci.30.1.545.
- (11) A. M. SMITH and S. NIE, "Semiconductor nanocrystals: Structure, properties, and band gap engineering", *Acc. Chem. Res.*, 2010, **43**, 190–200, DOI: 10.1021/ar9001069.
- (12) C. ZIEGLER, A. WOLF, W. LIU, A. K. HERRMANN, N. GAPONIK and A. EYCHMÜLLER, "Modern Inorganic Aerogels", *Angew. Chem. Int. Ed.*, 2017, **56**, 13200–13221, DOI: 10.1002/anie.201611552.
- (13) S. SANCHEZ-PARADINAS, D. DORFS, S. FRIEBE, A. FREYTAG, A. WOLF and N. C. BIGALL, "Aerogels from CdSe/CdS Nanorods with Ultra-long Exciton Lifetimes and High Fluorescence Quantum Yields", *Adv. Mater.*, 2015, **27**, 6152–6156, DOI: 10.1002/adma.201502078.
- (14) S. NASKAR, J. F. MIETHE, S. SÁNCHEZ-PARADINAS, N. SCHMIDT, K. KANTHASAMY, P. BEHRENS, H. PFNÜR and N. C. BIGALL, "Photoluminescent Aerogels from Quantum Wells", *Chem. Mater.*, 2016, **28**, 2089–2099, DOI: 10.1021/acs.chemmater.5b04872.
- (15) S. NASKAR, A. FREYTAG, J. DEUTSCH, N. WENDT, P. BEHRENS, A. KÖCKRITZ and N. C. BIGALL, "Porous Aerogels from Shape-Controlled Metal Nanoparticles Directly from Nonpolar Colloidal Solution", *Chem. Mater.*, 2017, **29**, 9208–9217, DOI: 10.1021/acs.chemmater.7b03088.
- (16) T. KODANEK, A. FREYTAG, A. SCHLOSSER, S. NASKAR, T. HÄRTLING, D. DORFS and N. C. BIGALL, "Macroscopic Aerogels with Retained Nanoscopic Plasmonic Properties", *Z. Phys. Chem.*, 2018, **232**, 1675–1689, DOI: 10.1515/zpch-2017-1045.
- (17) I. U. ARACHCHIGE and S. L. BROCK, "Highly luminescent quantum-dot monoliths", *J. Am. Chem. Soc.*, 2007, **129**, 1840–1841, DOI: 10.1021/ja066749c.

- 
- (18) F. PIETRA, R. J. VAN DIJK - MOES, X. KE, S. BALS, G. VAN TENDELOO, C. DE MELLO DONEGA and D. VANMAEKELBERGH, "Synthesis of Highly Luminescent Silica-Coated CdSe/CdS Nanorods", *Chem. Mater.*, 2013, **25**, 3427–3434, DOI: 10.1021/cm401169t.
- (19) L. M. LIZ-MARZÁN, M. GIERSIG and P. MULVANEY, "Synthesis of nanosized gold-silica core-shell particles", *Langmuir*, 1996, **12**, 4329–4335, DOI: 10.1021/la9601871.
- (20) X. TANG, E. KRÖGER, A. NIELSEN, C. STRELOW, A. MEWS and T. KIPP, "Ultrathin and Highly Passivating Silica Shells for Luminescent and Water-Soluble CdSe/CdS Nanorods", *Langmuir*, 2017, **33**, 5253–5260, DOI: 10.1021/acs.langmuir.7b00615.
- (21) Y. MA, Y. LI, S. MA and X. ZHONG, "Highly bright water-soluble silica coated quantum dots with excellent stability", *J. Mater. Chem. B*, 2014, **2**, 5043–5051, DOI: 10.1039/C4TB00458B.
- (22) Y. KOBAYASHI, H. KATAKAMI, E. MINE, D. NAGAO, M. KONNO and L. M. LIZ-MARZÁN, "Silica coating of silver nanoparticles using a modified Stöber method", *J. Colloid Interface Sci.*, 2005, **283**, 392–396, DOI: 10.1016/j.jcis.2004.08.184.
- (23) S. JUN, J. LEE and E. JANG, "Highly Luminescent and Photostable Quantum Dot–Silica Monolith and Its Application to Light-Emitting Diodes", *ACS Nano*, 2013, **7**, 1472–1477, DOI: 10.1021/nn3052428.
- (24) A. F. DEMIRÖRS, A. van BLAADEREN and A. IMHOF, "A General Method to Coat Colloidal Particles with Titania", *Langmuir*, 2010, **26**, 9297–9303, DOI: 10.1021/la100188w.
- (25) Z. ZHELEV, H. OHBA and R. BAKALOVA, "Single quantum dot-micelles coated with silica shell as potentially non-cytotoxic fluorescent cell tracers", *J. Am. Chem. Soc.*, 2006, **128**, 6324–6325, DOI: 10.1021/ja061137d.
- (26) S. T. SELVAN, P. K. PATRA, C. Y. ANG and J. Y. YING, "Synthesis of silica-coated semiconductor and magnetic quantum dots and their use in the imaging of live cells", *Angew. Chem. Int. Ed.*, 2007, **46**, 2448–2452, DOI: 10.1002/anie.200604245.
- (27) M. VERT, Y. DOI, K. H. HELLWICH, M. HESS, P. HODGE, P. KUBISA, M. RINAUDO and F. SCHUÉ, "Terminology for biorelated polymers and applications (IUPAC recommendations 2012)", *Pure Appl. Chem.*, 2012, **84**, 377–410, DOI: 10.1351/pac-rec-10-12-04.

- (28) P. ALIVISATOS, "The use of nanocrystals in biological detection", *Nat. Biotechnol.*, 2004, **22**, 47–52, DOI: 10.1038/nbt927.
- (29) L. N. LEWIS, "Chemical Catalysis by Colloids and Clusters", *Chem. Rev.*, 1993, **93**, 2693–2730, DOI: 10.1021/cr00024a006.
- (30) D. ASTRUC, F. LU and J. R. ARANZAES, "Nanoparticles as recyclable catalysts: The frontier between homogeneous and heterogeneous catalysis", *Angew. Chem. Int. Ed.*, 2005, **44**, 7852–7872, DOI: 10.1002/anie.200500766.
- (31) E. RODUNER, "Size matters: Why nanomaterials are different", *Chem. Soc. Rev.*, 2006, **35**, 583–592, DOI: 10.1039/b502142c.
- (32) T. TRINDADE, P. O'BRIEN and N. L. PICKETT, "Nanocrystalline semiconductors: Synthesis, properties, and perspectives", *Chem. Mater.*, 2001, **13**, 3843–3858, DOI: 10.1021/cm000843p.
- (33) A. P. ALIVISATOS, "Semiconductor Clusters, Nanocrystals, and Quantum Dots", *Science*, 1996, **271**, 933–937, DOI: 10.1126/science.271.5251.933.
- (34) M. BAWENDI, M. L. STEIGERWALD and L. E. BRUS, "The Quantum Mechanics Of Larger Semiconductor Clusters ("Quantum Dots")", *Ann. Rev. Phys. Chem.*, 1990, **41**, 477–496, DOI: 10.1146/annurev.physchem.41.1.477.
- (35) Q. A. AKKERMAN, "Lead Halide Perovskite Nanocrystals - A New Age of Semiconductive Nanocrystals", *University of Genoa*, 2018.
- (36) M. L. STEIGERWALD and L. E. BRUS, "Semiconductor Crystallites: A Class of Large Molecules", *Acc. Chem. Res.*, 1990, **23**, 183–188, DOI: 10.1021/ar00174a003.
- (37) A. L. EFROS and A. L. EFROS, "Interband Absorption of Light in a Semiconductor Sphere", *Sov. Phys.: Semiconduct.*, 1982, **16**, 772–775.
- (38) A. EKIMOV, A. ONUSHCHENKO and A. ÉFROS, "Quantization of the energy spectrum of holes in the adiabatic potential of the electron", *J. Exp. Theor. Phys.*, 1986, **43**, 376.
- (39) Y. WANG and N. HERRON, "Nanometer-sized semiconductor clusters: Materials synthesis, quantum size effects, and photophysical properties", *J. Phys. Chem.*, 1991, **95**, 525–532, DOI: 10.1021/j100155a009.

- 
- (40) L. E. BRUS, "Electron-electron and electron-hole interactions in small semiconductor crystallites: The size dependence of the lowest excited electronic state", *J. Chem. Phys.*, 1984, **80**, 4403–4409, DOI: 10.1063/1.447218.
- (41) F. LÜBKEMANN, "Semiconductor Nanoheteroparticles and Superstructures Thereof – Synthesis, Modification and Patterning via Inkjet Printing", *Leibniz Universität Hannover*, 2020.
- (42) D. V. TALAPIN, A. L. ROGACH, A. KORNOWSKI, M. HAASE and H. WELLER, "Highly Luminescent Monodisperse CdSe and CdSe/ZnS Nanocrystals Synthesized in a Hexadecylamine-Trioctylphosphine Oxide-Trioctylphosphine Mixture", *Nano Lett.*, 2001, **1**, 207–211, DOI: 10.1021/nl10155126.
- (43) B. O. DABBOUSI, J. RODRIGUEZ-VIEJO, F. V. MIKULEC, J. R. HEINE, H. MATTOUSSI, R. OBER, K. F. JENSEN and M. G. BAWENDI, "(CdSe)ZnS core-shell quantum dots: Synthesis and characterization of a size series of highly luminescent nanocrystallites", *J. Phys. Chem. B*, 1997, **101**, 9463–9475, DOI: 10.1021/jp971091y.
- (44) L. LI and P. REISS, "One-pot synthesis of highly luminescent InP/ZnS nanocrystals without precursor injection", *J. Am. Chem. Soc.*, 2008, **130**, 11588–11589, DOI: 10.1021/ja803687e.
- (45) S. HAUBOLD, M. HAASE, A. KORNOWSKI and H. WELLER, "Strongly Luminescent InP/ZnS Core-Shell Nanoparticles", *ChemPhysChem*, 2001, **2**, 331–334, DOI: 10.1002/1439-7641(20010518)2:5<331::AID-CPHC331>3.0.CO;2-0.
- (46) D. DORFS, A. SALANT, I. POPOV and U. BANIN, "ZnSe quantum dots within CdS nanorods: A seeded-growth type-II system", *Small*, 2008, **4**, 1319–1323, DOI: 10.1002/smll.200800084.
- (47) S. A. IVANOV, A. PIRYATINSKI, J. NANDA, S. TRETIAK, K. R. ZAVADIL, W. O. WALLACE, D. WERDER and V. I. KLIMOV, "Type-II core/shell CdS/ZnSe nanocrystals: Synthesis, electronic structures, and spectroscopic properties", *J. Am. Chem. Soc.*, 2007, **129**, 11708–11719, DOI: 10.1021/ja068351m.

- (48) V. I. KLIMOV, S. A. IVANOV, J. NANDA, M. ACHERMANN, I. BEZEL, J. A. MCGUIRE and A. PIRYATINSKI, "Single-exciton optical gain in semiconductor nanocrystals", *Nature*, 2007, **447**, 441–446, DOI: 10.1038/nature05839.
- (49) S. KUMAR, M. JONES, S. S. LO and G. D. SCHOLES, "Nanorod heterostructures showing photoinduced charge separation", *Small*, 2007, **3**, 1633–1639, DOI: 10.1002/smll.200700155.
- (50) D. ORON, M. KAZES and U. BANIN, "Multiexcitons in type-II colloidal semiconductor quantum dots", *Phys. Rev. B Condens. Matter Mater. Phys.*, 2007, **75**, 1–7, DOI: 10.1103/PhysRevB.75.035330.
- (51) S. KIM, B. FISHER, H. J. EISLER and M. BAWENDI, "Type-II quantum dots: CdTe/CdSe(core/shell) and CdSe/ZnTe(core/shell) heterostructures", *J. Am. Chem. Soc.*, 2003, **125**, 11466–11467, DOI: 10.1021/ja0361749.
- (52) Z. PAN, H. ZHANG, K. CHENG, Y. HOU, J. HUA and X. ZHONG, "Highly efficient inverted type-I CdS/CdSe core/shell structure QD-sensitized solar cells", *ACS Nano*, 2012, **6**, 3982–3991, DOI: 10.1021/nn300278z.
- (53) X. ZHONG, R. XIE, Y. ZHANG, T. BASCHÉ and W. KNOLL, "High-quality violet- To red-emitting ZnSe/CdSe core/shell nanocrystals", *Chem. Mater.*, 2005, **17**, 4038–4042, DOI: 10.1021/cm050948y.
- (54) D. BATTAGLIA, J. J. LI, Y. WANG and X. PENG, "Colloidal Two-Dimensional Systems: CdSe Quantum Shells and Wells", *Angew. Chem. Int. Ed.*, 2003, **42**, 5035–5039, DOI: 10.1002/anie.200352120.
- (55) A. MEWS, A. EYCHMUELLER, M. GIERSIG, D. SCHOOSS and H. WELLER, "Preparation, characterization, and photophysics of the quantum dot quantum well system cadmium sulfide/mercury sulfide/cadmium sulfide", *J. Phys. Chem.*, 1994, **98**, 934–941, DOI: 10.1021/j100054a032.
- (56) M. C. SCHLAMP, X. PENG and A. P. ALIVISATOS, "Improved efficiencies in light emitting diodes made with CdSe(CdS) core/shell type nanocrystals and a semiconducting polymer", *J. Appl. Phys.*, 1997, **82**, 5837–5842, DOI: 10.1063/1.366452.

- 
- (57) O. CHEN, J. ZHAO, V. P. CHAUHAN, J. CUI, C. WONG, D. K. HARRIS, H. WEI, H. S. HAN, D. FUKUMURA, R. K. JAIN and M. G. BAWENDI, "Compact high-quality CdSe-CdS core-shell nanocrystals with narrow emission linewidths and suppressed blinking", *Nat. Mater.*, 2013, **12**, 445–451, DOI: 10.1038/nmat3539.
- (58) D. V. TALAPIN, J. H. NELSON, E. V. SHEVCHENKO, S. ALONI, B. SADTLER and A. P. ALIVISATOS, "Seeded Growth of Highly Luminescent CdSe/CdS Nanoheterostructures with Rod and Tetrapod Morphologies", *Nano Lett.*, 2007, **7**, 2951–2959, DOI: 10.1021/n1072003g.
- (59) B. N. PAL, Y. GHOSH, S. BROVELLI, R. LAOCHAROENSUK, V. I. KLIMOV, J. A. HOLLINGSWORTH and H. HTOON, "'Giant' CdSe/CdS core/shell nanocrystal quantum dots as efficient electroluminescent materials: Strong influence of shell thickness on light-emitting diode performance", *Nano Lett.*, 2012, **12**, 331–336, DOI: 10.1021/n1203620f.
- (60) X. PENG, M. C. SCHLAMP, A. V. KADAVANICH and A. P. ALIVISATOS, "Epitaxial growth of highly luminescent CdSe/CdS core/shell nanocrystals with photostability and electronic accessibility", *J. Am. Chem. Soc.*, 1997, **119**, 7019–7029, DOI: 10.1021/ja970754m.
- (61) D. V. TALAPIN, R. KOEPPE, S. GÖTZINGER, A. KORNOWSKI, J. M. LUPTON, A. L. ROGACH, O. BENSON, J. FELDMANN and H. WELLER, "Highly Emissive Colloidal CdSe/CdS Heterostructures of Mixed Dimensionality", *Nano Lett.*, 2003, **3**, 1677–1681, DOI: 10.1021/n1034815s.
- (62) Y. NANDAN and M. S. MEHATA, "Wavefunction Engineering of Type-I/Type-II Excitons of CdSe/CdS Core-Shell Quantum Dots", *Sci. Rep.*, 2019, **9**, 1–11, DOI: 10.1038/s41598-018-37676-3.
- (63) H. ESHET, M. GRÜNWARD and E. RABANI, "The electronic structure of CdSe/CdS Core/shell seeded nanorods: Type-I or quasi-type-II?", *Nano Lett.*, 2013, **13**, 5880–5885, DOI: 10.1021/n1402722n.
- (64) S. VEZZOLI, M. MANCEAU, G. LEMÉNAGER, Q. GLORIEUX, E. GIACOBINO, L. CARBONE, M. DE VITTORIO and A. BRAMATI, "Exciton Fine Structure of CdSe/CdS Nanocrystals Determined by Polarization Microscopy at Room Temperature", *ACS Nano*, 2015, **9**, 7992–8003, DOI: 10.1021/acsnano.5b01354.

- (65) A. SIFT, F. DELLA SALA, G. MENAGEN and U. BANIN, "Multiexciton engineering in seeded core/shell nanorods: Transfer from type-I to quasi-type-II regimes", *Nano Lett.*, 2009, **9**, 3470–3476, DOI: 10.1021/nl901679q.
- (66) L. T. KUNNEMAN, M. ZANELLA, L. MANNA, L. D. SIEBBELES and J. M. SCHINS, "Mobility and spatial distribution of photoexcited electrons in CdSe/CdS nanorods", *J. Phys. Chem. C*, 2013, **117**, 3146–3151, DOI: 10.1021/jp3117984.
- (67) S. A. MAIER, *Plasmonics: Fundamentals and Applications*, Springer US, New York, NY, 2007, DOI: 10.1007/0-387-37825-1.
- (68) G. MIE, "Beiträge zur Optik trüber Medien, speziell kolloidaler Metallösungen", *Ann. Phys.*, 1908, **330**, 377–445, DOI: 10.1002/andp.19083300302.
- (69) U. KREIBIG and M. VOLLMER, *Optical Properties of Metal Clusters*, Springer Berlin Heidelberg, Berlin, Heidelberg, 1995, vol. 25, DOI: 10.1007/978-3-662-09109-8.
- (70) J. PARK, J. JOO, G. K. SOON, Y. JANG and T. HYEON, "Synthesis of monodisperse spherical nanocrystals", *Angew. Chem. Int. Ed.*, 2007, **46**, 4630–4660, DOI: 10.1002/anie.200603148.
- (71) V. K. LAMER and R. H. DINEGAR, "Theory, Production and Mechanism of Formation of Monodispersed Hydrosols", *J. Am. Chem. Soc.*, 1950, **72**, 4847–4854, DOI: 10.1021/ja01167a001.
- (72) M. FARADAY, "Experimental Relations of Gold (and other Metals) to Light.", *Phil. Trans. R. Soc.*, 1857, **147**, 145–181, DOI: 10.1098/rstl.1857.0011.
- (73) D. J. BARBER and I. C. FREESTONE, "An Investigation of the Origin of the Colour of the Lycurus Cup by Analytical Transmission Electron Microscopy", *Archaeometry*, 1990, **32**, 33–45, DOI: 10.1111/j.1475-4754.1990.tb01079.x.
- (74) P. P. EDWARDS and J. M. THOMAS, "Gold in a metallic divided state - From Faraday to present-day nanoscience", *Angew. Chem. Int. Ed.*, 2007, **46**, 5480–5486, DOI: 10.1002/anie.200700428.

- 
- (75) J. TURKEVICH, P. C. STEVENSON and J. HILLIER, "A study of the nucleation and growth processes in the synthesis of colloidal gold", *Faraday Discuss.*, 1951, **11**, 55–75, DOI: 10.1039/DF9511100055.
- (76) W. STÖBER, A. FINK and E. BOHN, "Controlled growth of monodisperse silica spheres in the micron size range", *J. Colloid Interface Sci.*, 1968, **26**, 62–69, DOI: 10.1016/0021-9797(68)90272-5.
- (77) A. R. TAO, S. HABAS and P. YANG, "Shape control of colloidal metal nanocrystals", *Small*, 2008, **4**, 310–325, DOI: 10.1002/smll.200701295.
- (78) T. K. SAU and A. L. ROGACH, "Nonspherical noble metal nanoparticles: Colloid-chemical synthesis and morphology control", *Adv. Mater.*, 2010, **22**, 1781–1804, DOI: 10.1002/adma.200901271.
- (79) M. NIEDERBERGER and G. GARNWEITNER, "Organic reaction pathways in the nonaqueous synthesis of metal oxide nanoparticles", *Chem. Eur. J.*, 2006, **12**, 7282–7302, DOI: 10.1002/chem.200600313.
- (80) J. P. RAO and K. E. GECKELER, "Polymer nanoparticles: Preparation techniques and size-control parameters", *Prog. Polym. Sci.*, 2011, **36**, 887–913, DOI: 10.1016/j.progpolymsci.2011.01.001.
- (81) A. L. ROGACH, T. FRANZL, T. A. KLAR, J. FELDMANN, N. GAPONIK, V. LESNYAK, A. SHAVEL, A. EYCHMÜLLER, Y. P. RAKOVICH and J. F. DONEGAN, "Aqueous synthesis of thiol-capped CdTe nanocrystals: State-of-the-art", *J. Phys. Chem. C*, 2007, **111**, 14628–14637, DOI: 10.1021/jp072463y.
- (82) Z. A. PENG and X. PENG, "Formation of high-quality CdTe, CdSe, and CdS nanocrystals using CdO as precursor", *J. Am. Chem. Soc.*, 2001, **123**, 183–184, DOI: 10.1021/ja003633m.
- (83) B. PAN, R. HE, F. GAO, D. CUI and Y. ZHANG, "Study on growth kinetics of CdSe nanocrystals in oleic acid/dodecylamine", *J. Cryst. Growth*, 2006, **286**, 318–323, DOI: 10.1016/j.jcrysgro.2005.10.003.

- (84) L. QU, Z. A. PENG and X. PENG, "Alternative Routes toward High Quality CdSe Nanocrystals", *Nano Lett.*, 2001, **1**, 333–337, DOI: 10.1021/n10155532.
- (85) W. W. YU, Y. A. WANG and X. PENG, "Formation and Stability of Size-, Shape-, and Structure-Controlled CdTe Nanocrystals: Ligand Effects on Monomers and Nanocrystals", *Chem. Mater.*, 2003, **15**, 4300–4308, DOI: 10.1021/cm034729t.
- (86) Z. A. PENG and X. PENG, "Mechanisms of the shape evolution of CdSe nanocrystals", *J. Am. Chem. Soc.*, 2001, **123**, 1389–1395, DOI: 10.1021/ja0027766.
- (87) L. MANNA, E. C. SCHER and A. P. ALIVISATOS, "Synthesis of soluble and processable rod-, arrow-, teardrop-, and tetrapod-shaped CdSe nanocrystals", *J. Am. Chem. Soc.*, 2000, **122**, 12700–12706, DOI: 10.1021/ja003055+.
- (88) D. V. TALAPIN, S. HAUBOLD, A. L. ROGACH, A. KORNOWSKI, M. HAASE and H. WELLER, "A novel organometallic synthesis of highly luminescent CdTe nanocrystals", *J. Phys. Chem. B*, 2001, **105**, 2260–2263, DOI: 10.1021/jp003177o.
- (89) N. KUMBHOJKAR, V. V. NIKESH, A. KSHIRSAGAR and S. MAHAMUNI, "Photophysical properties of ZnS nanoclusters", *J. Appl. Phys.*, 2000, **88**, 6260–6264, DOI: 10.1063/1.1321027.
- (90) M. A. HINES and P. GUYOT-SIONNEST, "Bright UV-blue luminescent colloidal ZnSe nanocrystals", *J. Phys. Chem. B*, 1998, **102**, 19–21, DOI: 10.1021/jp9810217.
- (91) A. ROGACH, S. KERSHAW, M. BURT, M. HARRISON, A. KORNOWSKI, A. EYCHMÜLLER and H. WELLER, "Colloidally prepared HgTe nanocrystals with strong room-temperature infrared luminescence", *Adv. Mater.*, 1999, **11**, 552–555, DOI: 10.1002/(SICI)1521-4095(199905)11:7<552::AID-ADMA552>3.0.CO;2-Q.
- (92) B. L. WEHRENBURG, C. WANG and P. GUYOT-SIONNEST, "Interband and intraband optical studies of PbSe colloidal quantum dots", *J. Phys. Chem. B*, 2002, **106**, 10634–10640, DOI: 10.1021/jp021187e.
- (93) I. MOREELS, Y. JUSTO, B. DE GEYTER, K. HAUSTRAETE, J. C. MARTINS and Z. HENS, "Size-tunable, bright, and stable PbS quantum dots: A surface chemistry study", *ACS Nano*, 2011, **5**, 2004–2012, DOI: 10.1021/nn103050w.

- 
- (94) L. CADEMARTIRI, J. BERTOLOTTI, R. SAPIENZA, D. S. WIERSMA, G. VON FREYMANN and G. A. OZIN, "Multigram scale, solventless, and diffusion-controlled route to highly monodisperse PbS nanocrystals", *J. Phys. Chem. B*, 2006, **110**, 671–673, DOI: 10.1021/jp0563585.
- (95) M. A. HINES and G. D. SCHOLES, "Colloidal PbS Nanocrystals with Size-Tunable Near-Infrared Emission: Observation of Post-Synthesis Self-Narrowing of the Particle Size Distribution", *Adv. Mater.*, 2003, **15**, 1844–1849, DOI: 10.1002/adma.200305395.
- (96) O. I. MIĆIĆ, C. J. CURTIS, K. M. JONES, J. R. SPRAGUE and A. J. NOZIK, "Synthesis and characterization of InP quantum dots", *J. Phys. Chem.*, 1994, **98**, 4966–4969, DOI: 10.1021/j100070a004.
- (97) M. A. OLSHAVSKY, A. N. GOLDSTEIN and A. P. ALIVISATOS, "Organometallic Synthesis of GaAs Crystallites Exhibiting Quantum Confinement", *J. Am. Chem. Soc.*, 1990, **112**, 9438–9439, DOI: 10.1021/ja00181a080.
- (98) H. UCHIDA, C. J. CURTIS, P. V. KAMAT, K. M. JONES and A. J. NOZIK, "Optical properties of gallium arsenide nanocrystals", *J. Phys. Chem.*, 1992, **96**, 1156–1160, DOI: 10.1021/j100182a026.
- (99) O. I. MIĆIĆ, S. P. AHRENKIEL, D. BERTRAM and A. J. NOZIK, "Synthesis, structure, and optical properties of colloidal GaN quantum dots", *Appl. Phys. Lett.*, 1999, **75**, 478–480, DOI: 10.1063/1.124414.
- (100) F. MONTANARELLA and M. V. KOVALENKO, "Three Millennia of Nanocrystals", *ACS Nano*, 2022, DOI: 10.1021/acsnano.1c11159.
- (101) P. REISS, M. PROTIERE and L. LI, "Core/shell semiconductor nanocrystals", *Small*, 2009, **5**, 154–168, DOI: 10.1002/smll.200800841.
- (102) L. CARBONE and P. D. COZZOLI, "Colloidal heterostructured nanocrystals: Synthesis and growth mechanisms", *Nano Today*, 2010, **5**, 449–493, DOI: 10.1016/j.nantod.2010.08.006.
- (103) I. SCHICK, S. LORENZ, D. GEHRIG, S. TENZER, W. STORCK, K. FISCHER, D. STRAND, F. LAQUAI and W. TREMEL, "Inorganic Janus particles for biomedical applications", *Beilstein J. Nanotechnol.*, 2014, **5**, 2346–2362, DOI: 10.3762/bjnano.5.244.

- (104) D. V. TALAPIN, I. MEKIS, S. GÖTZINGER, A. KORNOWSKI, O. BENSON and H. WELLER, “CdSe/CdS/ZnS and CdSe/ZnSe/ZnS core-shell-shell nanocrystals”, *J. Phys. Chem. B*, 2004, **108**, 18826–18831, DOI: 10.1021/jp046481g.
- (105) A. L. ROGACH, D. NAGESHA, J. W. OSTRANDER, M. GIERSIG and N. A. KOTOV, “Raisin bun’-type composite spheres of silica and semiconductor nanocrystals”, *Chem. Mater.*, 2000, **12**, 2676–2685, DOI: 10.1021/cm000244i.
- (106) J. J. LI, Y. A. WANG, W. GUO, J. C. KEAY, T. D. MISHIMA, M. B. JOHNSON and X. PENG, “Large-scale synthesis of nearly monodisperse CdSe/CdS core/shell nanocrystals using air-stable reagents via successive ion layer adsorption and reaction”, *J. Am. Chem. Soc.*, 2003, **125**, 12567–12575, DOI: 10.1021/ja0363563.
- (107) S. ITHURRIA and D. V. TALAPIN, “Colloidal Atomic Layer Deposition (c-ALD) using self-limiting reactions at nanocrystal surface coupled to phase transfer between polar and nonpolar media”, *J. Am. Chem. Soc.*, 2012, **134**, 18585–18590, DOI: 10.1021/ja308088d.
- (108) S. DEKA, A. QUARTA, M. G. LUPO, A. FALQUI, S. BONINELLI, C. GIANNINI, G. MORELLO, M. DE GIORGI, G. LANZANI, C. SPINELLA, R. CINGOLANI, T. PELLEGRINO and L. MANNA, “CdSe/CdS/ZnS double shell nanorods with high photoluminescence efficiency and their exploitation as biolabeling probes”, *J. Am. Chem. Soc.*, 2009, **131**, 2948–2958, DOI: 10.1021/ja808369e.
- (109) L. CARBONE, C. NOBILE, M. DE GIORGI, F. DELLA SALA, G. MORELLO, P. POMPA, M. HYTCH, E. SNOECK, A. FIORE, I. R. FRANCHINI, M. NADASAN, A. F. SILVESTRE, L. CHIODO, S. KUDERA, R. CINGOLANI, R. KRAHNE and L. MANNA, “Synthesis and micrometer-scale assembly of colloidal CdSe/CdS nanorods prepared by a seeded growth approach”, *Nano Lett.*, 2007, **7**, 2942–2950, DOI: 10.1021/nl0717661.
- (110) M. R. KIM, K. MISZTA, M. POVIA, R. BRESCIA, S. CHRISTODOULOU, M. PRATO, S. MARRAS and L. MANNA, “Influence of chloride ions on the synthesis of colloidal branched CdSe/CdS nanocrystals by seeded growth”, *ACS Nano*, 2012, **6**, 11088–11096, DOI: 10.1021/nn3048846.

- 
- (111) S. DEKA, K. MISZTA, D. DORFS, A. GENOVESE, G. BERTONI and L. MANNA, "Octapod-shaped colloidal nanocrystals of cadmium chalcogenides via "one-Pot" cation exchange and seeded growth", *Nano Lett.*, 2010, **10**, 3770–3776, DOI: 10.1021/nl102539a.
- (112) L. MANNA, D. J. MILLIRON, A. MEISEL, E. C. SCHER and A. P. ALIVISATOS, "Controlled growth of tetrapod-branched inorganic nanocrystals", *Nat. Mater.*, 2003, **2**, 382–385, DOI: 10.1038/nmat902.
- (113) J. GAO, B. ZHANG, Y. GAO, Y. PAN, X. ZHANG and B. XU, "Fluorescent magnetic nanocrystals by sequential addition of reagents in a one-pot reaction: A simple preparation for multifunctional nanostructures", *J. Am. Chem. Soc.*, 2007, **129**, 11928–11935, DOI: 10.1021/ja0731017.
- (114) J. ZHANG, Y. TANG, K. LEE and M. OUYANG, "Nonepitaxial Growth of Hybrid Core-Shell Nanostructures with Large Lattice Mismatches", *Science*, 2010, **327**, 1634–1638, DOI: 10.1126/science.1184769.
- (115) H. KIM, M. ACHERMANN, L. P. BALET, J. A. HOLLINGSWORTH and V. I. KLIMOV, "Synthesis and characterization of Co/CdSe core/shell nanocomposites: Bifunctional magnetic-optical nanocrystals", *J. Am. Chem. Soc.*, 2005, **127**, 544–546, DOI: 10.1021/ja047107x.
- (116) S. NASKAR, F. LÜBKEMANN, S. HAMID, A. FREYTAG, A. WOLF, J. KOCH, I. IVANOVA, H. PFNÜR, D. DORFS, D. W. BAHNEMANN and N. C. BIGALL, "Synthesis of Ternary and Quaternary Au and Pt Decorated CdSe/CdS Heteronanoplatelets with Controllable Morphology", *Adv. Funct. Mater.*, 2017, **27**, 1–11, DOI: 10.1002/adfm.201604685.
- (117) W. CHEN, X. LI, F. WANG, S. JAVAID, Y. PANG, J. CHEN, Z. YIN, S. WANG, Y. LI and G. JIA, "Nonepitaxial Gold-Tipped ZnSe Hybrid Nanorods for Efficient Photocatalytic Hydrogen Production", *Small*, 2020, **16**, 1–10, DOI: 10.1002/smll.201902231.
- (118) G. MENAGEN, J. E. MACDONALD, Y. SHEMESH, I. POPOV and U. BANIN, "Au growth on semiconductor nanorods: Photoinduced versus thermal growth mechanisms", *J. Am. Chem. Soc.*, 2009, **131**, 17406–17411, DOI: 10.1021/ja9077733.

- (119) C. O'SULLIVAN, S. AHMED and K. M. RYAN, "Gold tip formation on perpendicularly aligned semiconductor nanorod assemblies", *J. Mater. Chem.*, 2008, **18**, 5218–5222, DOI: 10.1039/b810543j.
- (120) Y. KHALAVKA and C. SÖNNICHSEN, "Growth of gold tips onto hyperbranched CdTe nanostructures", *Adv. Mater.*, 2008, **20**, 588–591, DOI: 10.1002/adma.200701518.
- (121) A. E. SAUNDERS, I. POPOV and U. BANIN, "Synthesis of hybrid CdS-Au colloidal nanostructures", *J. Phys. Chem. B*, 2006, **110**, 25421–25429, DOI: 10.1021/jp065594s.
- (122) T. MOKARI, E. ROTHENBERG, I. POPOV and R. COSTI, "Selective Growth of Metal Tips onto Semiconductor Quantum Rods and Tetrapods", *Science*, 2004, **304**, 1787–1790, DOI: DOI:10.1126/science.1097830.
- (123) J. MAYNADIÉ, A. SALANT, A. FALQUI, M. RESPAUD, E. SHAVIV, U. BANIN, K. SOULANTICA and B. CHAUDRET, "Cobalt growth on the tips of CdSe nanorods", *Angew. Chem. - Int. Ed.*, 2009, **48**, 1814–1817, DOI: 10.1002/anie.200804798.
- (124) A. GUERRERO-MARTÍNEZ, J. PÉREZ-JUSTE and L. M. LIZ-MARZÁN, "Recent progress on silica coating of nanoparticles and related nanomaterials", *Adv. Mater.*, 2010, **22**, 1182–1195, DOI: 10.1002/adma.200901263.
- (125) I. PASTORIZA-SANTOS, J. PÉREZ-JUSTE and L. M. LIZ-MARZÁN, "Silica-coating and hydrophobation of CTAB-stabilized gold nanorods", *Chem. Mater.*, 2006, **18**, 2465–2467, DOI: 10.1021/cm060293g.
- (126) N. ERATHODIYIL and J. Y. YING, "Functionalization of inorganic nanoparticles for bioimaging applications", *Acc. Chem. Res.*, 2011, **44**, 925–935, DOI: 10.1021/ar2000327.
- (127) M. LIONG, J. LU, M. KOVOCHICH, T. XIA, S. G. RUEHM, A. E. NEL, F. TAMANOI and J. I. ZINK, "Multifunctional inorganic nanoparticles for imaging, targeting, and drug delivery", *ACS Nano*, 2008, **2**, 889–896, DOI: 10.1021/nn800072t.
- (128) H. S. DONG, S. M. HUGHES, Y. YIN and A. P. ALIVISATOS, "Cation exchange reactions in ionic nanocrystals", *Science*, 2004, **306**, 1009–1012, DOI: 10.1126/science.1103755.

- 
- (129) H. LI, M. ZANELLA, A. GENOVESE, M. POVIA, A. FALQUI, C. GIANNINI and L. MANNA, “Sequential cation exchange in nanocrystals: Preservation of crystal phase and formation of metastable phases”, *Nano Lett.*, 2011, **11**, 4964–4970, DOI: 10.1021/nl202927a.
- (130) L. DE TRIZIO and L. MANNA, “Forging colloidal nanostructures via cation exchange reactions”, *Chem. Rev.*, 2016, **116**, 10852–10887, DOI: 10.1021/acs.chemrev.5b00739.
- (131) J. B. RIVEST and P. K. JAIN, “Cation exchange on the nanoscale: An emerging technique for new material synthesis, device fabrication, and chemical sensing”, *Chem. Soc. Rev.*, 2013, **42**, 89–96, DOI: 10.1039/c2cs35241a.
- (132) K. MISZTA, D. DORFS, A. GENOVESE, M. R. KIM and L. MANNA, “Cation Exchange Reactions in Colloidal Branched Nanocrystals”, *ACS Nano*, 2011, **5**, 7176–7183, DOI: 10.1021/nn201988w.
- (133) P. ADEL, A. WOLF, T. KODANEK and D. DORFS, “Segmented CdSe@CdS/ZnS Nanorods Synthesized via a Partial Ion Exchange Sequence”, *Chem. Mater.*, 2014, **26**, 3121–3127, DOI: 10.1021/cm500431m.
- (134) F. MATTER, A. L. LUNA and M. NIEDERBERGER, “From colloidal dispersions to aerogels: How to master nanoparticle gelation”, *Nano Today*, 2020, **30**, 100827, DOI: 10.1016/j.nantod.2019.100827.
- (135) P. RUSCH, D. ZÁMBÓ and N. C. BIGALL, “Control over Structure and Properties in Nanocrystal Aerogels at the Nano-, Micro-, and Macroscale”, *Acc. Chem. Res.*, 2020, **53**, 2414–2424, DOI: 10.1021/acs.accounts.0c00463.
- (136) H. HAMAKER, “The London—van der Waals attraction between spherical particles”, *Physica*, 1937, **4**, 1058–1072, DOI: 10.1016/S0031-8914(37)80203-7.
- (137) A. BISSON, A. RIGACCI, D. LECOMTE, E. RODIER and P. ACHARD, “Drying of Silica Gels to Obtain Aerogels: Phenomenology and Basic Techniques”, *Dry. Technol.*, 2003, **21**, 593–628, DOI: 10.1081/drt-120019055.
- (138) S. S. KISTLER, “Coherent Expanded Aerogels and Jellies”, *Nature*, 1931, **127**, 741–741, DOI: 10.1038/127741a0.

- (139) P. H. TEWARI, A. J. HUNT and K. D. LOFFTUS, “Ambient-temperature supercritical drying of transparent silica aerogels”, *Mater. Lett.*, 1985, **3**, 363–367, DOI: 10.1016/0167-577X(85)90077-1.
- (140) G. W. SCHERER, “Freezing gels”, *J. Non-Cryst. Solids*, 1993, **155**, 1–25, DOI: 10.1016/0022-3093(93)90467-C.
- (141) A. FREYTAG, S. SÁNCHEZ-PARADINAS, S. NASKAR, N. WENDT, M. COLOMBO, G. PUGLIESE, J. POPPE, C. DEMIRCI, I. KRETSCHMER, D. W. BAHNEMANN, P. BEHRENS and N. C. BIGALL, “Versatile Aerogel Fabrication by Freezing and Subsequent Freeze-Drying of Colloidal Nanoparticle Solutions”, *Angew. Chem. Int. Ed.*, 2016, **55**, 1200–1203, DOI: 10.1002/anie.201508972.
- (142) A. SCHLOSSER, L. C. MEYER, F. LÜBKEMANN, J. F. MIETHE and N. C. BIGALL, “Nanoplatelet cryoaerogels with potential application in photoelectrochemical sensing”, *Phys. Chem. Chem. Phys.*, 2019, **21**, 9002–9012, DOI: 10.1039/C9CP00281B.
- (143) S. S. PRAKASH, C. J. SANKARAN, A. J. HURD and S. M. RAO, “Silica aerogel films prepared at ambient pressure by using surface derivatization to induce reversible drying shrinkage”, *Nature*, 1995, **374**, 439–443, DOI: 10.1038/374439a0.
- (144) V. D. LAND, T. M. HARRIS and D. C. TEETERS, “Processing of low-density silica gel by critical point drying or ambient pressure drying”, *J. Non-Cryst. Solids*, 2001, **283**, 11–17, DOI: 10.1016/S0022-3093(01)00485-9.
- (145) N. LEVENTIS, A. PALCZER, L. MCCORKLE, G. ZHANG and C. SOTIRIOU-LEVENTIS, “Nanoengineered silica-polymer composite aerogels with No need for supercritical fluid drying”, *J. Sol-Gel Sci. Technol.*, 2005, **35**, 99–105, DOI: 10.1007/s10971-005-1372-7.
- (146) S. D. BHAGAT, C. S. OH, Y. H. KIM, Y. S. AHN and J. G. YEO, “Methyltrimethoxysilane based monolithic silica aerogels via ambient pressure drying”, *Microporous Mesoporous Mater.*, 2007, **100**, 350–355, DOI: 10.1016/j.micromeso.2006.10.026.
- (147) N. LEVENTIS, “Three-Dimensional Core-Shell Superstructures: Mechanically Strong Aerogels”, *Acc. Chem. Res.*, 2007, **40**, 874–884, DOI: 10.1021/ar600033s.

- 
- (148) T. GACOIN, L. MALIER and J. P. BOILOT, “New Transparent Chalcogenide Materials Using a Sol-Gel Process”, *Chem. Mater.*, 1997, **9**, 1502–1504, DOI: 10.1021/cm970103p.
- (149) T. GACOIN, K. LAHLIL, P. LARREGARAY and J. P. BOILOT, “Transformation of CdS colloids: Sols, gels, and precipitates”, *J. Phys. Chem. B*, 2001, **105**, 10228–10235, DOI: 10.1021/jp0117381.
- (150) J. L. MOHANAN and S. L. BROCK, “A new addition to the aerogel community: Unsupported CdS aerogels with tunable optical properties”, *J. Non-Crystal. Solids*, 2004, **350**, 1–8, DOI: 10.1016/j.jnoncrysol.2004.05.020.
- (151) J. L. MOHANAN, I. U. ARACHCHIGE and S. L. BROCK, “Porous semiconductor chalcogenide aerogels.”, *Science*, 2005, **307**, 397–400, DOI: 10.1126/science.1106525.
- (152) I. U. ARACHCHIGE, J. L. MOHANAN and S. L. BROCK, “Sol-gel processing of semiconducting metal chalcogenide xerogels: Influence of dimensionality on quantum confinement effects in a nanoparticle network”, *Chem. Mater.*, 2005, **17**, 6644–6650, DOI: 10.1021/cm0518325.
- (153) N. GAPONIK, A. WOLF, R. MARX, V. LESNYAK, K. SCHILLING and A. EYCHMÜLLER, “Three-Dimensional Self-Assembly of Thiol-Capped CdTe Nanocrystals: Gels and Aerogels as Building Blocks for Nanotechnology”, *Adv. Mater.*, 2008, **20**, 4257–4262, DOI: 10.1002/adma.200702986.
- (154) A. HITIHAMI-MUDIYANSELAGE, K. SENEVIRATHNE and S. L. BROCK, “Bottom-up assembly of Ni<sub>2</sub>P nanoparticles into three-dimensional architectures: An alternative mechanism for phosphide gelation”, *Chem. Mater.*, 2014, **26**, 6251–6256, DOI: 10.1021/cm5030958.
- (155) A. HITIHAMI-MUDIYANSELAGE, K. SENEVIRATHNE and S. L. BROCK, “Assembly of Phosphide Nanocrystals into Porous Networks: Formation of InP Gels and Aerogels”, *ACS Nano*, 2013, **7**, 1163–1170, DOI: 10.1021/nn305959q.
- (156) N. BIGALL, A.-K. HERRMANN, M. VOGEL, M. ROSE, P. SIMON, W. CARRILLO-CABRERA, D. DORFS, S. KASKEL, N. GAPONIK and A. EYCHMÜLLER, “Hydrogels and Aerogels from Noble Metal Nanoparticles”, *Angew. Chem. Int. Ed.*, 2009, **48**, 9731–9734, DOI: 10.1002/anie.200902543.

- (157) T. BERESTOK, P. GUARDIA, R. DU, J. B. PORTALS, M. COLOMBO, S. ESTRADÉ, F. PEIRÓ, S. L. BROCK and A. CABOT, “Metal Oxide Aerogels with Controlled Crystallinity and Faceting from the Epoxide-Driven Cross-Linking of Colloidal Nanocrystals”, *ACS Appl. Mater. Interfaces*, 2018, **10**, 16041–16048, DOI: 10.1021/acsami.8b03754.
- (158) D. ZÁMBÓ, A. SCHLOSSER, P. RUSCH, F. LÜBKEMANN, J. KOCH, H. PFNÜR and N. C. BIGALL, “A Versatile Route to Assemble Semiconductor Nanoparticles into Functional Aerogels by Means of Trivalent Cations”, *Small*, 2020, 1906934, DOI: 10.1002/smll.201906934.
- (159) V. LESNYAK, S. V. VOITEKHOVICH, P. N. GAPONIK, N. GAPONIK and A. EYCHMÜLLER, “CdTe Nanocrystals Capped with a Tetrazolyl Analogue of Thioglycolic Acid: Aqueous Synthesis, Characterization, and Metal-Assisted Assembly”, *ACS Nano*, 2010, **4**, 4090–4096, DOI: 10.1021/nn100563c.
- (160) A. WOLF, V. LESNYAK, N. GAPONIK and A. EYCHMÜLLER, “Quantum-dot-based (Aero)gels: Control of the optical properties”, *J. Phys. Chem. Lett.*, 2012, **3**, 2188–2193, DOI: 10.1021/jz300726n.
- (161) M. V. KOVALENKO, M. SCHEELE and D. V. TALAPIN, “Colloidal Nanocrystals with Molecular Metal Chalcogenide Surface Ligands”, *Science*, 2009, **324**, 1417–1420, DOI: 10.1126/science.1170524.
- (162) V. SAYEVICH, B. CAI, A. BENAD, D. HAUBOLD, L. SONNTAG, N. GAPONIK, V. LESNYAK and A. EYCHMÜLLER, “3D Assembly of All-Inorganic Colloidal Nanocrystals into Gels and Aerogels”, *Angew. Chem. Int. Ed.*, 2016, **55**, 6334–6338, DOI: 10.1002/anie.201600094.
- (163) A. SINGH, B. A. LINDQUIST, G. K. ONG, R. B. JADRIK, A. SINGH, H. HA, C. J. ELLISON, T. M. TRUSKETT and D. J. MILLIRON, “Linking semiconductor nanocrystals into gel networks through all-inorganic bridges”, *Angew. Chem. Int. Ed.*, 2015, **54**, 14840–14844, DOI: 10.1002/anie.201508641.
- (164) C. C. HEWA-RAHINDUWAGE, X. GENG, K. L. SILVA, X. NIU, L. ZHANG, S. L. BROCK and L. LUO, “Reversible Electrochemical Gelation of Metal Chalcogenide Quantum Dots”, *J. Am. Chem. Soc.*, 2020, **142**, 12207–12215, DOI: 10.1021/jacs.0c03156.

- 
- (165) C. C. HEWA-RAHINDUWAGE, K. L. SILVA, X. GENG, S. L. BROCK and L. LUO, "Electrochemical gelation of quantum dots using non-noble metal electrodes at high oxidation potentials", *Nanoscale*, 2021, **13**, 20625–20636, DOI: 10.1039/d1nr06615c.
- (166) C. C. HEWA-RAHINDUWAGE, K. L. SILVA, S. L. BROCK and L. LUO, "Quantum Dot Assembly Driven by Electrochemically Generated Metal-Ion Crosslinkers", *Chem. Mater.*, 2021, **33**, 4522–4528, DOI: 10.1021/acs.chemmater.1c00832.
- (167) Z. LIU, K. XU, P. SHE, S. YIN, X. ZHU and H. SUN, "Self-assembly of 2D MnO<sub>2</sub> nanosheets into high-purity aerogels with ultralow density", *Chem. Sci.*, 2016, **7**, 1926–1932, DOI: 10.1039/c5sc03217b.
- (168) Y. FUJIKI, S. SHINKAI and K. SADA, "Aerogel-like three-dimensional gold nanoparticle network via sublimation of volatile organic crystals decorated with gold nanoparticles", *Chem. Lett.*, 2007, **36**, 608–609, DOI: 10.1246/c1.2007.608.
- (169) F. J. HEILIGTAG, N. KRÄNZLIN, M. J. SÜESS and M. NIEDERBERGER, "Anatase-silica composite aerogels: A nanoparticle-based approach", *J. Sol-Gel Sci. Technol.*, 2014, **70**, 300–306, DOI: 10.1007/s10971-013-3232-1.
- (170) T. BERESTOK, P. GUARDIA, M. IBÁÑEZ, M. MEYNS, M. COLOMBO, M. V. KOVALENKO, F. PEIRÓ and A. CABOT, "Electrostatic-Driven Gelation of Colloidal Nanocrystals", *Langmuir*, 2018, **34**, 9167–9174, DOI: 10.1021/acs.langmuir.8b01111.
- (171) F. J. HEILIGTAG, M. D. ROSSELL, M. J. SÜESS and M. NIEDERBERGER, "Template-free co-assembly of preformed Au and TiO<sub>2</sub> nanoparticles into multicomponent 3D aerogels", *J. Mater. Chem. C*, 2011, **21**, 16893–16899, DOI: 10.1039/c1jm11740h.
- (172) F. RECHBERGER, G. ILARI and M. NIEDERBERGER, "Assembly of antimony doped tin oxide nanocrystals into conducting macroscopic aerogel monoliths", *Chem. Comm.*, 2014, **50**, 13138–13141, DOI: 10.1039/c4cc05648e.
- (173) R. DESHMUKH, E. TERVOORT, J. KÄCH, F. RECHBERGER and M. NIEDERBERGER, "Assembly of ultrasmall Cu<sub>3</sub>N nanoparticles into three-dimensional porous monolithic aerogels", *Dalton Trans.*, 2016, **45**, 11616–11619, DOI: 10.1039/c6dt01451h.

- (174) F. RECHBERGER, E. TERVOORT and M. NIEDERBERGER, “Nonaqueous sol-gel synthesis of InTaO<sub>4</sub> nanoparticles and their assembly into macroscopic aerogels”, *J. Am. Chem. Soc.*, 2017, **100**, 4483–4490, DOI: 10.1111/jace.15018.
- (175) H. YU and S. L. BROCK, “Effects of Nanoparticle Shape on the Morphology and Properties of Porous CdSe Assemblies (Aerogels)”, *ACS Nano*, 2008, **2**, 1563–1570, DOI: 10.1021/nn8002295.
- (176) K. G. S. RANMOHOTTI, X. GAO and I. U. ARACHCHIGE, “Salt-Mediated Self-Assembly of Metal Nanoshells into Monolithic Aerogel Frameworks”, *Chem. Mater.*, 2013, **25**, 3528–3534, DOI: 10.1021/cm401968j.
- (177) X. GAO, R. J. ESTEVES, T. T. H. LUONG, R. JAINI and I. U. ARACHCHIGE, “Oxidation-induced self-assembly of Ag nanoshells into transparent and opaque Ag hydrogels and aerogels”, *J. Am. Chem. Soc.*, 2014, **136**, 7993–8002, DOI: 10.1021/ja5020037.
- (178) B. CAI, A. DIANAT, R. HÜBNER, W. LIU, D. WEN, A. BENAD, L. SONNTAG, T. GEMMING, G. CUNIBERTI and A. EYCHMÜLLER, “Multimetallic Hierarchical Aerogels: Shape Engineering of the Building Blocks for Efficient Electrocatalysis”, *Adv. Mater.*, 2017, **29**, DOI: 10.1002/adma.201605254.
- (179) F. LÜBKEMANN, P. RUSCH, S. GETSCHMANN, B. SCHREMMER, M. SCHÄFER, M. SCHULZ, B. HOPPE, P. BEHRENS, N. C. BIGALL and D. DORFS, “Reversible cation exchange on macroscopic CdSe/CdS and CdS nanorod based gel networks”, *Nanoscale*, 2020, **12**, 5038–5047, DOI: 10.1039/c9nr09875e.
- (180) Q. YAO, I. U. ARACHCHIGE and S. L. BROCK, “Expanding the Repertoire of Chalcogenide Nanocrystal Networks: Ag<sub>2</sub>Se Gels and Aerogels by Cation Exchange Reactions”, *J. Am. Chem. Soc.*, 2009, **131**, 2800–2801, DOI: 10.1021/ja900042y.
- (181) B. CAI, R. HÜBNER, K. SASAKI, Y. ZHANG, D. SU, C. ZIEGLER, M. B. VUKMIROVIC, B. RELLINGHAUS, R. R. ADZIC and A. EYCHMÜLLER, “Core-Shell Structuring of Pure Metallic Aerogels towards Highly Efficient Platinum Utilization for the Oxygen Reduction Reaction”, *Angew. Chem. Int. Ed.*, 2018, **57**, 2963–2966, DOI: 10.1002/anie.201710997.

- 
- (182) T. HENDEL, V. LESNYAK, L. KÜHN, A. K. HERRMANN, N. C. BIGALL, L. BORCHARDT, S. KASKEL, N. GAPONIK and A. EYCHMÜLLER, “Mixed aerogels from Au and CdTe nanoparticles”, *Adv. Funct. Mater.*, 2013, **23**, 1903–1911, DOI: 10.1002/adfm.201201674.
- (183) R. WENDT, B. MÄRKER, A. DUBAVIK, A. K. HERRMANN, M. WOLLGARTEN, Y. P. RAKOVICH, A. EYCHMÜLLER, K. RADEMANN and T. HENDEL, “Versatile H<sub>2</sub>O<sub>2</sub>-driven mixed aerogel synthesis from CdTe and bimetallic noble metal nanoparticles”, *J. Mater. Chem. C.*, 2017, **5**, 10251–10259, DOI: 10.1039/c7tc01707c.
- (184) S. SEKIGUCHI, K. NIKURA, N. IYO, Y. MATSUO, A. EGUCHI, T. NAKABAYASHI, N. OHTA and K. IJIRO, “PH-dependent network formation of quantum dots and fluorescent quenching by Au nanoparticle embedding”, *ACS Appl. Mater. Inter.*, 2011, **3**, 4169–4173, DOI: 10.1021/am201013n.
- (185) J. L. DAVIS, K. L. SILVA and S. L. BROCK, “Exploiting kinetics for assembly of multi-component nanoparticle networks with programmable control of heterogeneity”, *Chem. Comm.*, 2020, **56**, 458–461, DOI: 10.1039/C9CC09027D.
- (186) L. KORALA and S. L. BROCK, “Aggregation kinetics of metal chalcogenide nanocrystals: Generation of transparent CdSe (ZnS) core (shell) gels”, *J. Phys. Chem. C*, 2012, **116**, 17110–17117, DOI: 10.1021/jp305378u.
- (187) H. YU, Y. LIU and S. L. BROCK, “Tuning the optical band gap of quantum dot assemblies by varying network density”, *ACS Nano*, 2009, **3**, 2000–2006, DOI: 10.1021/nn900456f.
- (188) F. LÜBKEMANN, J. F. MIETHE, F. STEINBACH, P. RUSCH, A. SCHLOSSER, D. ZÁMBÓ, T. HEINEMEYER, D. NATKE, D. ZOK, D. DORFS and N. C. BIGALL, “Patterning of Nanoparticle-Based Aerogels and Xerogels by Inkjet Printing”, *Small*, 2019, **15**, 1–8, DOI: 10.1002/smll.201902186.
- (189) L. KORALA, J. R. GERMAIN, E. CHEN, I. R. PALA, D. LI and S. L. BROCK, “CdS aerogels as efficient photocatalysts for degradation of organic dyes under visible light irradiation”, *Inorg. Chem. Front.*, 2017, **4**, 1451–1457, DOI: 10.1039/c7qi00140a.

- (190) F. RECHBERGER and M. NIEDERBERGER, “Translucent nanoparticle-based aerogel monoliths as 3-dimensional photocatalysts for the selective photoreduction of CO<sub>2</sub> to methanol in a continuous flow reactor”, *Mater. Horiz.*, 2017, **4**, 1115–1121, DOI: 10.1039/C7MH00423K.
- (191) W. LIU, A.-K. HERRMANN, D. GEIGER, L. BORCHARDT, F. SIMON, S. KASKEL, N. GAPONIK and A. EYCHMÜLLER, “High-Performance Electrocatalysis on Palladium Aerogels”, *Angew. Chem. Int. Ed.*, 2012, **51**, 5743–5747, DOI: 10.1002/anie.201108575.
- (192) R. DU, Y. HU, R. HÜBNER, J. O. JOSWIG, X. FAN, K. SCHNEIDER and A. EYCHMÜLLER, “Specific ion effects directed noble metal aerogels: Versatile manipulation for electrocatalysis and beyond”, *Sci. Adv.*, 2019, **5**, 1–10, DOI: 10.1126/sciadv.aaw4590.
- (193) D. WEN, W. LIU, D. HAUBOLD, C. ZHU, M. OSCHATZ, M. HOLZSCHUH, A. WOLF, F. SIMON, S. KASKEL and A. EYCHMÜLLER, “Gold Aerogels: Three-Dimensional Assembly of Nanoparticles and Their Use as Electrocatalytic Interfaces”, *ACS Nano*, 2016, **10**, 2559–2567, DOI: 10.1021/acsnano.5b07505.
- (194) W. LIU, P. RODRIGUEZ, L. BORCHARDT, A. FOELSKE, J. YUAN, A.-K. HERRMANN, D. GEIGER, Z. ZHENG, S. KASKEL, N. GAPONIK, R. KÖTZ, T. J. SCHMIDT and A. EYCHMÜLLER, “Bimetallic Aerogels: High-Performance Electrocatalysts for the Oxygen Reduction Reaction”, *Angew. Chem. Int. Ed.*, 2013, **52**, 9849–9852, DOI: 10.1002/anie.201303109.
- (195) S. GANGULY and S. L. BROCK, “Toward nanostructured thermoelectrics: synthesis and characterization of lead telluride gels and aerogels”, *J. Mater. Chem.*, 2011, **21**, 8800, DOI: 10.1039/c1jm11015b.
- (196) S. GANGULY, C. ZHOU, D. MORELLI, J. SAKAMOTO and S. L. BROCK, “Synthesis and characterization of telluride aerogels: Effect of gelation on thermoelectric performance of Bi<sub>2</sub>Te<sub>3</sub> and Bi<sub>2-x</sub>Sb<sub>x</sub>Te<sub>3</sub> nanostructures”, *J. Phys. Chem. C*, 2012, **116**, 17431–17439, DOI: 10.1021/jp3055608.
- (197) J. N. DE FREITAS, L. KORALA, L. X. REYNOLDS, S. A. HAQUE, S. L. BROCK and A. F. NOGUEIRA, “Connecting the (quantum) dots: towards hybrid photovoltaic devices based on chalcogenide gels”, *Phys. Chem. Chem. Phys.*, 2012, **14**, 15180, DOI: 10.1039/c2cp42998e.

- 
- (198) J. F. MIETHE, F. LÜBKEMANN, A. SCHLOSSER, D. DORFS and N. C. BIGALL, “Revealing the Correlation of the Electrochemical Properties and the Hydration of Inkjet Printed CdSe/CdS Semiconductor Gels”, *Langmuir*, 2020, [acs.langmuir.9b03708](https://doi.org/10.1021/acs.langmuir.9b03708), DOI: 10.1021/acs.langmuir.9b03708.
- (199) Q. YAO and S. L. BROCK, “Optical sensing of triethylamine using CdSe aerogels”, *Nanotechnology*, 2010, **21**, DOI: 10.1088/0957-4484/21/11/115502.



# 5 Optical Properties of Nanocrystal-Based Aerogel Networks

## 5.1 Summary

The (size dependent) optical properties of nanomaterials and the connected electronic properties are one of their core characteristics making them interesting in applications from illumination to sensing. As has been described earlier it is possible to retain such optical properties of the nanocrystalline building blocks when assembling them into a manageable macroscopic structure in case of aerogels. As stated in section 3.3 it is moreover even possible for the resulting aerogel to exhibit new optical properties based on the connection of the building blocks. One remarkable example are aerogels based on CdSe/CdS dot/rod nanocrystals. Due to the band structure of these CdSe/CdS building blocks an excited electron is delocalized over a part of the connected network larger than the original building block. This results in ultra-long photoluminescence lifetimes in these aerogel structures. In this chapter the optical properties of such networks are investigated in detail.

The publication in section 5.2 contains a temperature dependent investigation of the optical properties down to cryogenic temperatures. The photoluminescence decay of the structures can be seen to be highly temperature dependent, initially increasing in speed with lower temperatures and then splitting into two processes with drastically different time scales. This can be attributed to bright and dark states in the CdSe cores and can be described with an established three-level model. Additionally, the structures are prepared starting from either 2.8 or 3.5 nm CdSe cores resulting in different band structures and therefore different emission colors. The

interaction within networks of mixed building blocks is investigated and a straight-forward color tunability between green and red is shown.

## **5.2 Temperature and Composition Dependent Optical Properties of CdSe/CdS Dot/Rod-Based Aerogel Networks**

Pascal Rusch, Denis Pluta, Franziska Lübke, Dirk Dorfs, Dániel Zámbo, Nadja C. Bigall

Published in: *ChemPhysChem*, 2021, 22,

DOI: 10.1002/cphc.202100755

Published by Wiley-VCH GmbH



# Temperature and Composition Dependent Optical Properties of CdSe/CdS Dot/Rod-Based Aerogel Networks

Pascal Rusch,<sup>[a, b]</sup> Denis Pluta,<sup>[a, b, c]</sup> Franziska Lübke, <sup>[a, b]</sup> Dirk Dorfs,<sup>[a, b, d]</sup>  
 Dániel Zámbo,<sup>[a, b]</sup> and Nadja C. Bigall\*<sup>[a, b, d]</sup>

Employing nanocrystals (NCs) as building blocks of porous aerogel network structures allows the conversion of NC materials into macroscopic solid structures while conserving their unique nanoscopic properties. Understanding the interplay of the network formation and its influence on these properties like size-dependent emission is a key to apply techniques for the fabrication of novel nanocrystal aerogels. In this work, CdSe/CdS dot/rod NCs possessing two different CdSe core sizes were synthesized and converted into porous aerogel network structures. Temperature-dependent steady-state and time-resolved photoluminescence measurements were performed to expand the understanding of the optical and

electronic properties of these network structures generated from these two different building blocks and correlate their optical with the structural properties. These investigations reveal the influence of network formation and aerogel production on the network-forming nanocrystals. Based on the two investigated NC building blocks and their aerogel networks, mixed network structures with various ratios of the two building blocks were produced and likewise optically characterized. Since the different building blocks show diverse optical response, this technique presents a straightforward way to color-tune the resulting networks simply by choosing the building block ratio in connection with their quantum yield.

## Introduction

With the introduction of network structures based on colloidal CdS dispersions<sup>[1,2]</sup> and the conversion of these nanocrystal-(NC) based gels to aerogels<sup>[3,4]</sup> – porous network structures – an exciting new class of materials emerged. In analogy to the well-established sol-gel method, this allows for the transformation of nanoscopic materials into macroscopic, self-supported solids.<sup>[5,6]</sup> A number of methods<sup>[3,7–12]</sup> to produce aerogel networks based on most of the available NCs<sup>[13–18]</sup> has been developed and first demonstrations of applications have been published. These

were focused on the sensing<sup>[19,20]</sup> or catalytic<sup>[21–25]</sup> properties of the NC building blocks but much less attempts have been made to utilize the inherent photoluminescence (PL) of the semiconducting NC building blocks. Compared to the more classical sol-gel approach to produce aerogel networks, a key advantage of NC-based aerogels is that it allows for the synthesis of the individual NC building blocks in a separate step prior to the network formation. In turn, enabling the use of the vast library of NC synthesis and modification procedures to be used to fine-tune the building blocks and in consequence the later network itself. As these NC-based structures bridge from the nanoscopic scale of each building block up to the macroscopic shape of the resulting monolith, the tuning of their properties can similarly be performed on the level of the individual building block (e.g. shape-selective synthesis<sup>[10,26]</sup> or bandgap engineering<sup>[26,27]</sup>), and the macroscopic ensemble (e.g. patterning<sup>[28]</sup>). In addition to these nano- and macrostructuring possibilities, a level of control can also be exerted at the intermediate scale to tune the microstructure and the building block connection.<sup>[29]</sup> Multicomponent networks, formed of more than one building block material, are often used to connect semiconducting materials with metallic ones for the generation of catalytically active networks. This can be done by the isolated synthesis of two different NC building blocks,<sup>[30–34]</sup> assembling hybrid nanoparticles<sup>[35–37]</sup> or even via the direct deposition of the metal to the forming network.<sup>[38,39]</sup> The idea of connecting two different semiconducting NC building blocks into one network has been explored much less frequently. The nature of the interparticle connection,<sup>[8]</sup> the ligands<sup>[40,41]</sup> and the composition<sup>[42]</sup> play a governing role in the control over the assembled gel structures in terms of the structural as well as optical properties. When combining two differently-sized CdTe NC building blocks or CdTe and ZnSe NC building blocks which

[a] P. Rusch, D. Pluta, Dr. F. Lübke, Dr. D. Dorfs, Dr. D. Zámbo, Prof. N. C. Bigall  
 Institute of Physical Chemistry and Electrochemistry,  
 Leibniz Universität Hannover  
 Callinstr. 3A, 30167 Hannover, Germany  
 E-mail: nadja.bigall@pci.uni-hannover.de

[b] P. Rusch, D. Pluta, Dr. F. Lübke, Dr. D. Dorfs, Dr. D. Zámbo, Prof. N. C. Bigall  
 Laboratory of Nano and Quantum Engineering,  
 Leibniz Universität Hannover  
 Schneiderberg 39, 30167 Hannover, Germany

[c] D. Pluta  
 Hannover School for Nanotechnology,  
 Leibniz Universität Hannover  
 Schneiderberg 39, 30167 Hannover, Germany

[d] Dr. D. Dorfs, Prof. N. C. Bigall  
 Cluster of Excellence, PhoenixD  
 (Photonics, Optics and Engineering – Innovation Across Disciplines),  
 Leibniz Universität Hannover  
 30167 Hannover, Germany

Supporting information for this article is available on the WWW under <https://doi.org/10.1002/cphc.202100755>

© 2021 The Authors. ChemPhysChem published by Wiley-VCH GmbH. This is an open access article under the terms of the Creative Commons Attribution Non-Commercial License, which permits use, distribution and reproduction in any medium, provided the original work is properly cited and is not used for commercial purposes.

differ in their band positions into one network, energy and charge transfer within these semiconductor multicomponent networks could be confirmed by the change in the emission spectra between the building block solution and the connected networks. In turn, this could then be used to tune the ratios of the different components to generate white emitting aerogels.<sup>[42]</sup>

In the present work, we aim to increase our understanding of the optical properties of these multicomponent semiconductor NC-based networks namely within the system of CdSe/CdS dot/rod NC building blocks by analyzing their temperature-dependent optical properties. The measurements are performed by steady-state as well as time-resolved photoluminescence (PL) spectroscopy. Additionally, expanding this established system of CdSe/CdS dot/rod NC-based aerogels *via* the use of building blocks with differently sized CdSe cores and therefore varying emission colors is also targeted, as schematically drawn out in Figure 1A. These systems of connected CdSe/CdS dot/rod NCs are remarkable due to their optical properties, i.e. the difference in PL lifetimes at the level of the individual building blocks and a connected network.<sup>[8]</sup> The measured PL decay of the connected network is considerably longer than the decay of the isolated particles which could be attributed to the interparticle connection and a resulting delocalization of the excited electron over several connected building blocks.<sup>[8,43]</sup>

## Results and Discussion

### Optical Properties of CdSe/CdS Dot/Rod Building Blocks and Their Aerogel Networks

The nanocrystal building blocks were synthesized along well-known literature routes by hot injection method (see Experimental Section for details). To this end, CdSe QDs in two sizes were produced. For the sake of simplicity, these will be called small core for 2.0 nm CdSe QDs and large core for 3.9 nm CdSe QDs in the following. These CdSe QDs were then used as seeds

for the growth of an elongated CdS shell, which resulted in the production of CdSe/CdS dot/rods with dimensions of ca.  $4 \times 50$  nm independent of the CdSe core size (see Figure 2A,B and S1) The ensemble optical properties (see Figure 2E,F) were tuned via the size of the CdSe core embedded into a CdS shell showing a size-dependent CdSe absorption maxima at 537 nm (small core) and 605 nm (large core) and the emission at 555 nm and 608 nm for CdSe/CdS dot/rods, respectively. For both heteroparticle systems, a strong absorption can be observed below 500 nm due to the band edge of the CdS shell material accounting for the majority of the dot/rods.

These well-defined dot/rod building blocks were then assembled into interconnected porous network structures (i.e. gels) by controlled oxidative removal of their protective ligands (3-mercaptopropionic acid) *via* the addition of low concentrations of hydrogen peroxide (see Figure 2C,D). This process favorably attacks the ligands on the NC tips (due to steric considerations) and also facilitates the generation of sulfur-sulfur bonds resulting in the NCs forming a mostly tip-to-tip connected crystal-crystal bound network.<sup>[8]</sup> As has been shown in earlier works, these networks show considerably longer PL lifetimes compared to their individual NC building blocks. This effect was previously attributed to the delocalization of excited electrons within several connected building blocks, thereby decreasing electron-hole overlap.<sup>[8]</sup> As can be seen in Figure 2F, this effect is also clearly visible in the large core sample for this study with the PL lifetimes increasing from 15 ns for individual building blocks to 28 ns in the network structure. In the small core sample, the increase in PL lifetime between individual NCs and an interconnected network is likewise observed with an increase of the PL lifetime from 22 ns to 29 ns. This confirms the influence of the interconnection of the CdSe/CdS dot/rod building blocks as well as the conduction band-offset between the combined semiconductors on the PL decay behavior similarly to the earlier reported red-emitting CdSe/CdS dot/rod based aerogel networks.<sup>[8]</sup> Networks build-up from building blocks based on much smaller CdSe cores not investigated yet. This is interesting as these smaller CdSe core-based structures have been reported to behave differently to larger CdSe core-based ones in certain aspects. With smaller CdSe cores and as consequence a larger bandgap of the core material, the conduction band offset between the CdSe core and the CdS shell is expected to decrease (see scheme in Figure 1B), leading to an increased leaking of the electron wavefunction into the CdS shell in the excited dot/rod.<sup>[44-47]</sup> This leads to longer PL lifetimes in CdSe/CdS dot/rods with smaller cores due to the increased delocalization of the excited electron. Meanwhile, the steady-state optical properties (see Figure 2E) of these CdSe/CdS dot/rod-based aerogel networks are similar to their building blocks. The CdSe absorption is clearly visible at 525 nm (small core) and 590 nm (large core) with the CdS absorption edge around 480 nm in both instances. As can be seen in the spectra, the absorption of the network structures reaches a saturation around this CdS band edge whereby higher energy of the incident light does not lead to a higher measured absorption – as would be the case for diluted dispersions of the building blocks. This is due to the optically dense sample being

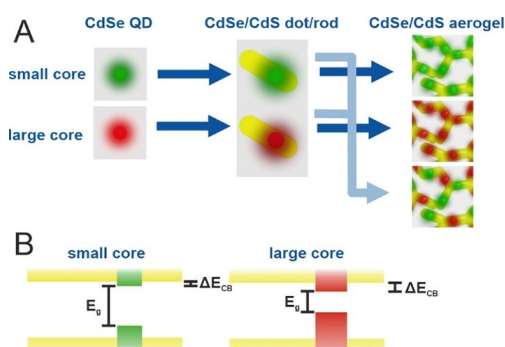


**Figure 1.** Schematic depiction of (A) the synthesis route of the investigated CdSe/CdS NC-based aerogel networks and (B) the band structure of the two NCs based on differently sized CdSe cores.

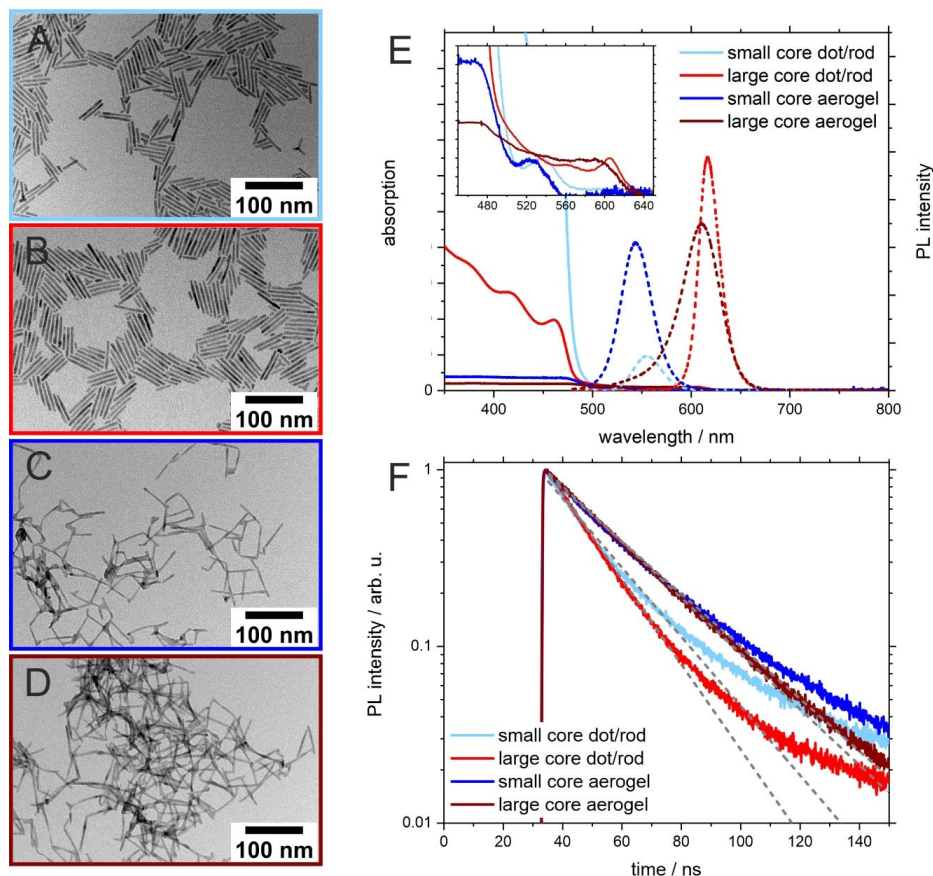


**Figure 2.** CdSe/CdS dot/rod NC-based aerogel network structures and the individual building block NCs. TEM micrographs of CdSe/CdS dot/rod NCs synthesized from (A) 2.0 nm CdSe cores and (B) 3.9 nm CdSe cores and the respective (C, D) network structures. (E) Absorption (solid lines) and emission (dashed lines) spectra with inset showing the magnified area of CdSe absorption and (F) PL decays of these CdSe/CdS dot/rod NC-based aerogel networks and the individual building blocks (2.0 nm CdSe core-based structures in blue colors, 3.9 nm CdSe core-based structures in red colors).

a macroscopic monolith comparable to a very highly concentrated dispersion. Like their building blocks, the assembled network structures show emission from the CdSe core at 544 nm and 608 nm respectively. The PL quantum yield (PLQY) increases from 6% (small core) and 23% (large core) in the respective aqueous dispersions to 26% (small core) and 38% (large core) in the aerogels (see Figure S6). This increase in PLQY is most likely caused by the removal of solvent and therefore a removal of certain non-radiative recombination pathways.<sup>[48,49]</sup> Additionally, by the crystal-to-crystal connection of the inorganic building blocks *via* the tips, surface traps on the tips are likely to be eliminated.

#### Temperature Dependent Optical Properties of CdSe/CdS Dot/Rod Aerogel Networks

The aerogel networks, as well as their building blocks as a reference, were then systematically investigated with regards to their optical properties at lower temperatures. The steady-state emission spectra change consistently with the changing temperature for the network structures and their building blocks (see Figure 3 and S3). The emission maxima shift to higher energy at lower temperatures accompanied by a decreasing full width at half maximum (FWHM). These parameters can be extracted from the experimental spectra by fitting with a single Gaussian. This temperature-dependent emission behavior is well-known and documented for semiconducting NCs<sup>[50-52]</sup> and can be attributed to exciton-phonon coupling as well as lattice deformation both being temperature-dependent

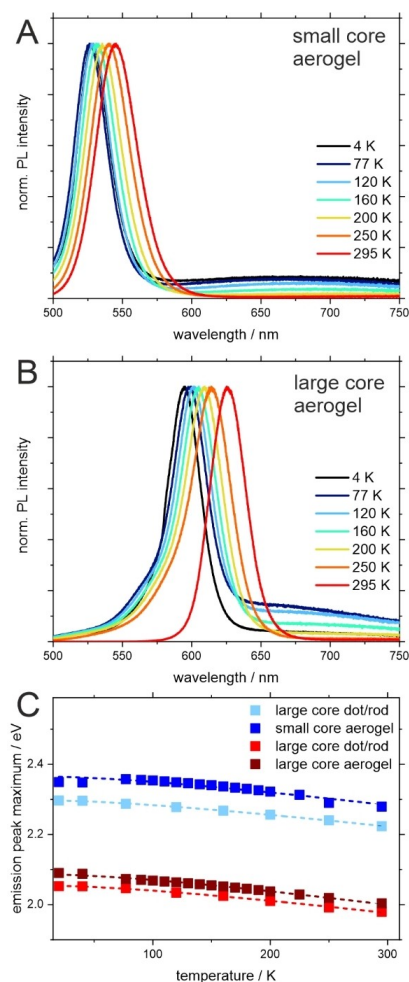


**Figure 3.** Change of PL with temperature. Temperature dependent emission spectra of CdSe/CdS dot/rod NC-based aerogel networks with (A) CdSe core diameter of 2.0 nm and (B) CdSe core diameter of 3.9 nm. (C) Change in emission maxima depending on temperature and Varshni law fit for CdSe/CdS dot/rod NC-based network structures with different CdSe core sizes (blue colors for small cores, red colors for large cores) and the respective individual building blocks.

themselves and influencing the electronic properties of the NCs. The temperature dependent emission maxima, i.e. bandgap ( $E_g(T)$ ), can be fitted by the empirical Varshni law<sup>[53]</sup> (Equation 1).

$$E_g(T) = E_g(T=0) - \frac{\alpha T^2}{(T + \beta)} \quad (1)$$

The thermal dependency of the respective emission maxima can be fitted by the Varshni law using 195 K as  $\beta$  (which is

roughly the Debye temperature) and ca.  $4 \cdot 10^{-4}$  as  $\alpha$  (a measure for the electron-phonon coupling) for individual NC building blocks and their networks alike (see Figure 3C), yielding values close to the ones reported for these CdSe/CdS dot/rods before.<sup>[52]</sup> The theoretical bandgap at 0 K ( $E_g(T=0)$ ) as determined by this fit agrees well with the observed emission colors, while a slight difference between building blocks and assembled networks can be observed (see Table S1).

Looking at the time-resolved PL spectroscopy, the CdSe cores (see Figure S4) show a non-monoexponential decay behavior at higher temperatures, probably due to the lack of surface passivation. After the growth of CdS shells, the PL decay is much closer to a mono-exponential behavior, which would be expected for an ideal system. A longer decay component tail can be observed. This has been seen in the past for these types of core-shell NC systems and has been attributed to shallow electron traps causing a delayed emission.<sup>[54]</sup> For all samples, building blocks and networks alike, a similar trend can be observed with the PL lifetimes decreasing with decreasing temperature (see Figure 4 and S5). This phenomenon has been discussed in literature for the CdSe/CdS dot/rod system<sup>[51]</sup> (which are employed here as individual building blocks) but has not been investigated for the resulting network structures, yet. For the building blocks, several different factors have been argued to cause this behavior of decreasing PL lifetimes at lower temperatures, starting with (i) a shifting conduction band offset altering the extend of delocalization into the CdS shell,<sup>[51]</sup> (ii) the thermal lattice fluctuations introducing asymmetry in electron and hole wavefunction,<sup>[52]</sup> and (iii) the contribution of higher excited electron states by thermal mixing.<sup>[52]</sup> All of these proposed mechanisms would alter the electron-hole overlap which results in a change in radiative lifetimes. These effects described for the individual building blocks can be assumed to likewise take place in their interconnected network structures, and similar trends in the change of PL lifetimes with temperature can be observed for both different CdSe core sizes. Interestingly, the PL lifetimes observed for the aerogel network structures exceed the ones of the individual building blocks over the full temperature range.

The effect detailed above of decreasing PL lifetimes with decreasing temperature can be observed until roughly a temperature of 80 K. Below this and down to temperatures of 20 K a different trend can be seen with the lifetimes increasing again with decreasing temperature and easily surpassing the lifetimes measured at room temperature (see Figure 4). With continuously lower temperatures down to 4 K, the evolution of two separated processes (one with very short lifetimes and one with extremely long lifetimes) is found. As shown in Figure 4D, the measured PL lifetime decreases from initially 15 ns at room temperature to 8 ns at 77 K in case of large core dot/rods and below this temperature rises again, to then split up into two distinct processes. For clarification, it should be noted that deviation from ideal mono-exponential behavior at higher temperatures, as can be seen in some cases (see Figure 4, S4, S5) can be attributed to surface states, as has been stated earlier,<sup>[54]</sup> and should not be confused with the processes at cryogenic temperatures. Similarly, the measured PL of large

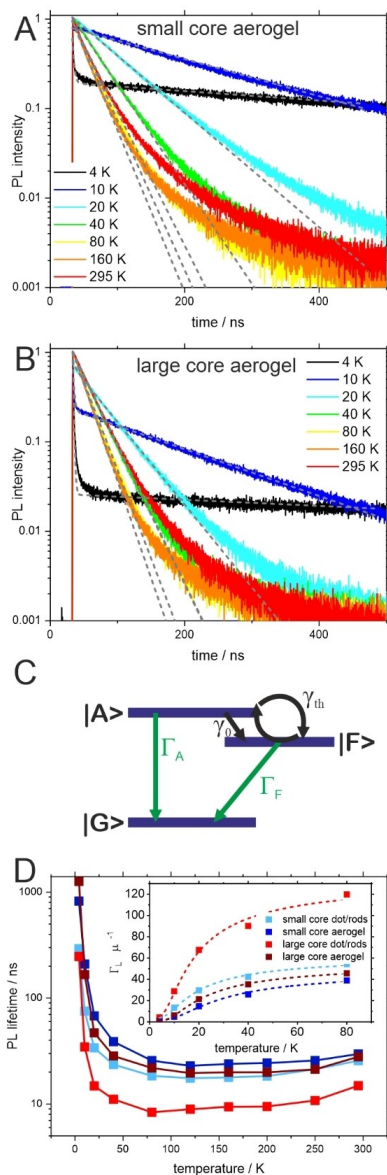


**Figure 4.** Temperature-dependent time-resolved PL properties. PL decay and single exponential fits at different temperatures of CdSe/CdS dot/rod NC-based network structures with (A) 2.0 nm CdSe core diameter and (B) 3.9 nm CdSe core diameter, grey lines indicate the exponential fit of the data. (C) Three-level model used to describe the PL kinetics at cryogenic temperatures. (D) Temperature-dependent PL lifetime extracted by single exponential fit (at  $T > 10$  K) or single exponential fit of the long decay component (4–10 K), inset shows the fit of the extracted lifetimes following equation 3 (derived from a three-level model).

core aerogels decrease from 28 ns (room temperature) to 22 ns (120 K) to then increase and split into the aforementioned two processes. This behavior is also seen in the small core samples with PL lifetimes decreasing from 22 ns and 29 ns at room temperature to 18 ns and 26 ns at 77 K for small core dot/rods and SC aerogels, respectively. Again, below 77 K the increase in PL lifetime and eventual evolution of two processes can be observed for the small core samples. The transition point from PL lifetimes decreasing with decreasing temperature to then increase with decreasing temperature, i.e. the minimum measured PL lifetime, is slightly different between samples within the region of 77–120 K. The fast process of the cryogenic decays at 4 K shows lifetimes between 2.7 ns (large core dot/rods) and 1.2 ns (large core aerogels), while the slow process varies between 247 ns (in large core dot/rods) and 1262 ns (in the respective large core aerogels). Comparable results are obtained for the small core sample with a fast component, 2.4 ns (small core dot/rods) and 2.2 ns (small core aerogels), and a slow component, 292 ns (small core dot/rods) and 822 ns (small core aerogels). Similar to these observations, two processes have been shown for CdSe/ZnS NCs in the past<sup>[55]</sup> and have been attributed to the bright and dark exciton (with the first showing extremely fast recombination and the latter showing very slow recombination due to the spin forbidden transition). This behavior is very much alike in the CdSe/CdS dot/rod building blocks as has been shown in reference<sup>[51]</sup> and in their network structures as observed in the present work. As has been demonstrated in the past,<sup>[55,56]</sup> these systems can be explained by a three-level model with the ground state ( $|G\rangle$ ), the bright, allowed state ( $|A\rangle$ ) and the dark, forbidden state ( $|F\rangle$ ) (see Figure 4C). The two excited states are different in energy by  $\Delta E$ , the bright-dark splitting. They exhibit respective radiative recombination rates ( $\Gamma_A$  and  $\Gamma_F$ ) with a spin-flip from bright to dark state denoted by  $\gamma_0$  and a thermally induced spin-flip  $\gamma_{th} = \gamma_0 N_B$  mixing bright and dark states with  $N_B = 1/(e^{\Delta E/k_B T} - 1)$  being the Bose-Einstein phonon occupation. As has been detailed elsewhere,<sup>[56]</sup> under the assumption of the PL signal being proportional to  $(\Gamma_A \rho_A + \Gamma_F \rho_F)$ , with the time-dependent populations of the bright ( $\rho_A$ ) and dark ( $\rho_F$ ) exciton states an expression for the PL signal ( $S(t)$ ) can be derived (Equation 2).

$$S(t) = \frac{\Gamma_A N_B + \Gamma_F}{1 + 2N_B} e^{-r_i t} + \frac{\Gamma_A}{2(1 + 2N_B)} e^{-r_s t} \quad (2)$$

In this equation, the long ( $\Gamma_L$ ) and short ( $\Gamma_S$ ) component of the observed PL decay can be expressed as follows:<sup>[56]</sup>

$$\Gamma_L = \frac{\Gamma_A + \Gamma_F}{2} - \frac{\Gamma_A - \Gamma_F}{2} \tanh\left(\frac{\Delta E}{2k_B T}\right) \quad (3)$$

$$\Gamma_S = \gamma_0(1 + 2N_B) \quad (4)$$

This results in biexponential decays at very low temperatures with a short component caused by recombination from the bright state before relaxation and a long component caused by the recombination from the dark state. At higher temper-

atures, this transforms into a mono-exponential decay. This expression (Equation 3) can be used to fit the experimentally observed slow component of the PL decay to extract the bright-dark splitting  $\Delta E$  as well as the radiative recombination rates of the bright ( $\Gamma_A$ ) and the dark ( $\Gamma_F$ ) state (see Figure 4D and Table S3). The CdSe/CdS building blocks show cryogenic decay curves quite similar to their respective initial CdSe cores. The domination of the PL behavior at cryogenic temperatures by the CdSe cores can be expected due to the recombination taking place solely in these cores. Minor differences might be caused by the CdS shell as this alters surface passivation and dielectric surrounding of the cores in the dot/rods. However, interestingly, as seen in the present work, the assembly of these CdSe/CdS dot/rod building blocks into aerogel networks results in increased PL lifetimes not only at room temperature but at all temperatures down to 4 K. This is unexpected so far, as the assumption for these network structures would likewise be a domination of the CdSe core in the PL decay behavior at cryogenic temperatures, if these cores are unaffected by the network assembly and drying procedure generating the aerogels. While it has been shown that the cryogenic PL decay of CdSe/CdS dot/rods depends strongly on the nanorod width, the nanorod length has shown no noticeable influence.<sup>[56]</sup> Comparing these observations to the networks in this study, the connection of the dot/rod building blocks into network structures should yield similar results as elongating the rod further. As can be seen, the width of the network structure corresponds well to the width of the individual building blocks (see Figure S1 and S2). A change in width can therefore be excluded as the reason for the difference in cryogenic decay behavior between building blocks and networks. This might in turn hint at additional processes taking place during the drying process. In the first description of CdSe/CdS dot/rod NC-based aerogel networks, the difference in decay behavior between the freshly assembled hydro- and acetogels to the dried aerogels was monitored. It was attributed to the removal of the solvent and potential sintering processes improving the connection of the building blocks to each other during the supercritical drying, which takes place at elevated pressure and slightly elevated temperature.<sup>[8]</sup> These processes, elevated pressure leading to sintering as well as the washing process during solvent exchange (which is part of the synthetic process to produce such dried aerogels), can principally all influence the surface of the NC building blocks resulting in differences in surface passivation and therefore modified PL kinetics. The cryogenic PL decay measurements presented here might also hint at these processes influencing not only the interparticle connection but likewise the internal structure of the building blocks, e.g. the CdSe to CdS interface.

#### Optical Properties of Aerogel Networks Assembled from Two Different CdSe/CdS Building Blocks

For further insight into the interaction between the individual building blocks inside of these CdSe/CdS network structures the two building blocks described above (small core and large core)

were then combined into one network, varying the mixing ratio of these two components. The mixing of two CdSe/CdS dot/rods possessing different emission colors in colloidal solution resulted in a colloidal mixture exhibiting both emission features (Figure 5A). The resulting spectra were fitted with a system of two Gaussians with the parameters for the peaks (peak maximum and FWHM) taken from the Gaussian fit of the emission spectrum of the individual respective dot/rods or their corresponding network structures. The area of the two peaks in the mixtures is therefore left as the only free parameter. From the ratio of the respective peak areas in combination with the PLQY of the unmixed samples, an estimation of the ratio of the two building blocks can be made (see Figure 5D and Table S4). From this ratio, a small systematic error is visible slightly shifting these ratios compared to the targeted ratios, most likely due to the error in calculating the particle concentration (using the  $\text{Cd}^{2+}$  concentration, the NC size as measured from transmission electron microscopy (TEM) and the bulk density of CdS). For the building block mixtures, as one would expect for these low concentration colloidal solutions, in which the NC building blocks can be assumed to be isolated from each other, no interaction between the two building blocks could be observed. The ratios, interestingly, could be found in the respective mixed networks with only minor deviations between mixed colloids and the mixed interconnected network (see Figure 5, for the intermediate acetogels see Figure S7). The evaluation of the emission intensity by fitting with two Gaussians worked reasonably well for all but one sample. In this instance, the fitting was not possible for the assembled networks with a high content of red-emitting (large core) building blocks (targeted ratio: 1–10). This is caused by the overlap of the more intense red emission peak and the low intensity green emission peak in conjunction with slight deviations from the ideal Gaussian peak shape. These factors did not allow for a correct fitting of the emission curve with a combination of two Gaussians. Earlier reports on other mixed semiconductor NC aerogel systems indicate a shift of emission in the case of a network consisting of two different sized CdTe QDs due to charge and energy transfer from the larger bandgap building block to the small bandgap building block which in that case needed to be taken into account upon color tuning the aerogel monolith.<sup>[42]</sup> This is very much not the case in the structures described in this work, with no strong difference between a mixture of two building blocks emitting different colors and the network assembled from them. This can be explained by the CdS shell of the building blocks. While the excited electron is delocalized over multiple connected rods as discussed earlier, the localization of the hole to the CdSe core of the building block is happening within less than 1 ps.<sup>[44,57]</sup> The recombination, therefore, happens solely in the cores after a few ps.<sup>[58]</sup> The emission color staying rather constant between the colloidal mixture of CdSe/CdS building blocks and their assembled networks does allow for a less complex approach to the color tuning of the resulting macroscopic network structures. This can be done simply by varying the ratios of the building blocks used in accordance with their quantum yields as demonstrated here with a color space from red to yellow to green (see Figure 5B).

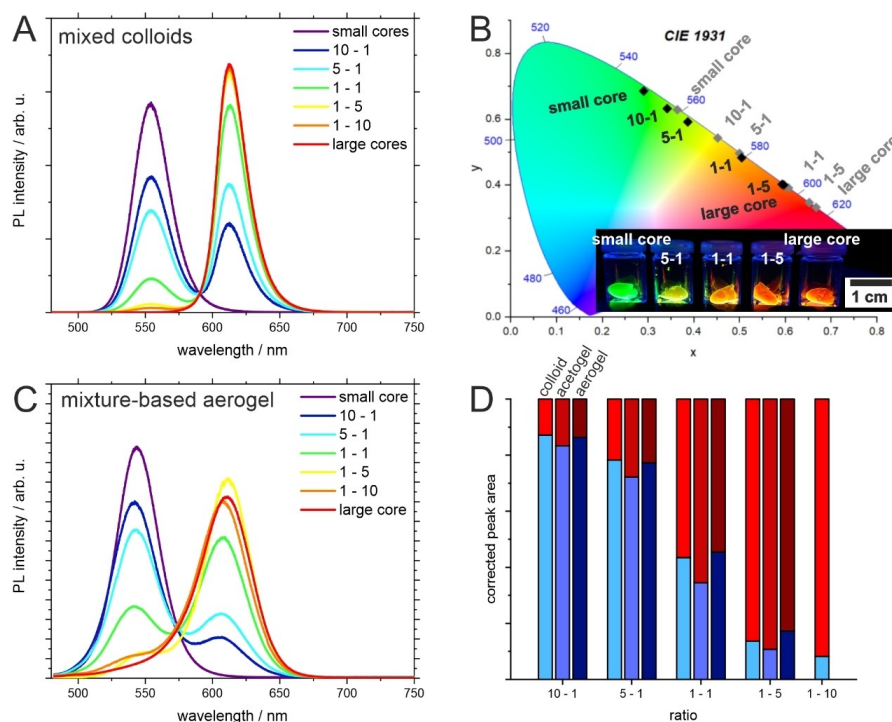


**Figure 5.** Emission properties of CdSe/CdS dot/rod-based network structures with two different CdSe core sizes and their mixtures (targeted molar ratios of the two mixed building block NCs are given). Emission spectra of (A) colloidal dispersions and mixtures of the building block NCs and (C) the resulting aerogel networks. (B) Chromaticity coordinates of the colloidal mixtures (grey) and the aerogels (black), inset shows a photograph of the aerogels under UV illumination. (D) Contribution to emission peak areas of the mixed colloidal NC and network structures of the small CdSe core (blue colors) and large CdSe core (red colors) NCs corrected by the quantum yield of the unmixing samples. As discussed in the main text, the evaluation of the peak areas for 1–10 ratio was only possible in colloidal mixtures.

The networks formed from different mixed building blocks also show the behavior observed for single component networks when investigating their temperature dependent optical properties (see Figure 6). The emission maxima shift and the FWHMs narrow with lower temperature. Additionally, a prominent shift in the ratio of the two emission peaks is visible. The change of emission intensity with temperature in the CdSe/CdS dot/rod system is rather complex with multiple processes contributing to a non-radiative recombination<sup>[46]</sup> which can be favored or hindered by lower temperatures. A difference in PL intensity with temperature between the building blocks of two different CdSe core sizes can also be observed in the individual single component aerogel networks (see Figure S8). While the small core aerogel shows a more or less steady increase of PL intensity at lower temperatures, the large core aerogel shows a slight loss in intensity at moderate temperatures (down to ca. 150 K) to only then increase with decreasing temperature (Figure S8). The interplay of these two behaviors results in the effect observed in the mixed aerogel network of both building blocks. Here, the intensity of the green emission (emanating from the small core part of the network) compared to the red

emission (from the large core part) increases to roughly this temperature of 150 K then decrease again down to 77 K below which it stays constant and comparable to the ratio of green to red emission observed at room temperature. The PL kinetics likewise are very similar to the measurements of the single component networks described above. A slight decrease in PL lifetime is seen down to ca. 80 K and below that, a drastic increase with a split into two processes can be observed. These measurements taken at the emission maxima of one of the building blocks are very much in line with the measurements of the networks formed solely from the respective building block as displayed in Figure 6D. This is also true for the PL decay behavior of mixed networks assemble from other ratios of SC and LC building blocks, as shown in Figure S9. This again reinforces the point that the emission properties are mostly governed by the CdSe core within these CdSe/CdS dot/rod aerogel networks. The effect of increased PL lifetimes between individual building blocks and assembled networks as reported earlier could likewise be confirmed in this study and may be attributed to the CdS-to-CdS connection within the network enabling further delocalization of the excited electron<sup>[8,43]</sup> as has

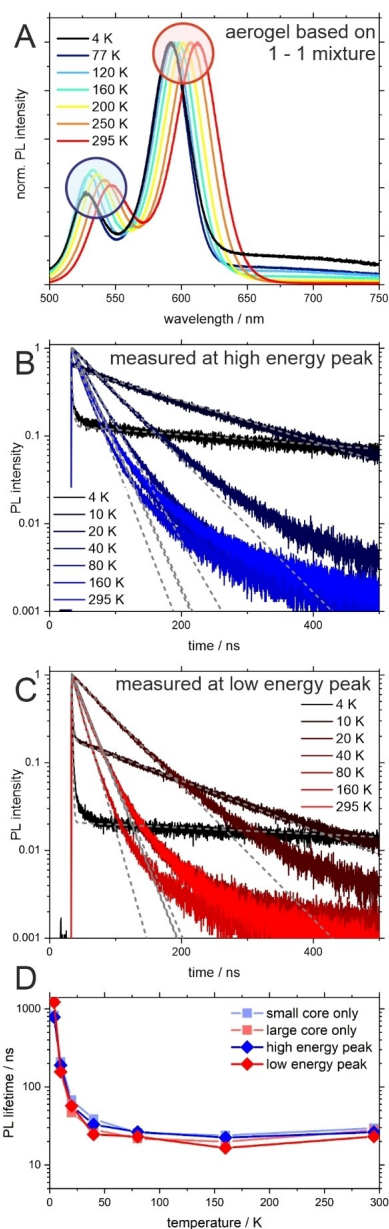


**Figure 6.** Temperature-dependent optical properties of CdSe/CdS dot/rod NC-based aerogel network consisting of a 1/1 molar ratio small CdSe core (2.0 nm) and large CdSe core (3.9 nm) building blocks. (A) Emission spectra at different temperatures and PL decay measured at the (B) higher energy (small cores, marked blue in panel A) emission peak, corresponding to detection at 525 nm (4 K)–555 nm (295 K), and (C) low energy (large cores, marked red in panel A) emission peak, corresponding to detection at 590 nm (4 K)–615 nm (295 K). (D) PL lifetimes extracted from the decay curves in panel B and C compared to PL lifetimes of aerogels based on one NC building block only.

similarly been demonstrated by increasing the length of the CdS rod-shaped shell.<sup>[59]</sup> An interaction between building blocks of different core sizes and therefore different band gaps within a mixed network of these two components with regards to emission color or cryogenic PL kinetics could not be observed here.

## Conclusions

In summary, CdSe/CdS dot/rod-based aerogel networks were synthesized, and the optical properties of these networks produced starting from two differently sized CdSe cores were investigated. In this context, the known effect of prolonged photoluminescence lifetimes caused by the network formation could be confirmed also for the much smaller CdSe core samples. For the first time the cryogenic PL properties of these networks and their building blocks have been investigated. While the general temperature dependent PL behavior was similar between CdSe QDs, CdSe/CdS dot/rods and CdSe/CdS dot/rod-based aerogel networks, distinct differences from individual NCs to interconnected NC networks could be found. Namely, a remarkably slow dark exciton recombination was observed, which might appear due to the process of aerogel fabrication. The two investigated nanoparticles were subsequently assembled into mixed networks of controlled ratios presenting a convenient approach to color tuning of the macroscopic aerogel networks, as the emission color of the mixed networks can be controlled solely by the mixture of the individual components and no additional interaction between the two differently emitting building blocks during network formation was found. This underlines the governing effect of the CdSe cores on the overall optics of the mixed CdSe/CdS dot/rod aerogel networks.

## Experimental Methods

### Chemicals

Tri-*n*-octylphosphine oxide (TOPO), Sulfur, 3-mercaptopropionic acid (MPA), potassium hydroxide, methanol, chloroform and hydrogen peroxide (35% aqueous solution) were purchased from Sigma Aldrich. Cadmium oxide and selenium were purchased from Alfa Aesar. Octadecylphosphonic acid and Hexylphosphonic acid were purchased from PCI Synthesis. Tri-*n*-octylphosphine (TOP) was purchased from ABCR. Toluene and acetone were purchased from Merck. All chemicals were used without further purification.

### Synthesis of CdSe/CdS Building Blocks

The synthesis of the CdSe cores and the CdSe/CdS dot/rods was performed along with established literature methods.<sup>[8,60]</sup>

Briefly, 180 mg CdO, 840 mg ODPA and 9 g TOPO were degassed at 150 °C and then heated to 300 °C under nitrogen. 5.4 mL TOP were injected, and the temperature was raised to 350 °C. At this point, a solution of Se in TOP (0.174 g Se in 5.4 mL TOP) was quickly injected, and the reaction mixture was kept at this temperature until the desired size of CdSe NCs was reached (10 s for small cores

and 4.5 min for large cores respectively). The CdSe NCs were separated and cleaned by repeated precipitation with methanol and dispersion in toluene.

For CdSe/CdS dot/rods 60 mg CdO, 280 mg ODPA, 80 mg HPA and 3 g TOPO were degassed at 150 °C and then heated to 300 °C under nitrogen. 1.8 mL TOP were injected, and the temperature was raised to 350 °C. A solution of S in TOP (0.13 g S in 1.8 mL TOP) containing 80 nmol of CdSe core NCs (as determined by optical spectroscopy<sup>[61]</sup>) was injected swiftly. The reaction mixture was kept at this temperature for 8 min and then cooled down. The particles were collected and cleaned by repeated precipitation with methanol and dispersion in toluene. Each sample was finally dispersed in 5 mL toluene for storage.

#### Phase Transfer of CdSe/CdS Building Blocks

The CdSe/CdS dot/rods were phase transferred *via* ligand exchange to MPA.<sup>[62,63]</sup> 4.5 mL of CdSe/CdS dot/rod solution was added to a phase transfer solution containing 250  $\mu$ L MPA and 0.2 g KOH in 10 mL MeOH. This mixture was shaken overnight, the NCs were separated by centrifugation and dispersed in 0.1 M KOH. This solution was cleaned of organic contaminants by the addition of 3 mL chloroform and 10 mL acetone. The NCs were again separated by centrifugation and dispersed in 0.01 M KOH. The Cd<sup>2+</sup> concentration was measured via atom absorption spectroscopy (AAS) and adjusted to 3.6 g/L.

#### Gelation and Drying of CdSe/CdS Networks

CdSe/CdS dot/rod based networks were produced via oxidative removal of the ligands.<sup>[8]</sup> Small amounts of hydrogen peroxide (75  $\mu$ L 0.035% solution) were added to 800  $\mu$ L of aqueous CdSe/CdS dot/rod solution. For mixtures of the two CdSe/CdS dot/rods (small core and large core) the respective volumina were calculated using the particle concentration as obtained from the Cd<sup>2+</sup> concentration and the dot/rod size determined by TEM. These gelation mixtures were heated to 80 °C for 1 min and then kept undisturbed in the dark until a syneresis is visible. The gels are washed by repeated replacement of the supernatant by fresh solvent, first with water and later acetone. After the completed solvent exchange to water-free acetone, the gels can be converted to aerogels by supercritical drying using a critical point dryer (Quorum Technologies E3100). In this, the solvent is first thoroughly exchanged to liquid CO<sub>2</sub> which is afterwards brought to 35 °C at 75 bar (above its critical point). The CO<sub>2</sub> is subsequently released from the dryer to yield NC-based aerogels.

#### Optical Characterization

Optical spectroscopy was performed using an Edinburgh Instruments FLS 1000. For time-resolved measurements the samples were excited using an Edinburgh Instruments EPL-450 (445.1 nm wavelength, 60 ps pulse width) with a repetition rate of 100 kHz if not stated otherwise, scattered excitation light was filtered out using a colored glass filter. Samples were measured in either 3 mL quartz cuvettes (Hellma Analytics) for solutions or in demountable quartz cuvettes (Hellma Analytics) for solid samples. For temperature-resolved measurements, this spectrometer was coupled with an Oxford Instruments OptistatCF cryostat cooled either by liquid nitrogen or liquid helium with the sample in helium gas. In this case, solid samples were loaded into 1.5 mL quartz cuvettes (Hellma Analytics) and liquids were drop-cast onto quartz glass slides. Time-resolved PL decays were fitted by a monoexponential decay ( $f(x) = A e^{-x/\tau} + B$ ) to extract the PL lifetimes ( $\tau$ ). Quantum yield

and absorption measurements were performed using an Edinburgh Instruments integration sphere using 3 mL quartz cuvettes (Hellma Analytics) or Edinburgh Instruments Teflon solid sample holders with quartz cover slides. Quantum yields were calculated using the integrated area of the scattered excitation peak and the integrated area of the emission peak in the integrating sphere measured with and without the sample. Sample absorption was measured by moving excitation and emission monochromator in synchronous and calculating the difference with and without a sample in the integrating sphere. Absorption measurements of colloidal solutions were performed using an Agilent Cary 5000 spectrometer using 3 mL quartz cuvettes. AAS measurements were performed using a Varion AA140, samples were dissolved in aqua regia prepared from AAS grade acids.

#### Electron Microscopy

TEM measurements were performed using a FEI Technai G2 F20. Samples were drop-cast onto carbon foil on copper grids (Quantifoil), for aerogel samples small amounts of aerogel were dispersed in acetone by ultrasonication for 5 seconds before drop-casting.

#### Acknowledgements

The project leading to these results was funded by the European Research Council (ERC) under the European Union's Horizon 2020 research and innovation program (grant agreement 714429). D.D. and N.C.B. would like to thank the German Research Foundation (Deutsche Forschungsgemeinschaft, DFG) for funding under Germany's excellence strategy within the cluster of excellence PhoenixD (EXC 2122, project ID 390833453). D.P. is thankful for support from the Hannover School for Nanotechnology (HSN). The authors thank the Laboratory of Nano and Quantum Engineering (LNQE) for providing the TEM facility. Open Access funding enabled and organized by Projekt DEAL.

#### Conflict of Interest

The authors declare no conflict of interest.

**Keywords:** semiconductor · nanocrystals · aerogels · low temperature spectroscopy · optical characterization · CdSe/CdS dot/rod

- [1] T. Gacoin, L. Malier, J. P. Boilot, *Chem. Mater.* **1997**, *9*, 1502.
- [2] T. Gacoin, K. Lahlil, P. Larregaray, J. P. Boilot, *J. Phys. Chem. B* **2001**, *105*, 10228.
- [3] J. L. Mohanan, I. U. Arachchige, S. L. Brock, *Science* **2005**, *307*, 397.
- [4] I. U. Arachchige, J. L. Mohanan, S. L. Brock, *Chem. Mater.* **2005**, *17*, 6644.
- [5] C. Ziegler, A. Wolf, W. Liu, A. K. Herrmann, N. Gaponik, A. Eychmüller, *Angew. Chem. Int. Ed.* **2017**, *56*, 13200.
- [6] F. Matter, A. L. Luna, M. Niederberger, *Nano Today* **2020**, *30*, 100827.
- [7] A. Singh, B. A. Lindquist, G. K. Ong, R. B. Jadrich, A. Singh, H. Ha, C. J. Ellison, T. M. Truskett, D. J. Milliron, *Angew. Chem. Int. Ed.* **2015**, *54*, 14840.
- [8] S. Sanchez-Paradinas, D. Dorfs, S. Friebe, A. Freytag, A. Wolf, N. C. Bigall, *Adv. Mater.* **2015**, *27*, 6152.

## 5.2. TEMPERATURE AND COMPOSITION DEPENDENT OPTICAL PROPERTIES

- [9] A. Freytag, S. Sánchez-Paradinas, S. Naskar, N. Wendt, M. Colombo, G. Pugliese, J. Poppe, C. Demirci, I. Kretschmer, D. W. Bahnemann, P. Behrens, N. C. Bigall, *Angew. Chem. Int. Ed.* **2016**, *55*, 1200.
- [10] S. Naskar, A. Freytag, J. Deutsch, N. Wendt, P. Behrens, A. Köckritz, N. C. Bigall, *Chem. Mater.* **2017**, *29*, 9208.
- [11] T. Berestok, P. Guardia, M. Ibáñez, M. Meyns, M. Colombo, M. V. Kovalenko, F. Peiró, A. Cabot, *Langmuir* **2018**, *34*, 9167.
- [12] D. Zámbo, A. Schlosser, P. Rusch, F. Lübckemann, J. Koch, H. Pfnür, N. C. Bigall, *Small* **2020**, 1906934.
- [13] N. C. Bigall, A.-K. Herrmann, M. Vogel, M. Rose, P. Simon, W. Carrillo-Cabrera, D. Dorfs, S. Kaskel, N. Gaponik, A. Eychmüller, *Angew. Chem. Int. Ed.* **2009**, *48*, 9731.
- [14] A. Hitihami-Mudiyanselage, K. Senevirathne, S. L. Brock, *ACS Nano* **2013**, *7*, 1163.
- [15] K. K. Kalebaila, S. L. Brock, *Z. Anorg. Allg. Chem.* **2012**, *638*, 2598.
- [16] A. Hitihami-Mudiyanselage, K. Senevirathne, S. L. Brock, *Chem. Mater.* **2014**, *26*, 6251.
- [17] R. Deshmukh, E. Tervoort, J. Käch, F. Rechberger, M. Niederberger, *Dalton Trans.* **2016**, *45*, 11616.
- [18] F. J. Heiligtag, N. Kränzlin, M. J. Süess, M. Niederberger, *J. Sol-Gel Sci. Technol.* **2014**, *70*, 300.
- [19] Q. Yao, S. L. Brock, *Nanotechnology* **2010**, *21*, DOI 10.1088/0957-4484/21/11/115502.
- [20] A. Schlosser, L. C. Meyer, F. Lübckemann, J. F. Miethe, N. C. Bigall, *Phys. Chem. Chem. Phys.* **2019**, *21*, 9002.
- [21] W. Liu, A.-K. Herrmann, D. Geiger, L. Borchardt, F. Simon, S. Kaskel, N. Gaponik, A. Eychmüller, *Angew. Chem. Int. Ed.* **2012**, *51*, 5743.
- [22] W. Liu, P. Rodriguez, L. Borchardt, A. Foelske, J. Yuan, A.-K. Herrmann, D. Geiger, Z. Zheng, S. Kaskel, N. Gaponik, R. Kötz, T. J. Schmidt, A. Eychmüller, *Angew. Chem. Int. Ed.* **2013**, *52*, 9849.
- [23] Z. Fang, P. Li, G. Yu, *Adv. Mater.* **2020**, DOI 10.1002/adma.202003191.
- [24] F. Rechberger, M. Niederberger, *Mater. Horiz.* **2017**, *4*, 1115.
- [25] L. Koralá, J. R. Germain, E. Chen, I. R. Pala, D. Li, S. L. Brock, *Inorg. Chem. Front.* **2017**, *4*, 1451.
- [26] S. Naskar, J. F. Miethe, S. Sánchez-Paradinas, N. Schmidt, K. Kanthasamy, P. Behrens, H. Pfnür, N. C. Bigall, *Chem. Mater.* **2016**, *28*, 2089.
- [27] I. U. Arachchige, S. L. Brock, *J. Am. Chem. Soc.* **2007**, *129*, 1840.
- [28] F. Lübckemann, J. F. Miethe, F. Steinbach, P. Rusch, A. Schlosser, D. Zámbo, T. Heinemeyer, D. Natke, D. Zok, D. Dorfs, N. C. Bigall, *Small* **2019**, *1902186*, 1902186.
- [29] P. Rusch, D. Zámbo, N. C. Bigall, *Acc. Chem. Res.* **2020**, *53*, 2414.
- [30] S. Sekiguchi, K. Niikura, N. Iyo, Y. Matsuo, A. Eguchi, T. Nakabayashi, N. Ohta, K. Jjiro, *ACS Appl. Mater. Interfaces* **2011**, *3*, 4169.
- [31] F. J. Heiligtag, M. D. Rossell, M. J. Süess, M. Niederberger, *J. Mater. Chem.* **2011**, *21*, 16893.
- [32] M. Rosebrock, D. Zámbo, P. Rusch, D. Pluta, F. Steinbach, P. Bessel, A. Schlosser, A. Feldhoff, K. D. J. Hindricks, P. Behrens, D. Dorfs, N. C. Bigall, *Adv. Funct. Mater.* **2021**, 2101628.
- [33] R. Wendt, B. Märker, A. Dubavik, A. K. Herrmann, M. Wollgarten, Y. P. Rakovich, A. Eychmüller, K. Rademann, T. Hendel, *J. Mater. Chem. C* **2017**, *5*, 10251.
- [34] T. Hendel, V. Lesnyak, L. Kühn, A. K. Herrmann, N. C. Bigall, L. Borchardt, S. Kaskel, N. Gaponik, A. Eychmüller, *Adv. Funct. Mater.* **2013**, *23*, 1903.
- [35] T. Mokari, E. Rothenberg, I. Popov, R. Costi, *Science* **2004**, *304*, 1787.
- [36] T. Mokari, C. G. Sztrum, A. Salant, E. Rabani, U. Banin, *Nat. Mater.* **2005**, *4*, 855.
- [37] J. Schlenkrich, D. Zámbo, A. Schlosser, P. Rusch, N. C. Bigall, *Adv. Opt. Mater.* **2021**, 2101712.
- [38] R. Lavieville, Y. Zhang, A. Casu, A. Genovese, L. Manna, E. Di Fabrizio, R. Krahne, *ACS Nano* **2012**, *6*, 2940.
- [39] D. Zámbo, A. Schlosser, R. T. Graf, P. Rusch, P. A. Kißling, A. Feldhoff, N. C. Bigall, *Adv. Opt. Mater.* **2021**, DOI 10.1002/adom.202100291.
- [40] S. F. Wuister, I. Swart, F. van Driel, S. G. Hickey, C. de Mello Donegá, *Nano Lett.* **2003**, *3*, 503.
- [41] F. Di Stasio, J. Q. Grim, V. Lesnyak, P. Rastogi, L. Manna, I. Moreels, R. Krahne, *Small* **2015**, *11*, 1328.
- [42] A. Wolf, V. Lesnyak, N. Gaponik, A. Eychmüller, *J. Phys. Chem. Lett.* **2012**, *3*, 2188.
- [43] P. Rusch, B. Schremmer, C. Strelow, A. Mews, D. Dorfs, N. C. Bigall, *J. Phys. Chem. Lett.* **2019**, *10*, 7804.
- [44] M. G. Lupo, F. Della Sala, L. Carbone, M. Zavelani-Rossi, A. Fiore, L. Lühr, D. Polli, R. Cingolani, L. Manna, G. Lanzani, *Nano Lett.* **2008**, *8*, 4582.
- [45] A. Sift, F. Della Sala, G. Menagen, U. Banin, *Nano Lett.* **2009**, *9*, 3470.
- [46] X. Wen, A. Sitt, P. Yu, Y. R. Toh, J. Tang, *Phys. Chem. Chem. Phys.* **2012**, *14*, 3505.
- [47] M. Grazia Lupo, F. Scotognella, M. Zavelani-Rossi, G. Lanzani, L. Manna, F. Tassone, *Phys. Chem. Chem. Phys.* **2012**, *14*, 7420.
- [48] A. S. Blum, M. H. Moore, B. R. Ratna, *Langmuir* **2008**, *24*, 9194.
- [49] M. G. Spirin, S. B. Brichkin, V. F. Razumov, *High Energy Chem.* **2015**, *49*, 193.
- [50] D. Valerini, A. Creti, M. Lomascolo, L. Manna, R. Cingolani, M. Anni, *Phys. Rev. B: Condens. Matter Mater. Phys.* **2005**, *71*, 1.
- [51] G. Rainò, T. Stöferle, I. Moreels, R. Gomes, J. S. Kamal, Z. Hens, R. F. Mahrt, *ACS Nano* **2011**, *5*, 4031.
- [52] A. D. Balan, H. Eshet, J. H. Olshansky, Y. V. Lee, E. Rabani, A. P. Alivisatos, *Nano Lett.* **2017**, *17*, 1629.
- [53] Y. P. Varshni, *Physica* **1967**, *34*, 149.
- [54] Y. Gao, X. Peng, *J. Am. Chem. Soc.* **2015**, *137*, 4230.
- [55] O. Labeau, P. Tamarat, B. Lounis, *Phys. Rev. Lett.* **2003**, *90*, 257404.
- [56] L. Biadala, B. Siebers, R. Gomes, Z. Hens, D. R. Yakovlev, M. Bayer, *J. Phys. Chem. C* **2014**, *118*, 22309.
- [57] M. G. Lupo, F. Della Sala, L. Carbone, M. Zavelani-Rossi, A. Fiore, L. Lühr, D. Polli, R. Cingolani, L. Manna, G. Lanzani, *Opt. InfoBase Conf. Pap.* **2009**, 1.
- [58] B. T. Diroll, C. B. Murray, *ACS Nano* **2014**, *8*, 6466.
- [59] A. Hinsch, S. H. Lohmann, C. Strelow, T. Kipp, C. Würth, D. Geißler, A. Kornowski, C. Wolter, H. Weller, U. Resch-Genger, A. Mews, *J. Phys. Chem. C* **2019**, *123*, 24338.
- [60] L. Carbone, C. Nobile, M. De Giorgi, F. Della Sala, G. Morello, P. Pompa, M. Hytch, E. Snoeck, A. Fiore, I. R. Franchini, M. Nadasan, A. F. Silvestre, L. Chiodo, S. Kudera, R. Cingolani, R. Krahne, L. Manna, *Nano Lett.* **2007**, *7*, 2942.
- [61] W. W. Yu, L. Qu, W. Guo, X. Peng, *Chem. Mater.* **2003**, *15*, 2854.
- [62] T. Kodanek, H. M. Banbela, S. Naskar, P. Adel, N. C. Bigall, D. Dorfs, *Nanoscale* **2015**, *7*, 19300.
- [63] H. G. Bagaria, E. T. Ada, M. Shamsuzzoha, D. E. Nikles, D. T. Johnson, *Langmuir* **2006**, *22*, 7732.

Manuscript received: October 19, 2021  
 Accepted manuscript online: November 4, 2021  
 Version of record online: November 23, 2021



## 6 Post-Gelation Approach for Structuring Nanocrystal-Based Aerogels

### 6.1 Summary

The formation of aerogels based on nanocrystalline building blocks made from a wide range of different materials has been exhaustively described. One important advantage of these methods is the meticulous control over the building block properties (size, shape, crystal structure, etc.) achieved through the separated synthesis and the methods of nanoparticle chemistry. It is, however, also possible to treat the assembled gel as a substrate which can be further transformed by processes established in nanoparticle chemistry after the network formation (*post-gelation*).

The publication in section 6.2 presents a process to modify whole nanocrystal-based aerogels by wet-chemical methods of nanochemistry. This results in a macroscopic network of assembled connected nanocrystals surrounded by a thin uniform metal oxide. These shells can be demonstrated to significantly increase the mechanical resilience of the networks the modification is applied to, thereby resolving the common problem of the mechanical fragility of NC-based aerogels. The process is developed for a silica shell grown around a substrate of connected CdSe/CdS dot/rod NC building blocks, but is demonstrated to be adaptable to different shell materials (i.e. titania) or network substrates (i.e. based on connected noble metal NCs) by minor modifications in procedure.

## 6.2 Versatile Route to Core-Shell Reinforced Network Nanostructures

Pascal Rusch, Fabian Niemeyer, Denis Pluta, Björn Schremmer, Franziska Lübke, Marina Rosebrock, Malte Schäfer, Mandy Jahns, Peter Behrens, Nadja C. Bigall

Published in: *Nanoscale*, **2019**, 11, 15270-15278

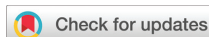
DOI: 10.1039/c9nr03645h

Published by The Royal Society of Chemistry 2019



## Nanoscale

PAPER

View Article Online  
View Journal | View IssueCite this: *Nanoscale*, 2019, **11**, 15270

## Versatile route to core–shell reinforced network nanostructures†

Pascal Rusch,<sup>a</sup> Fabian Niemeyer,<sup>a,c</sup> Denis Pluta,<sup>a,c</sup> Björn Schremmer,<sup>a</sup> Franziska Lübke,<sup>a</sup> Marina Rosebrock,<sup>a</sup> Malte Schäfer,<sup>b,c</sup> Mandy Jahns,<sup>b</sup> Peter Behrens<sup>id</sup><sup>b,c,d</sup> and Nadja C. Bigall<sup>id</sup><sup>\*a,c,d</sup>

In this work we present the generation of new core–shell network nanostructures of macroscopic dimensionality by a two-step process analogous to the seeded-growth method in colloidal nanoparticle modification. The nanoparticle-based core network is assembled first and in a separate second step it is coated with a continuous metal oxide shell by sol–gel methods. The interparticle contact of the nanoparticles comprising the core network is kept intact throughout the process. By analyzing the local elemental distribution, the shells can be shown to be homogeneous over the macroscopic network monolith. The shell network can be used to considerably reinforce the mechanical strength of the final core–shell network structure.

Received 29th April 2019,  
Accepted 19th July 2019  
DOI: 10.1039/c9nr03645h

rsc.li/nanoscale

## Introduction

After the introduction of aerogels in 1931 by Kistler<sup>1</sup> and the optimistic outlook to extend the list of materials from which aerogels can be generated, it still took the better part of a century until a method was used to generate nanocrystal-based aerogel networks in 2005.<sup>2,3</sup> This method to form randomly oriented network structures out of pre-formed colloidal nanoparticles offers higher customizability as it allows the fine tuning of the individual building blocks by modern colloid chemical routes as opposed to the one-step generation of particles and networks in molecular routes of conventional sol-gel chemistry. In recent years the number of nanoparticle materials that were converted into such macroscopic and porous network structures steadily increased<sup>4–7</sup> and was expanded to noble metals<sup>8</sup> as well as a number of intricate particles provided by the well advanced chemical synthesis of nanoparticles.<sup>9–13</sup> The procedure usually includes the controlled destabilization of a colloidally stable nanoparticle solution, often by attacking the stabilizing ligand shell of the particle, *e.g.*, by oxidation agents. More recently different methods

were described based on connecting the particles – sometimes also reversibly – *via* the interaction of ligands, organic and inorganic, with added cations.<sup>14,15</sup> Also methods completely free of chemical interactions but rather based on physical procedures have been employed.<sup>16</sup> Still, as the catalogue of new nanoparticles grows and the number of these converted into self-supporting 3D networks increases, generally this innovation stops once a network is indeed generated.

In this work we want to show that the network formation alone does not need to be the last step, but instead some of the modification procedures developed for colloidal nanoparticles can – under the right conditions – be applied to a nanoparticle network substrate as well. Network structures build up from metal nanoparticle building blocks have shown very promising results as catalysts in the oxygen evolution reaction<sup>17,18</sup> as well as fuel cell applications.<sup>19</sup> Similarly semiconductor nanoparticle based networks were employed as photocatalysts.<sup>20</sup> Our group recently demonstrated a semiconductor network based sensor also showing the higher sensitivity of the network compared to plain nanoparticles.<sup>21</sup> One drawback of the monolithic network structures is their poor mechanical stability which is widely regarded as the point inhibiting application of these networks.<sup>22,23</sup> Here, we propose the method of post-assembly shell growth as a new way to increase mechanical stability and thereby resolve one major problem holding self-supporting nanoparticle network structures back from their potential applications. For example, in recent studies of the catalytic activity of nanoparticle aerogels, it was found that either the networks had to be broken apart and dispersed<sup>24</sup> or the reaction conditions needed to be changed drastically<sup>13</sup> to accommodate this problem. It has recently been shown that it is possible to grow metallic shells

<sup>a</sup>Institute of Physical Chemistry and Electrochemistry, Leibniz Universität Hannover, Callinstrasse 3A, 30167 Hannover, Germany.  
E-mail: nadja.bigall@pci.uni-hannover.de

<sup>b</sup>Institute for Inorganic Chemistry, Leibniz Universität Hannover, Callinstrasse 9, 30167 Hannover, Germany

<sup>c</sup>Laboratory of Nano and Quantum Engineering, Leibniz Universität Hannover, Schneiderberg 39, 30167 Hannover, Germany

<sup>d</sup>Cluster of Excellency PhoenixD (Photonics, Optics, and Engineering – Innovation Across Disciplines), Hannover, Germany

†Electronic supplementary information (ESI) available: Rehydration experiments, further TEM and SEM measurements. See DOI: 10.1039/c9nr03645h



Nanoscale

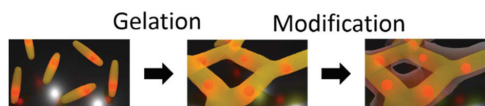


Fig. 1 Schematic depiction of the two-step process employed: first, the assembly of individual nanocrystal building blocks into a porous network structure and second the modification of this network by shell growth.

around nanoparticle-based networks by electrochemical deposition.<sup>25</sup> Our method also entails another modification step after the initial nanoparticle network formation but using wet-chemical methods. The method employed is similar to a seeded growth mechanism in colloid chemistry, where first nanocrystal seeds are synthesized and subsequently a different compound can be grown onto the seeds under conditions of heterogeneous nucleation only. In our method, however, instead of the seed nanoparticle we employ a seed nanoparticle network, as schematically shown in Fig. 1. More specifically, we propose the growth of metal oxide shells around the whole NANOparticle-based NETWORK Structure (NANONETS) (consisting of interconnected nanocrystal building blocks) using sol-gel processes. The method presented in this work is applicable for different substrates as shown by the shell growth onto the semiconductor NANONETS as well as metallic ones. It can also be used to grow not only silica shells but also titania alike (also see Fig. 2). This indicates the versatility of our approach.

Contrary to other methods already published in the literature we do not embed particles in a gel matrix made of the metal oxide.<sup>26–29</sup> Instead the original network is made up of the nanoparticle based “core” network which is encased in a second “shell” network applying a post-assembly coating step. The crystal-to-crystal contact between the nanoparticles in the “core” network is still present in the newly formed structure, as schematically illustrated in Fig. 1.

## Experimental

### Chemicals used

Tri-*n*-octylphosphine oxide (TOPO, 99%), 3-mercaptopropionic acid (MPA, 99%), potassium hydroxide (KOH, >85%), hexane (99%), toluene (99.7%), methanol (99.8%), sulfur (S, 99.98%), ammonia (NH<sub>3</sub>, 28.0–30.0% aqueous solution), titanium(IV) butoxide (97%), sodium borohydride (98%), (3-aminopropyl)-trimethoxysilane (APTMS, 97%) and tetraethyl orthosilicate (TEOS, 99.999%) were purchased from Sigma-Aldrich. Acetone (99.5%) and hydrogen peroxide (35% aqueous solution) were purchased from Honeywell. Cadmium oxide (CdO, 99.998%), hydrogen tetrachloroaurate trihydrate (99.99%), silver nitrate (99.9%) and selenium (Se, 99.999%) were purchased from Alfa Aesar. Hexylphosphonic acid (HPA, >99%) and octadecylphosphonic acid (ODPA, >99%) were purchased from PCI Synthesis. Tri-*n*-octylphosphine (TOP, 97%) and trisodium citrate dihydrate (99.0%) were purchased from ABCR. Acetylacetone

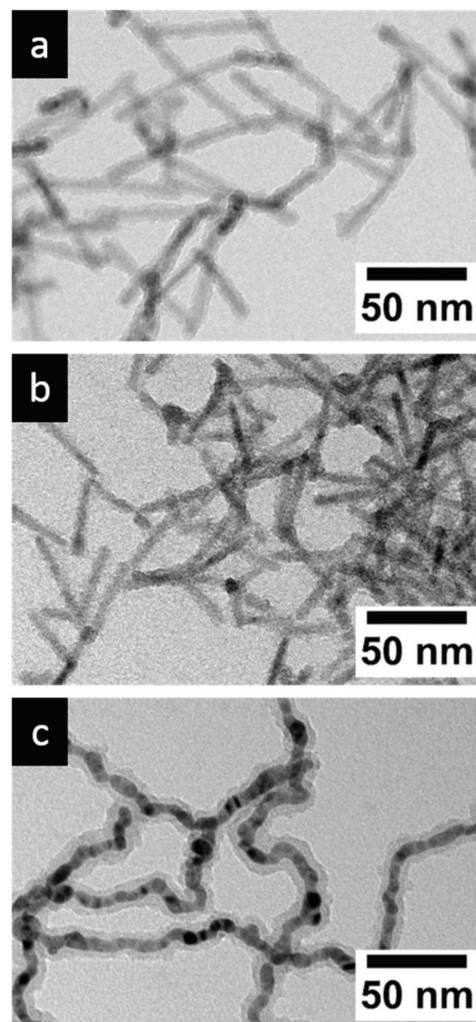


Fig. 2 Different material combination of post-gelation modified networks. (a) CdSe/CdS nanorod core network with a silica shell, (b) CdSe/CdS nanorod core network with a titania shell and (c) Au–Ag mixed core network with a silica shell.

(acac, 99%) was purchased from Merck. Ethanol (99.8%) was purchased from Roth. All chemicals were used as received.

### Synthesis procedures

The CdSe/CdS nanorods used for network formation were synthesized according to the literature procedure<sup>30</sup> and assembled as described in earlier studies of our group.<sup>12</sup> The whole process will be described briefly here.

**Synthesis of CdSe cores.** CdSe quantum dots were synthesized by mixing 60 mg of CdO with 280 mg of ODPA and



3 g of TOPO in a 25 mL three-neck-flask and degassed at 150 °C for one hour. The temperature was raised to 300 °C under a nitrogen atmosphere to dissolve CdO. 1.8 mL of TOP was added and the mixture was heated to 380 °C. At this point 58 mg of Se powder dissolved in 1.8 mL of TOP (equimolar mixture) was injected by a syringe. Due to the injection the temperature of the mixture decreased, it was allowed to reach 380 °C again, and then the reaction mixture was cooled down to room temperature. The quantum dots were precipitated by the addition of methanol and centrifuged. The quantum dots were washed twice by dispersion in toluene and precipitation by methanol and afterwards stored in toluene.

**Synthesis of CdSe/CdS nanorods by the seeded growth method.** For the growth of rod shaped shells around the CdSe quantum dots 60 mg of CdO were mixed with 280 mg of ODPa, 80 mg of HPA, and 3 g of TOPO and degassed at 150 °C for one hour. Under a nitrogen atmosphere the temperature was increased to 300 °C and 1.8 mL of TOP is added. The temperature was raised to 380 °C and a mixture of S in TOP (130 mg S in 1.8 mL TOP) and the dissolved CdSe cores (400 µM, concentration estimated by optical spectroscopy<sup>31</sup>) was injected. After six minutes of reaction time the mixture was allowed to cool to room temperature. The nanorods produced by this method were precipitated, washed in a similar way to the quantum dots in the first step and stored in 6 mL of toluene.

**Transfer of CdSe/CdS nanorods into aqueous solution.** The phosphine capped nanorods need to be transferred into water for network formation. This was done by exchanging the ligands with mercaptopropionic acid (MPA) as described in the literature.<sup>32,33</sup>

The nanorods in solution (750 µL) were precipitated by the addition of methanol and centrifuged at 5000 rcf. The supernatant was discarded and the particles were dissolved in 10 mL of hexane. To this solution 242 µL of MPA was added as well as 10 mL of a 0.1 M solution of KOH in methanol. The mixture is shaken for 24 hours during which the now MPA capped nanorods precipitated. The particles were separated from the remaining phase transfer solution by centrifugation and could be dissolved in 0.1 M aqueous KOH.

**Assembly of the CdSe/CdS nanorod network.** The aqueous solution of nanorods was diluted to a cadmium ion concentration of 3.6 mg mL<sup>-1</sup> and 800 µL of this solution were mixed with 75 µL of 0.35% hydrogen peroxide. The solution was thoroughly mixed and heated to 80 °C for one minute. It was then left undisturbed in the dark for one hour and afterwards a macroscopic network structure is formed. The network was washed by multiple additions of water and removal of the supernatant.

**Synthesis of noble metal nanoparticle network structures.** Noble metal nanoparticles were prepared and assembled into network structures according to literature procedures.<sup>8</sup> For the preparation of Au nanoparticles 36.2 mL of a 0.2 wt% H[AuCl<sub>4</sub>]:3H<sub>2</sub>O solution was added to 465 mL of distilled water. To this solution 11.6 mL of 1% sodium citrate solution was added and after 30 seconds 5.5 mL of sodium borohydride solution (prepared by dissolving 39 mg of NaBH<sub>4</sub> in 50 mL of

1% sodium citrate solution) was quickly added. This was left to stir for 30 minutes. The prepared nanoparticle dispersion was concentrated by filtration down to a volume of 10 mL. During this the particles were washed by repeatedly adding 5 mL of distilled water and concentrated by filtration. Ag nanoparticles were prepared in a similar manner using 12 mL of 0.2% AgNO<sub>3</sub> solution as a noble metal precursor and by performing the reduction in boiling solution. The two noble metal nanoparticle dispersions were mixed in equal volumes (here 0.5 mL) and 0.4 mL of 1% hydrogen peroxide solution was added to the mixture. Network formation took place within 5 weeks.

**Modification of networks with a metal oxide shell.** As the first step of modification of the nanoparticle network with a silica shell the solvent surrounding the network had to be thoroughly exchanged to methanol as residual water will influence the formation of silica. The solvent exchange was done by discarding the liquid above the network and adding fresh methanol. This process was repeated twice a day for at least five days. Afterwards tetraethyl orthosilicate (TEOS) as a silica precursor was added and the sample was left undisturbed for 24 hours to give the precursor time to diffuse into the network pores. The amount of TEOS used is calculated in relation to the cadmium amount inside the network. A typical network contained 2.88 mg or 26 µmol of cadmium. For an equimolar relation of cadmium and silicon, 5.7 µL of TEOS was needed. After the one-day period a specific amount of water (0–50 mmol) and ammonia (0–400 µmol) was added to the sample and it was again left undisturbed for 24 hours to react. After the reaction the network structure was washed with methanol by repeatedly exchanging the solvent to fresh methanol to flush out byproducts.

The coating of networks with titania was performed accordingly using titanium *n*-butoxide as a metal oxide precursor. As the hydrolysis of titanium alkoxides is much faster than the reaction of the equivalent silicon compounds acetylacetonate was added in this case to slow down the reaction by complexing the titanium cation. The amount of acetylacetonate was chosen in relation to the amount of titania precursor added.

The coating of noble metal nanoparticle based networks was performed in an identical manner. In this case the addition of a linker, namely, APTMS, at a 0.1 ratio compared to the noble metal concentration could be used to improve the uniformity of the shells.

**Supercritical drying.** To dry the nanoparticle network, structures were transferred into dry acetone by exchanging the solvent twice per day for at least five days with acetone dried over molecular sieves, 3 Å. The samples prepared by this solvent exchange were carefully loaded into a critical point dryer (Quorum Technologies E3100). The apparatus was filled and additionally flushed for five minutes with liquid CO<sub>2</sub> at a pressure of 55 bar at 20 °C. CO<sub>2</sub> was allowed to diffuse into the network overnight and flushing was repeated once before drying. For supercritical drying the drier was heated above the critical point of CO<sub>2</sub> at 31.1 °C. During the process the pressure inside the drying chamber rose to about 73 bar. Once



CO<sub>2</sub> was in the supercritical state it was allowed to slowly vent into the atmosphere while retaining temperatures above 31 °C. Once the pressure inside the drying chamber was at the atmospheric value the dried networks could be recovered from the apparatus and were further characterized.

### Characterization

**Electron microscopy.** TEM samples of nanoparticles in solution were prepared by drop casting diluted solutions in chloroform onto a carbon coated copper grid (300 mesh) by Quantifoil. For sample preparation of dried networks, the mentioned grids were pulled along the sample, thereby keeping small parts of the network stuck to the grid. The bright-field (BF-TEM) measurements were carried out using a FEI Tecnai G2 F20 transmission electron microscope with a field emission gun operating at 200 kV. For high-angle annular dark field (HAADF-STEM) measurements coupled with energy-dispersive X-ray spectroscopy (EDX) a JEOL JEM-2100F with an acceleration voltage of 200 kV was employed.

SEM samples were prepared by finely slicing off a part of the macroscopic network structure with a scalpel. This section was stuck to the adhesive carbon film and measured. The SEM used was a JEOL JSM 6700F field emission scanning electron microscope with an acceleration voltage of 2 kV and a secondary electron detector at a working distance of 8 mm. In the SEM, elemental analysis was performed using an Oxford Instruments INCA 300 energy dispersive X-ray spectrometer with the SEM operating at 10 kV at a working distance of 15 mm.

**Compression tests.** The compression tests were performed on an Instron 5565A by placing the monolithic dried network structure between the plates of the device. As the samples are not completely uniform, an irregular shape was assumed for the interpretation of the data. The contact area between the pressure plate and the sample was estimated by measuring the area of the sample from a photograph taken from above. The plates are pressed together at a constant rate of 0.2 mm s<sup>-1</sup> and the force acting on the plates is measured. The measurement was stopped when either the material showed a mechanical failure (in the case of the unmodified gel in the form of multiple breakages) or when the pressure reached 50 N. The stress and strain are calculated using the initial contact area of the monolith and plate and the initial height of the monolith, respectively.

**Physisorption measurements.** Physisorption measurements were carried out on a Quantachrome Autosorb-1 at 87 K employing Krypton as the measurement gas. Before the measurement the samples were degassed at room temperature for 24 h. The surface areas were estimated using the Brunauer–Emmett–Teller (BET) equation.<sup>34</sup>

## Results and discussion

For the functionalization of nanoparticles with a silica shell, a plethora of methods is described in the literature which are mostly based on the Stöber process.<sup>35</sup> Due to the substrate not being a nanoparticle in solution but rather a macroscopic

body (consisting of a network of nanocrystals), methods involving microemulsions<sup>36,37</sup> could not be used. We therefore opted for a synthesis that is similar to the direct coating methods reported,<sup>38,39</sup> with much simpler conditions than the microemulsion routes in terms of the solvent system since no surfactants are employed, see the Experimental section for details. This procedure could be used with small adaptations for the growth of titania shells as well as for the growth of silica on noble metal NANONETSs. The successful modification of the NANONETS with a metal oxide shell can be observed by transmission electron microscopy (TEM) as shown in Fig. 2.

For the pristine semiconductor NANONETS a smooth surface of the NRs forming the network is visible (Fig. 3b) in the TEM measurements. With increasing amounts of metal oxide precursor added to the structure there is no optical difference between the dried network structures as can be seen in the photographs under UV- and daylight (Fig. 3a). In electron microscopy an increase in surface roughness is visible due to small domains of silica forming on the nanocrystal surfaces (see Fig. 3c and d). In these cases, the difference in electronic TEM contrast between silica and the NRs is unfortunately not sufficient to make the new shell clearly distinguishable from cadmium sulfide. With higher amounts of silica precursor and consequently thicker shells, the core network and the surrounding silica shell become easily discernable (Fig. 3e). The porous structure of the network is visible in the SEM (Fig. 4d) and could also be measured by krypton physisorption. The surface area derived from the BET evaluation is 100 m<sup>2</sup> g<sup>-1</sup> for the unmodified network which is comparable to the ones reported for similar structures.<sup>11,40</sup> After the modification the BET surface areas increase considerably to 160–180 m<sup>2</sup> g<sup>-1</sup> potentially due to microporosity in the silica shell itself as well as the higher mechanical stability, preventing the network from damage during processing. It also indicates that the modification does not block the porosity of the network (see Fig. S11†).

The successful modification with a homogeneous silica shell is clearly visible in the nanometer size regime. However, this only shows the modification in a random spot test. Hence, to investigate the homogeneity of the modification on a much larger scale, scanning electron microscopy (SEM) with elemental analysis by energy-dispersive X-ray spectroscopy (EDX) is employed. The elemental distribution is measured at different positions of a section of the modified NANONETS. These samples are prepared by slicing a thin piece off the body of the network structure (possible for samples with Si/Cd ratios larger than 1) without further modification of the sample (schematically shown in Fig. 4a). It should be noted that this is to the best of our knowledge the first time that the dried network of nanoparticles can be cut easily by simply employing a scalpel, since “conventional” nanocrystal network structures are either far too brittle or far too deformable for such a preparation method. By our post-assembly silica growth route, it is possible to perform structural investigations of nanocrystal network structures to a greater extent. Here, we have investigated the ratio of Si/Cd at various points in the NANONETS (center, top, bottom, and outer areas) in order to determine



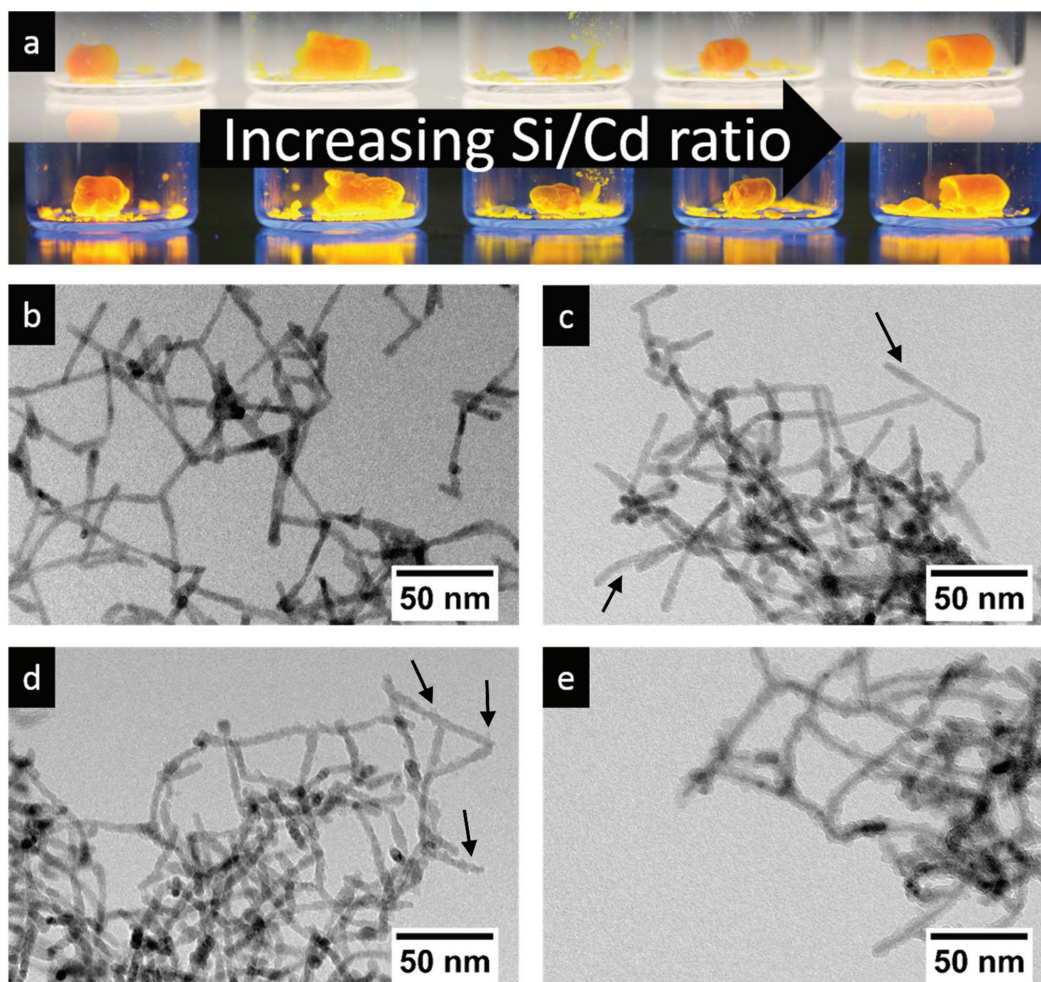


Fig. 3 Core-shell network structures prepared with different ratios of silica precursors relative to the cadmium content of the core network. (a) Photographs of the monolithic dried networks under ambient (top) and UV (bottom) light with increasing amounts of silica precursor added from left to right (starting at 0 to 10/1). TEM micrographs of networks modified with different silica/cadmium ratios, (b) 0/1, (c) 1/1, (d) 2/1 and (e) 10/1. Arrows are used to indicate some of the recognizable domains of silica growth on the building block surfaces.

the homogeneity of our silica shell growth route. The SEM images show the highly porous network structure expected for these types of nanoparticle assemblies (Fig. 4d). The elemental measurements illustrate the silica-shell modification as well as its homogeneity. In the case of low silica amounts ( $\text{Si}/\text{Cd} < 1/1$ ) the NANONETS breaks uncontrollably during sample preparation and random measurement positions were chosen (see the ESI†). Still, the elemental measurements fit well within our assumption of a largely homogeneous silica shell growth as discussed in the ESI.† For higher amounts of silica the NANONETS can be sliced in a controlled way and so the elemental distribution can be examined from the surface of

the NANONETS down to the center. As an example, the measurement positions for one sample are marked in Fig. 3c on an overview (for positions on other samples see Fig. S4–S6† for the corresponding EDX spectra). In the case of NANONETSs modified with an initial (that is, as inserted during synthesis) ratio of 2/1 of Si/Cd, this initial ratio is retained for the surface part of the final structure, while in the center the ratio drops to 1.64/1. When an initial ratio of 10/1 of Si/Cd is used, the ratio measured from the surface of the NANONETS is 7.5/1 (measured at the position “outside”) going down to 4.8/1 inside the structure (measured at the position “center”). This gradient in the Si/Cd ratio exemplifies the strong influence of



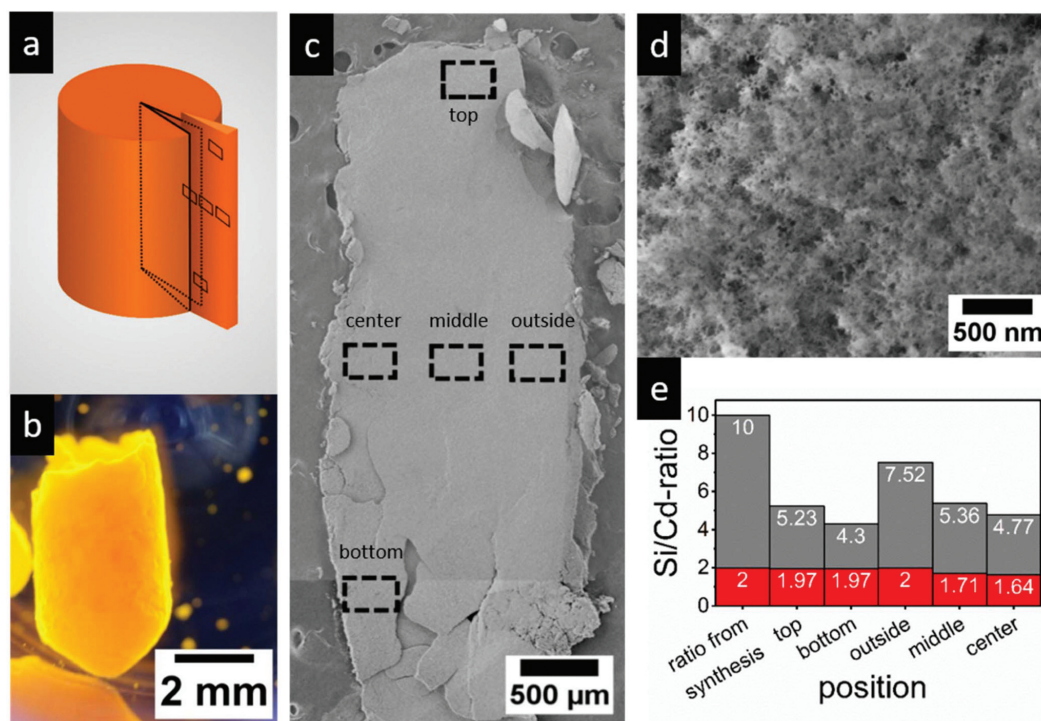


Fig. 4 Analysis of local elemental distribution to evaluate the homogeneity of the silica shells. (a) Schematic depiction of the SEM sample in relation to the whole network body and (b) photograph of a dried network monolith under UV light to demonstrate the shape analogy. (c) Large scale SEM micrograph of the network slice modified with an initial Si/Cd ratio of 10/1, depicting the measurement positions for EDX (assembled from two separate pictures) and (d) higher resolution SEM image of the same network structure displaying the porous structure. (e) Si/Cd ratio found by EDX measurements at various measurement positions for initial Si/Cd ratios of 10/1 in grey and 2/1 in red.

the transport limitation inside of the network pores, so that the modification is therefore not totally uniform for the whole of the macroscopic body of the NANONETS. On the other hand, it also shows that the modification is – while not completely uniform – present over the whole macroscopic network. It needs to be taken into account that transport is a major obstacle in the attempt of transferring nanoparticle modification methods in colloidal solution onto nanoparticle network substrates. Considering that the size regime of the distance that the silica precursors have to travel is increased from nanometers in a colloid to millimeters in such types of networks, the silica shells produced by this method throughout the structure are remarkably homogeneous.

The pH-value and concentration of water are key parameters for the Stöber synthesis. The standard parameters for this work have been adapted from literature procedures for the functionalization of noble metal nanoparticles with a silica shell in solution.<sup>41</sup> The parameters are then varied to optimize the functionalization for a NANONETS substrate. The amount of water and ammonia is varied from no addition of the reactant to a tenfold excess in the case of ammonia or a fivefold

excess in the case of water compared to the standard values adapted from the literature. All other parameters are kept constant. From the TEM micrographs of the NANONETS the clear necessity of both water and ammonia for the modification process can be derived. If neither water nor ammonia is added (Fig. S2a†) the shell growth is highly inhomogeneous even on a low size scale. Silica forms probably by reaction with residual water in the pores or from the atmosphere, but it does not form a clearly defined shell around the network. Instead some pores are filled with silica, while no silica is visible in other places. If only 30% ammonia solution is added but no additional water, the results are quite similar (Fig. S2b†). In this case a silica gel seems to form encasing the original NANONETS. The pores of the original structure are filled with the silica material. If water is added but no ammonia, the growth of silica also appears to be largely inhomogeneous (Fig. S3a†) with thicker silica shells visible at certain spots and no shell visible at other places. As soon as both reactants, water and ammonia, are added, the desired structure of the original NANONETS is surrounded by a continuous silica shell without any visible side nucleation. While the amount of



ammonia does not seem to have a pronounced influence for the volumes investigated as long as it is present (Fig. S3†), water concentrations between 2 and 10 mmol mL<sup>-1</sup> yield the most homogeneous and pronounced silica shells (Fig. S2†).

It was also investigated if it was possible to transfer these reaction conditions while changing either the core network material or the shell material. To this end similar conditions were applied while using titanium butoxide instead of tetraethyl orthosilicate (Fig. 1c). With this it was possible to grow titania shells in an equal manner (also see Fig. S7†). Slight adjustments in this procedure are needed such as the addition of acetylacetonate (acac). acac acts as a chelating ligand which considerably decreases the reactivity of the precursor. This counteracts the effect that titania alkoxides are in general much more reactive compared to silica alkoxides as has been described for similar processes in colloidal particle modification (also see Fig. S8†).<sup>42,43</sup> When examining the local elemental distribution by SEM-EDX as described for the silica shells earlier this influence is clearly visible. Without the addition of acac the homogeneous nucleation of titania outside of the network is immediately visible even by the eye. If the amount of acac in relation to the amount of titania precursor is increased the ratio of Ti/Cd measured inside the network increases due to the suppression of homogeneous nucleation. Also the homogeneity increases, indicated by the small difference in the Ti/Cd ratio measured at different spots on the gel. However, if very high amounts of acac are added the titania shell formation inside the gel is suppressed and there is almost no titania grown in this instance. A ratio of 2/1 acac/Ti-precursor seems to yield the most promising results in this study. The BET surface area of this titania modified network is ca. 140 m<sup>2</sup> g<sup>-1</sup> which is still higher than that of the unmodified networks (see Fig. S11†).

Furthermore, it was possible to use networks assembled from a mixture of gold and silver nanoparticles to grow a noble metal core silica shell network. Electron micrograms of these are shown in Fig. 5. The nanoparticles assemble into a chain-like interconnected highly porous network structure. In higher magnifications the silica shell is clearly visible homogeneously surrounding the whole continuous network (Fig. 5b). Measuring the elemental distribution at high magnifications is very difficult as the networks tend to move during the measurement. Still in the HAADF-STEM the shell is visible as a slightly brighter shell surrounding the noble metal chains. In the EDX signals of all three elements of interest (Au, Ag and Si) are detected along the chains of the network (Fig. 5c and d). The physisorption measurements revealed a BET surface area of the pristine Au-Ag nanoparticle networks of 25 m<sup>2</sup> g<sup>-1</sup> which is similar to the values reported in the literature.<sup>8</sup> As was the case for semiconductor nanoparticle based networks this surface area increases considerably with the silica modification to 105 m<sup>2</sup> g<sup>-1</sup> (see Fig. S11†). This hints at the large inner surface of the porous silica shell. Similar to the growth of titania shells in this instance it was also needed to minimally adjust the experimental procedure. The addition of low amounts of a silica linker (here: 3-aminopropyl-trimethoxy-

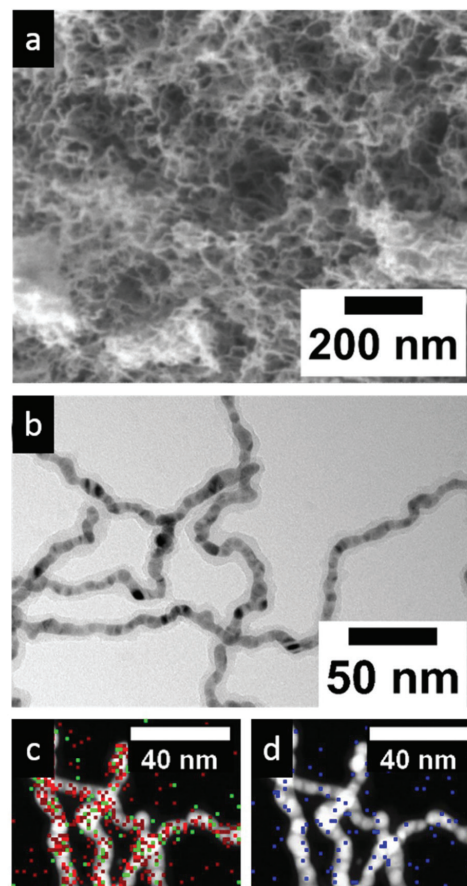


Fig. 5 Network consisting of a mixture of Au and Ag nanoparticles with a silica shell grown around the network in (a) SEM, (b) BF-TEM and (c, d) HAADF-STEM with the overlaying EDX measurement. Red color indicates Au, green Ag and blue Si.

silane, at a 0.1 ratio compared to the amount of silica precursor used) was needed to grow homogeneous shells (also see Fig. S9† for details). Without the addition of a linker the shell growth is not homogeneous and limited to randomly dispersed spots on the network structure.

The silica shell modification was expected to considerably increase the resistivity of the NANONETS towards mechanical stress as the network is essentially reinforced by the shell. Although the mechanical instability of nanoparticle networks is often a drawback it is seldom investigated or even mentioned in the literature. In fact the studies of mechanical properties have been reported only for organic aerogels,<sup>44,45</sup> carbon aerogels<sup>46,47</sup> or silica aerogels<sup>48,49</sup> and recently for other metal-oxide aerogels.<sup>50</sup> In this work a compression test was employed to evaluate the mechanical stability of silica



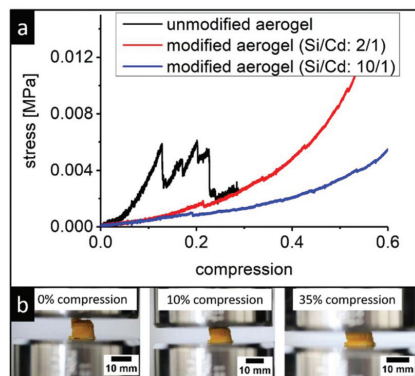


Fig. 6 (a) Mechanical measurement of dried silica shell modified and unmodified CdSe/CdS NR networks by compression tests. The photographs (b) show a silica shell modified network structure (Si/Cd 10/1) at various points of the measurement.

shell modified and unmodified NANONETSs. As the dimensions of the NANONETS are small, and as the forces the samples are subjected to are also very small, it is not possible to actually measure the Young's modulus (which is usually done in the area of elastic deformation at low strain levels). Still, information about the relative mechanical stability can be obtained by the measurements performed. The measurements of the unmodified NANONETS show a drastic drop in stress, which occurs when a large part of the structure breaks and is a signature of its brittleness.

This is not observed in the case of silica modified networks (see Fig. 6) within the measurement range investigated. In a more practical context this increased mechanical resistance can also be observed when the dried NANONETS is added back to a solvent, *i.e.*, water. The unmodified NANONETS falls apart in a few seconds into a multitude of small particles (Fig. S10<sup>†</sup>), which we attribute to the occurrence of capillary forces. In contrast, the silica shell modified NANONETS sinks to the bottom of the container after some time while still remaining largely in one piece (also see Fig. S10<sup>†</sup>). This result further emphasizes the benefit of post-assembly silica shell growth for nanoparticle aerogels, since it enables rehydration while keeping the advantageous properties of the nanocrystal networks in the macroscopic body.

## Conclusions

In summary, we have presented a novel approach to the metal oxide shell modification of the NANONETS which leaves the initial network and the interparticle crystal-to-crystal contact intact. To our knowledge this marks the first time that the possibility of modifying self-supporting nanocrystal networks by a sol-gel post-assembly modification with a thin inorganic shell has been described. This process leads to a new, formerly unknown structure. This method was employed to successfully

coat nanostructures of different compositions ranging from the semiconducting to metallic ones and is therefore highly versatile. It could also be expanded to the growth of titania instead of silica. The integrity of the nanocrystal network could be confirmed by electron microscopy measurements and the homogeneity of the silica shell was examined by local elemental analysis and found to be highly uniform over the whole body for all modifications performed. It could be shown that the modification with silica shells severely increases the mechanical stability of the structures, which can now be cut into pieces without breaking. All of this opens up a plethora of new possible applications of nanocrystal network assemblies in, *e.g.*, electrochemistry or catalysis where the network structures would need to be rehydrated with an electrolyte while maintaining the network properties. Due to the increased mechanical stability the fabrication of flow-through reactors can be imagined as well as the introduction of external stirring to facilitate mixing. All this can be done while retaining the monolithic structure, leading to an easy separation. As the particles forming the core network are still connected the networks should be able to conduct generated charge carriers, potentially improving the efficiency of the catalyst. Also the transfer of this method to other catalytically active metal oxides could prove interesting.

## Conflicts of interest

There are no conflicts to declare.

## Acknowledgements

The authors would like to thank Armin Feldhoff and Juergen Caro for the use of the SEM, as well as the Laboratory of Nano and Quantum Engineering for the use of the TEM and their support. The authors would also like to thank the REBIRTH cluster of excellence for access to the mechanical testing experiment. The project leading to these results received funding from the European Research Council (ERC) under the European Union's Horizon 2020 research and innovation programme (grant agreement No. 714429). N. C. B. furthermore acknowledges funding from German Federal Ministry of Education and Research (BMBF) within the framework of NanoMatFutur (support code 03X5525). This project was in part funded by the Deutsche Forschungsgemeinschaft (DFG, German Research Foundation) under Germany's Excellence Strategy within the Cluster of Excellence PhoenixD (EXC 2122). M. S. is grateful for a fellowship from the PhD programme "Hannover School for Nanotechnology-Sensors" of the LNQE, funded by the state of lower Saxony.

## Notes and references

- 1 S. S. Kistler, *Nature*, 1931, **127**, 741–741.
- 2 J. L. Mohanan, I. U. Arachchige and S. L. Brock, *Science*, 2005, **307**, 397–400.



- 3 I. U. Arachchige, J. L. Mohanan and S. L. Brock, *Chem. Mater.*, 2005, **17**, 6644–6650.
- 4 K. K. Kalebaila, D. G. Georgiev and S. L. Brock, *J. Non-Cryst. Solids*, 2006, **352**, 232–240.
- 5 A. Hitihami-Mudiyanselage, K. Senevirathne and S. L. Brock, *ACS Nano*, 2013, **7**, 1163–1170.
- 6 S. Ganguly and S. L. Brock, *J. Mater. Chem.*, 2011, **21**, 8800.
- 7 N. Gaponik, A. Wolf, R. Marx, V. Lesnyak, K. Schilling and A. Eychmüller, *Adv. Mater.*, 2008, **20**, 4257–4262.
- 8 N. C. Bigall, A.-K. Herrmann, M. Vogel, M. Rose, P. Simon, W. Carrillo-Cabrera, D. Dorfs, S. Kaskel, N. Gaponik and A. Eychmüller, *Angew. Chem., Int. Ed.*, 2009, **48**, 9731–9734.
- 9 H. Yu and S. L. Brock, *ACS Nano*, 2008, **2**, 1563–1570.
- 10 I. U. Arachchige and S. L. Brock, *J. Am. Chem. Soc.*, 2007, **129**, 1840–1841.
- 11 S. Naskar, J. F. Miethe, S. Sanchez-Paradinas, N. Schmidt, K. Kanthasamy, P. Behrens, H. Pfnür and N. C. Bigall, *Chem. Mater.*, 2016, **28**, 2089–2099.
- 12 S. Sanchez-Paradinas, D. Dorfs, S. Friebe, A. Freytag, A. Wolf and N. C. Bigall, *Adv. Mater.*, 2015, **27**, 6152–6156.
- 13 S. Naskar, A. Freytag, J. Deutsch, N. Wendt, P. Behrens, A. Köckritz and N. C. Bigall, *Chem. Mater.*, 2017, **29**, 9208–9217.
- 14 V. Lesnyak, S. V. Voitekhovich, P. N. Gaponik, N. Gaponik and A. Eychmüller, *ACS Nano*, 2010, **4**, 4090–4096.
- 15 V. Sayevich, B. Cai, A. Benad, D. Haubold, L. Sonntag, N. Gaponik, V. Lesnyak and A. Eychmüller, *Angew. Chem., Int. Ed.*, 2016, **55**, 6334–6338.
- 16 A. Freytag, S. Sánchez-Paradinas, S. Naskar, N. Wendt, M. Colombo, G. Pugliese, J. Poppe, C. Demirci, I. Kretschmer, D. W. Bahnemann, P. Behrens and N. C. Bigall, *Angew. Chem., Int. Ed.*, 2016, **55**, 1200–1203.
- 17 W. Liu, A.-K. Herrmann, D. Geiger, L. Borchardt, F. Simon, S. Kaskel, N. Gaponik and A. Eychmüller, *Angew. Chem., Int. Ed.*, 2012, **51**, 5743–5747.
- 18 W. Liu, P. Rodriguez, L. Borchardt, A. Foelske, J. Yuan, A.-K. Herrmann, D. Geiger, Z. Zheng, S. Kaskel, N. Gaponik, R. Kötz, T. J. Schmidt and A. Eychmüller, *Angew. Chem., Int. Ed.*, 2013, **52**, 9849–9852.
- 19 S. Henning, H. Ishikawa, L. Kühn, J. Herranz, E. Müller, A. Eychmüller and T. J. Schmidt, *Angew. Chem., Int. Ed.*, 2017, **56**, 10707–10710.
- 20 L. Korala, J. R. Germain, E. Chen, I. R. Pala, D. Li and S. L. Brock, *Inorg. Chem. Front.*, 2017, **4**, 1451–1457.
- 21 A. Schlosser, L. C. Meyer, F. Lübke, J. F. Miethe and N. C. Bigall, *Phys. Chem. Chem. Phys.*, 2019, **21**, 9002–9012.
- 22 B. Cai, V. Sayevich, N. Gaponik and A. Eychmüller, *Adv. Mater.*, 2018, **30**, 1707518.
- 23 W. Wan, R. Zhang, M. Ma and Y. Zhou, *J. Mater. Chem. A*, 2018, **6**, 754–775.
- 24 D. Wen, W. Liu, D. Haubold, C. Zhu, M. Oschatz, M. Holzschuh, A. Wolf, F. Simon, S. Kaskel and A. Eychmüller, *ACS Nano*, 2016, **10**, 2559–2567.
- 25 B. Cai, R. Hübner, K. Sasaki, Y. Zhang, D. Su, C. Ziegler, M. B. Vukmirovic, B. Rellinghaus, R. R. Adzic and A. Eychmüller, *Angew. Chem., Int. Ed.*, 2018, **57**, 2963–2966.
- 26 S. Jun, J. Lee and E. Jang, *ACS Nano*, 2013, **7**, 1472–1477.
- 27 Z. Li, L. Kong, S. Huang and L. Li, *Angew. Chem., Int. Ed.*, 2017, **56**, 8134–8138.
- 28 B. Belache, Y. Khelifaoui, M. Bououdina, T. Souier and W. Cai, *Mater. Sci. Semicond. Process.*, 2018, **76**, 42–49.
- 29 L. G. Tartuci, L. F. T. Domingos, J. Bettini, K. O. Vieira, E. Raphael, B. R. C. Vale, J. L. Ferrari and M. A. Schiavon, *J. Nanopart. Res.*, 2017, **19**, 250.
- 30 L. Carbone, C. Nobile, M. De Giorgi, F. Della Sala, G. Morello, P. Pompa, M. Hytch, E. Snoeck, A. Fiore, I. R. Franchini, M. Nadasan, A. F. Silvestre, L. Chiodo, S. Kudera, R. Cingolani, R. Krahne and L. Manna, *Nano Lett.*, 2007, **7**, 2942–2950.
- 31 W. W. Yu, L. Qu, W. Guo and X. Peng, *Chem. Mater.*, 2003, **15**, 2854–2860.
- 32 T. Kodanek, H. M. Banbela, S. Naskar, P. Adel, N. C. Bigall and D. Dorfs, *Nanoscale*, 2015, **7**, 19300–19309.
- 33 H. G. Bagaria, E. T. Ada, M. Shamsuzzoha, D. E. Nikles and D. T. Johnson, *Langmuir*, 2006, **22**, 7732–7737.
- 34 S. Brunauer, P. H. Emmett and E. Teller, *J. Am. Chem. Soc.*, 1938, **60**, 309–319.
- 35 W. Stöber, A. Fink and E. Bohn, *J. Colloid Interface Sci.*, 1968, **26**, 62–69.
- 36 X. Tang, E. Kröger, A. Nielsen, C. Strelow, A. Mews and T. Kipp, *Langmuir*, 2017, **33**, 5253–5260.
- 37 F. Pietra, R. J. A. van Dijk - Moes, X. Ke, S. Bals, G. Van Tendeloo, C. de Mello Donega and D. Vanmaekelbergh, *Chem. Mater.*, 2013, **25**, 3427–3434.
- 38 E. Mine, A. Yamada, Y. Kobayashi, M. Konno and L. M. Liz-Marzán, *J. Colloid Interface Sci.*, 2003, **264**, 385–390.
- 39 Y. Kobayashi, H. Katakami, E. Mine, D. Nagao, M. Konno and L. M. Liz-Marzán, *J. Colloid Interface Sci.*, 2005, **283**, 392–396.
- 40 H. Yu and S. L. Brock, *ACS Nano*, 2008, **2**, 1563–1570.
- 41 E. Mine, A. Yamada, Y. Kobayashi, M. Konno and L. M. Liz-Marzán, *J. Colloid Interface Sci.*, 2003, **264**, 385–390.
- 42 S. Lee, K. Lee, W. D. Kim, S. Lee, D. J. Shin and D. C. Lee, *J. Phys. Chem. C*, 2014, **118**, 23627–23634.
- 43 X. Zhang, H. Sun, X. Tao and X. Zhou, *RSC Adv.*, 2014, **4**, 31313–31317.
- 44 K. Kanamori, M. Aizawa, K. Nakanishi and T. Hanada, *Adv. Mater.*, 2007, **19**, 1589–1593.
- 45 H. Sehaqui, M. Salajková, Q. Zhou and L. A. Berglund, *Soft Matter*, 2010, **6**, 1824.
- 46 C. Zhu, T. Y.-J. Han, E. B. Duoss, A. M. Golobic, J. D. Kuntz, C. M. Spadaccini and M. A. Worsley, *Nat. Commun.*, 2015, **6**, 6962.
- 47 H.-W. Liang, Q.-F. Guan, L.-F. Chen, Z. Zhu, W.-J. Zhang and S.-H. Yu, *Angew. Chem., Int. Ed.*, 2012, **51**, 5101–5105.
- 48 J. P. Randall, M. A. B. Meador and S. C. Jana, *ACS Appl. Mater. Interfaces*, 2011, **3**, 613–626.
- 49 K. E. Parmenter and F. Milstein, *J. Non-Cryst. Solids*, 1998, **223**, 179–189.
- 50 A. Benad, F. Jürries, B. Vetter, B. Klemmed, R. Hübner, C. Leyens and A. Eychmüller, *Chem. Mater.*, 2018, **30**, 145–152.





# 7 Influencing Charge Carriers in Nanocrystal Aerogels

## 7.1 Summary

Aerogel networks build up from CdSe/CdS dot/rod nanocrystals show unique optical properties caused by their electronic structure that as such are found neither in the isolated nanocrystals nor the bulk materials. In these CdSe/CdS-based networks excited electrons are delocalized throughout the network over several CdSe/CdS building blocks because of the small conduction band offset between CdSe and CdS. However, the holes are confined and localized in the CdSe dots as the valence band offset is large between CdSe and CdS. By structuring either the network or the individual building blocks this interaction within the network can be influenced.

The publication in section 7.2 reports the optical investigation of CdSe/CdS dot/rod-based structures described in section 6.2, i.e. a core network of connected CdSe/CdS dot/rods surrounded by a silica shell. These systems are contrasted to a network of CdSe/CdS dot/rods modified by silica shell growth before the network assembly. This results in two comparable CdSe/CdS/SiO<sub>2</sub> structures in which one contains a connected CdSe/CdS network and the second contains isolated CdSe/CdS dot/rods embedded in a silica network. The difference in optical properties, here the photoluminescence decay, clearly shows the contrast between the aerogels containing connected and thereby coupled building blocks and the isolated and thereby decoupled variant.

The publication in section 7.3 builds further on this approach using a different procedure. Cd cations in the CdSe/CdS dot/rod building blocks are exchanged with Zn cations selectively

starting at the tip of the building blocks which results in building blocks with ZnS tips of different lengths. When connecting these building blocks into a network the ZnS tips are at the connection points between the CdSe/CdS segments and represent a barrier due to their larger bandgap. Through the amount of Zn exchanged into the building blocks the size of these barriers can be influenced. Thereby a more precise control of the interaction between the building blocks can be achieved, not simply coupling and decoupling but control the amount of interaction as confirmed by the optical properties (the photoluminescence decay behaviour) of the aerogel networks.

## **7.2 Nanocrystal Aerogels with Coupled and Decoupled Building Blocks**

Pascal Rusch, Björn Schremmer, Christian Strelow, Alf Mews, Dirk Dorfs, Nadja C. Bigall

Published in: *The Journal of Physical Chemistry Letters*, 2019, 10, 7804-7810

DOI: 10.1021/acs.jpcllett.9b02695

Published by American Chemical Society 2019

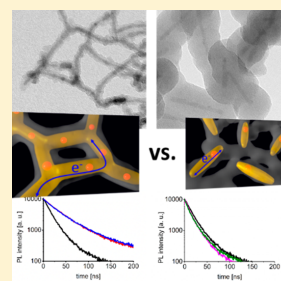


## Nanocrystal Aerogels with Coupled or Decoupled Building Blocks

Pascal Rusch,<sup>†,§</sup> Björn Schremmer,<sup>†,§</sup> Christian Strelow,<sup>‡</sup> Alf Mews,<sup>‡,¶</sup> Dirk Dorfs,<sup>†,§,⊥</sup> and Nadja C. Bigall<sup>\*,†,§,⊥</sup><sup>†</sup>Institute of Physical Chemistry and Electrochemistry, Leibniz Universität Hannover, Callinstraße 3A, 30167 Hannover, Germany<sup>§</sup>Laboratory of Nano and Quantum Engineering, Leibniz Universität Hannover, Schneiderberg 39, 30167 Hannover, Germany<sup>‡</sup>Institute of Physical Chemistry, University of Hamburg, Grindelallee 117, 20146 Hamburg, Germany<sup>⊥</sup>Cluster of Excellence PhoenixD (Photonics, Optics, and Engineering - Innovation Across Disciplines), 30167 Hannover, Germany

## Supporting Information

**ABSTRACT:** The influence of interparticle contact in nanoparticle-based aerogel network structures is investigated by selectively connecting or isolating the building blocks inside of the network, thereby coupling and decoupling them in regards to their optical and electronic properties. This is achieved by tuning the synthesis sequence and exchanging the point of shell growth and the point of particle assembly, leading to two distinctly different structures as examined by electron microscopy. By thorough examination of the resulting optical properties of the generated structures, the clear correlation between nanoscopic/microscopic structure and macroscopic optical properties is demonstrated. Temperature-dependent measurements and effective mass approximation calculations support our findings.



One potential method to immobilize nanoparticles and even form macroscopic solids while retaining the nanoscopic properties of colloid chemically synthesized nanocrystals is the assembly of said particles into three-dimensional network structures. The network formation is achieved by controlled destabilization of a colloidal nanoparticle solution. By carefully adjusting the speed of destabilization, instead of precipitation, the particles can form an interconnected macroscopic network often called a gel. This method has been introduced for semiconductor nanoparticles<sup>1–3</sup> and has been expanded to date with different materials,<sup>4–9</sup> shapes,<sup>10–12</sup> and assembly routes.<sup>13–15</sup> Already in the first instance of such semiconductor nanoparticle-based aerogel networks, the emission of the newly generated macroscopic body was described, although at low temperature.<sup>1</sup> It was shown that the monolithic assembly of nanoparticles in this instance shows a much higher intensity of the trap state emission compared to the initial nanoparticles. The reflectance spectroscopy still shows size quantization effects, which indicates that the nanoscopic properties of the nanoparticle building blocks can be transferred onto macroscopic bodies with these techniques.<sup>1</sup> By using core-shell particles, the trap state emission could be avoided and the fluorescence of the nanoparticle building blocks could be completely carried over to a macroscopic solid.<sup>16</sup> CdSe/CdS dot-in-rod nanostructures have already been investigated extensively regarding their optical properties and the underlying electronic processes.<sup>17–23</sup> Building further on this structure, our group was later able to show that the assembly of nanoparticle building blocks into a network structure can

actually not only be performed while retaining the optical properties of the particles but also can be used to introduce new optical properties into the final structure.<sup>24</sup> In the work reported, CdSe/CdS nanoparticles were used as pseudotype-II building blocks, and it could be shown that networks consisting of these building blocks have drastically increased fluorescence lifetimes. This was attributed to the excited electron being able to travel within the network of interconnected building blocks while the hole is localized in the CdSe cores of individual building blocks.<sup>24</sup> Similarly, an influence of the aspect ratio of the nanorod (NR) building blocks on their optical properties could be shown.<sup>25</sup> Recently, further studies have been undertaken using spectroelectrochemical measurements to understand the unique optical properties of semiconductor nanoparticle gels and suggest their applicability as sensors.<sup>26,27</sup>

In the present work, we aim to employ our recently introduced method of post-gelation modification<sup>28</sup> to build up nanoparticle-based network structures in two different sequences with the aim of selectively coupling and decoupling the individual building blocks, as illustrated in Figure 1. The silica encapsulation of singular dispersed nanoparticles has already been described.<sup>29</sup> A thin silica shell was grown according to this route, and such insulated nanoparticles were subsequently embedded into a silica gel monolith. The

Received: September 13, 2019

Accepted: November 5, 2019

Published: November 11, 2019



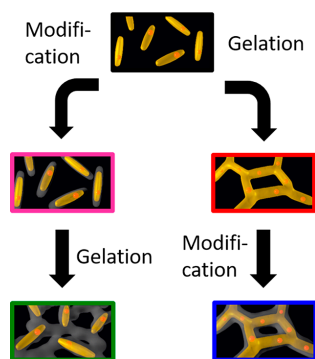


**Figure 1.** Schematic depiction of the two different synthesis sequences employed. Starting from (top) CdSe/CdS NR building blocks upon (right side) assembling into the network structure first and then modification by silica shell growth or (left side) first modification of the individual particles with a silica shell and then incorporation of them into a network, as illustrated by computer graphics.

silica shell essentially insulates the particles and prevents direct contact between the semiconductor NRs in the macroscopic monolith. In parallel, the same CdSe/CdS dot-in-rod nanoparticles were assembled first into an interconnected network structure. This network was afterward surrounded with a silica coating while leaving the interparticle connection intact. With this procedure, we have been able to generate a nanoparticle-based network with strongly enhanced mechanical stability,<sup>28</sup> but in this work, we aimed to employ it to synthesize two comparable solid macroscopic porous systems (sol-gels and, after supercritical drying, aerogels), one with and one without crystal-to-crystal contact between the semiconductor particles, allowing us to further investigate the influence of the interparticle contact on the optoelectronic properties.

The optical spectroscopy of the pristine CdSe/CdS NRs (Figure S2) in colloidal solution (which are the building blocks for the aerogels) in organic solution shows the characteristics of this nanoparticle structure. The absorption of the cadmium selenide core is visible as a small band at 570 nm, while the cadmium sulfide shell is responsible for the strong absorption band at 468 nm.<sup>30</sup> Due to the electronic structure of the NRs, the hole is trapped in the CdSe core after excitation. This leads to a strong fluorescence emission at 585 nm, slightly bathochromically shifted compared to the absorption of the core. The phase transfer<sup>31,32</sup> to aqueous solution only

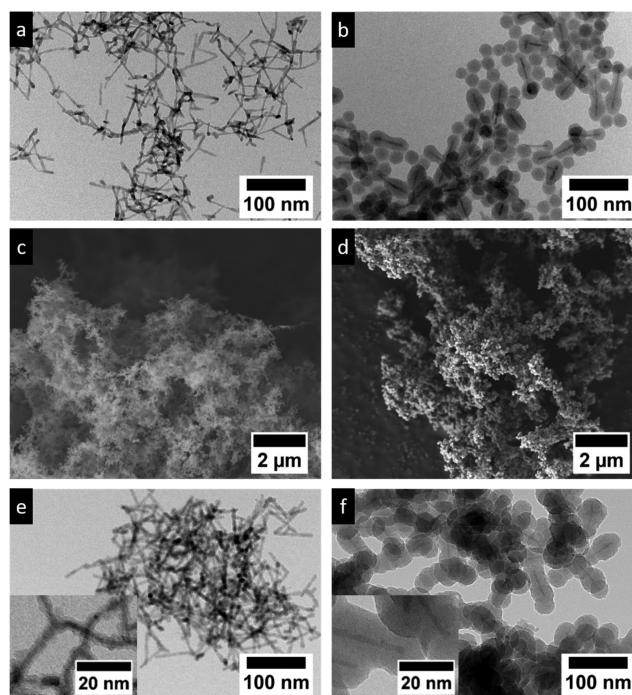


**Figure 2.** Electron microscopic images of the investigated structures comparing synthesis sequences starting with the gel network assembly (a,c,e) or starting with the particle modification (b,d,f). (a) Initial network of interconnected CdSe/CdS NRs before shell growth in TEM; (b) silica-modified CdSe/CdS NRs in TEM; network of CdSe/CdS NRs modified with silica after network formation (c) in SEM and (e) in TEM with the inset at higher magnification; and gel network generated from silica-modified CdSe/CdS NRs (d) in SEM and (f) in TEM, with the inset at higher magnification.

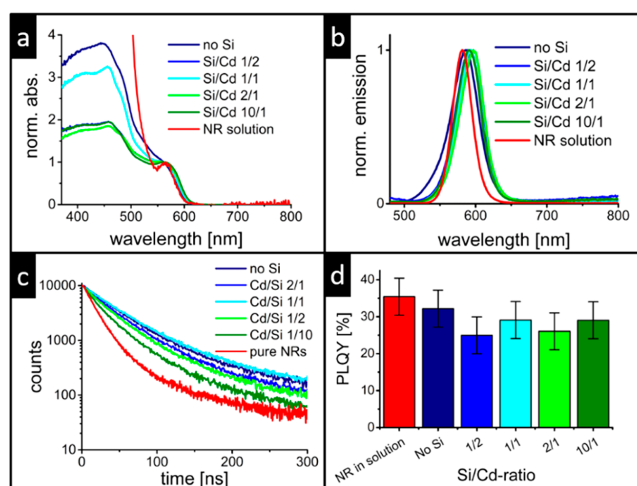


**Figure 3.** Optical properties of silica-modified CdSe/CdS NR aerogels: (a) absorption spectra, (b) emission spectra, (c) fluorescence lifetime decay, and (d) PLQYs of aerogels modified with different amounts of TEOS. As can be derived from the four panels, the silica shell modification does not significantly alter the optical properties (in absorption, emission, PL lifetime, and quantum yield) in comparison to the nonmodified CdSe/CdS NR aerogels.

marginally influences the absorption of the NRs; the position of the emission maximum does not change. However, the photoluminescence quantum yield (PLQY) is reduced slightly from 35 to 27%. The fluorescence lifetime also decreases from 18 ns in the organic solution to 16 ns in the aqueous solution (Figure S4a,b). These NRs are assembled by controlled destabilization by hydrogen peroxide into porous network structures, as can be seen in Figure 2a. The aerogels prepared this way show very similar optical features (Figure 3). In the nonmodified aerogels, the emission is visible at 588 nm. The absorption of the CdSe core can be seen at 563 nm, while the absorption of the CdS shell appears as a broad band at around 500 nm. Especially for the interpretation of the absorption spectra, it is important to keep the state of the sample in mind. Because of the high influence of scattering compared to a colloidal nanoparticle solution, the gel is measured using an integrating sphere. Also, the concentration of the nanoparticles is much higher than one would use for conventional nanoparticle spectroscopy in solution. This leads to the much larger prominence of the signal from the cadmium selenide core in the spectra, which is only barely visible in the spectrum of the colloidal solution. It also causes the spectra to reach saturation in the area of the cadmium sulfide absorption band. For light of energies higher than a certain value or below a certain wavelength, the gels simply become optically dense materials in which all incoming light is absorbed and the higher-energy features of the spectrum are not measurable. The findings discussed above are consistent with our previous data of such types of aerogels;<sup>24</sup> therefore, these samples can be employed as references for our new materials, as will be discussed in the next paragraph.

In a second step, the networks are modified with a continuous silica shell, as can be seen in TEM (Figure 2e); see the *Experimental Methods* section for details. The porous structure is still present after this modification, as can be seen in SEM images (Figure 2c) and based on the core network of

connected NRs. For silica-modified gels, the optical properties are almost identical compared to the unmodified gels, as shown in Figure 3 and discussed above. The emission wavelength is slightly shifted toward longer wavelengths from 590 to 597 nm. This could simply be due to the change in dielectric surrounding and minor inhomogeneities during the shell growth process, but as no clear relation to the amount of silica used or other variables in the synthesis procedure is visible, the exact reason is unclear. The absorption features are also similar to the absorption of the CdSe cores around 560 nm and the CdS absorption below 500 nm. The optical density of absorption saturation changes, which we attribute to a variation of illuminated sample areas (which is technically unavoidable due to inhomogeneities of the monolithic samples). The PLQY of all gels—modified and unmodified—is similar. The PLQY of the pristine NRs in toluene is measured to be 35%; the PLQY of an unmodified aerogel is very close to this at 32% and a bit higher than the PLQY of the water transferred NRs (27%). Shell-modified aerogels show PLQYs of 26–29% (Figure 2d). Within the uncertainty (5%, determined by reproducibility tests with the reference dye rhodamine 6G) estimated for these measurements, these differences are minimal. The loss of PLQY by the silica shell modification can thus be seen as insignificant. The fluorescence lifetime of the aerogels is especially interesting as the connection of the NRs with each other is a key factor in the fluorescence decay. In an earlier work of our group, a strongly increased fluorescence lifetime for CdSe/CdS NR aerogels compared to the NRs in solution was shown and attributed to the crystal-to-crystal type connection of the rods. We explained this effect with a higher delocalization of the electron after excitation, resulting in less overlap between electron and hole wave functions and therefore longer PL decay times.<sup>24</sup> The lifetime increase can therefore be seen as indication for an electronic coupling between interconnected nanoparticles in the aerogel networks. In fact, in the present work, we also

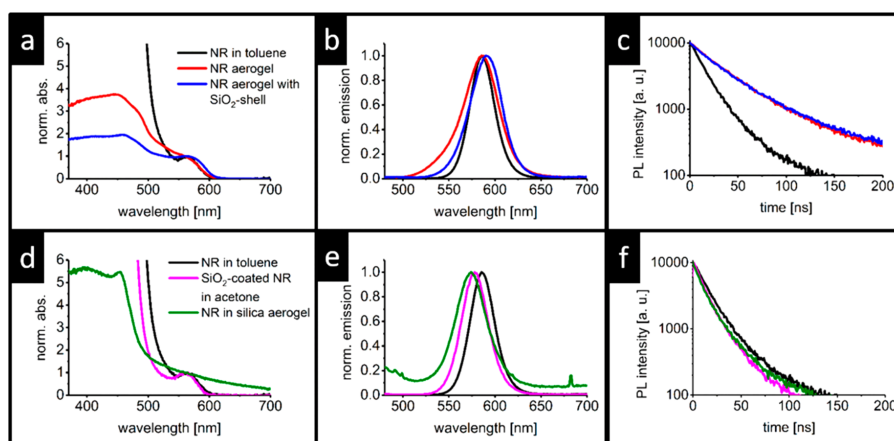


**Figure 4.** Differences in optical properties depending on the synthesis sequence: (top row) network formation first, (bottom row) silica modification first. (a,d) Absorption spectra normalized to the first excitonic transition of the CdSe core, (b,e) emission spectra, and (c,f) fluorescence decay measurements. Colors of the graphs also correspond to the borders used in Figure 1.

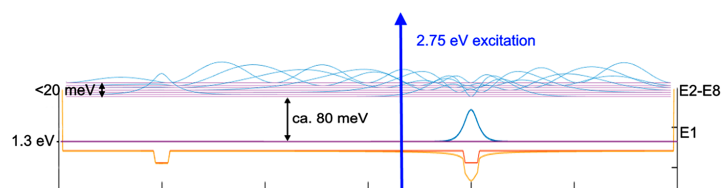


**Figure 5.** Wave functions of the first eight excited states in two connected CdSe/CdS NRs calculated by EMA with the hole fixed to the right side core. The external potential is shown in orange with the overall potential including coulomb interaction in yellow and the generated wave functions in blue.

observe increased fluorescence lifetimes for all aerogels—with and without a silica shell—compared to the lifetime of the NRs in solution. The fluorescence lifetime of unmodified CdSe/CdS NR aerogels is 40 ns, which is in accordance with our previous findings.<sup>24</sup> For modified aerogels, the lifetimes are in the range of 33–41 ns (Figures 2c and S3). This means that also the drastic lifetime increase is present for all Si/Cd ratios investigated for silica shell-modified aerogels, which is comparable to that of unmodified aerogels. Hence, we conclude that also in the silica shell-modified aerogels the electron seems to be able to travel within the network while the hole is located at the CdSe cores. If this explanation for the increase in fluorescence lifetime is to be believed, a network containing individual isolated particles—e.g., by the growth of an insulating silica shell before network formation—should show very much different behavior regarding the fluorescence lifetimes. In this instance, fluorescence lifetimes should not increase between a particle dispersion and the network.

To investigate whether the sequence of synthesis steps (namely, network formation and silica coating) influence the physical properties of the resulting nanocrystal aerogels in terms of fluorescence lifetime, the same NRs as those used for the production of the described modified gels were now first surrounded with silica shells according to literature procedures<sup>29</sup> (see the Experimental Methods section and Figure 2b) and subsequently gelled in the presence of further TEOS.

This resulted in a silica matrix with singular embedded NRs, which were not in direct contact with each other and should therefore have been decoupled, i.e., they should not have shown increased PL decay times (see also Figure S6 in the Supporting Information). These single NRs in a silica matrix can be seen in the TEM (Figure 2f). The larger structure of these silica networks can be seen in SEM (Figure 2d) and is now defined by the silica as opposed to the networks made up of connected NRs, which are defined by this NR core network (see also Figure 2 for comparison). The different structures are illustrated schematically in Figure 1. The silica aerogel is essentially utilized as an electronically isolating spacer between the NRs. The emission and absorption spectra of these silica-coated NRs in solution and in the silica gel only differ insignificantly from each other (Figure 4a–e). Also, no significant spectral difference of such gels and particles from the pristine NRs (before silica growth) or from the unmodified and modified aerogels is observed. The lifetime measurements confirm our initial expectation. While the aerogels produced from CdSe/CdS NRs as well as their post-gelation-modified counterparts show distinct ultralong lifetimes of ca. 40 ns, the aerogels with embedded NRs, which are each separated from one other by a thin silica shell, exhibit much shorter lifetimes of 13–14 ns (which are comparable to those of the initial NRs in organic solution) (Figure 4c,f). These observations further support our previous assumption of the influence of

interparticle contact on the fluorescence lifetime in NR gels<sup>24</sup> and show that this contact between the individual NRs is still present after post-gelation modification.

To understand the electronic processes underlying the observed fluorescence behavior, theoretical calculations based on the effective mass approximation were performed to simulate the excited electron wave functions of a network structure of crystal connected particles. Figure 5 shows the results for the eight lowest excited electron wave functions of two merged CdSe/CdS NRs that should represent the smallest subunit in the network exhibiting the properties of the whole structure. Due to its low effective mass and the high valence band discontinuity of CdS and CdSe, the hole always localizes inside of one of the two CdSe cores (not shown in Figure 5). The first excited electron state (E1 in Figure 5) also strongly localizes at the position of the hole due to the combination of the attractive potential formed by conduction band discontinuity and the coulomb interaction with the localized hole. The properties of this state do not differ from those of the corresponding state in an isolated particle and thus do not explain the observed increase in PL lifetime. The second excited electron state (E2) is also localized at the second CdSe core not occupied by the hole. Due to the strongly reduced coulomb interaction with the hole, it is lifted in energy by about 80 meV. However, the next higher excited electron states (E3–E8; see Figure 5 and additionally Figure S7 in the Supporting Information for the individual wave functions) exhibit an increasing delocalization over the merged CdSe/CdS NR system with increasing energy. The wave functions of these higher electron states indeed have a smaller overlap with the hole wave function. We thus attribute these higher electron states to be responsible for the observed fluorescence kinetics. Naturally, the question arises why the electron and the hole do not thermalize into the lowest-energy state that does not show a difference from the individual isolated CdSe/CdS NR.

We explain this contradiction as follows: the excitation with 450 nm light used in the measurements creates pairs of hot electrons and holes that occupy higher excited states. Subsequently, the electron and hole separate and thermalize independently, leading to either (i) the occupation of states in different cores or (ii) direct occupation of a delocalized higher electron state. The first case (i) would lead to zero overlap of the electron and hole wave functions and would not contribute to the measured fluorescence. However, as can be observed in Figure 5, the second excited electron state (E2) that is separated from the hole has an energy very close to a bunch of higher electron states (labeled E3–E8 in Figure 5), which are all within an energy range of 10–20 meV of each other. Thus, thermal activation of the separated electron into the delocalized states or even a thermal mixing of all higher excited electron states (E2–E8) is reasonable. This also includes the above-mentioned second case (ii), direct thermalization into a delocalized (thermally mixed) higher electron state. The wave functions of the thermally mixed higher excited electron states should in general have a reduced overlap with the localized hole and should thus lead to a reduced fluorescence lifetime and/or even to a suppression of the thermalization into the lowest excited electron state (E1).

Following this explanation, the influence of the states showing considerable delocalization (labeled E5–E8 in Figure S7) should decrease with lower temperature, leading to higher wave function overlap and shorter PL lifetimes. To confirm this temperature-dependent lifetime, measurements have been

carried out as well. These indeed show a decrease in PL lifetime with lower temperatures (see Figure S8 in the Supporting Information) contrary to classical theory, which assumes no influence of temperature on the radiative process and a slowing down of the non-radiative processes leading to increased PL lifetimes. Because we observe the opposite effect within our measurements, a different factor influencing the lifetimes has to exist, and our above-mentioned thermal mixing of higher excited states becomes reasonable.

In this work, the possibility to couple and decouple the nanoparticle building blocks when assembling them into a network structure is shown. This is achieved by switching the synthesis sequence during the generation of the network, i.e., either first generating a nanoparticle-based network and subsequently surrounding this network with a silica shell or first isolating the individual particles with silica shells and subsequently embedding them into a silica-based network. The pronounced effect of the interparticle contact on the optical properties in the first case could be illustrated by photoluminescence spectroscopy and further detailed with theoretical calculations. When a contact between the particles is established before silica shell growth, the ultralong lifetimes typical for these CdSe/CdS network structures are visible independently of the presence of a silica shell. If the direct contact between the semiconductor NRs is instead inhibited by silica coating of individual particles, an increase in lifetime can not be observed. This supports the underlying theory that electrons can travel within such nanocrystal networks. This model was supported by effective mass approximation simulations in combination with temperature-dependent lifetime measurements. Our work furthermore shows that the sequence of synthetic steps in nanochemistry is of utmost importance for controlling the optoelectronic properties of such elaborate materials.

## EXPERIMENTAL METHODS

The preparation of the CdSe/CdS building blocks has been described in earlier works<sup>30</sup> as well as their phase transfer,<sup>31,32</sup> assembly,<sup>24</sup> silica modification of dispersed particles,<sup>29</sup> and modification of networks.<sup>28</sup> It is additionally described briefly in the Supporting Information.

**Optical Characterization.** Absorption measurements were performed in an Agilent Cary 5000 spectrophotometer in 3 mL quartz cuvettes with a 10 mm path length. For the measurement of aerogels, a DRA-2500 integrating sphere was connected to the spectrophotometer, and the sample was mounted in reflection position. Photoluminescence measurements were carried out in a Horiba Fluoromax-4 spectrometer for emission and lifetime measurements. The lifetime was measured by time-correlated single-photon counting (TCSPC) using a NanoLED with a 455 nm wavelength as the excitation source. Each lifetime measurement was continued until the peak value reached 10000 counts. The measurement of PLQY was done by absolute measurements using a Horiba Dual-FL with a quanta- $\phi$  integrating sphere with an excitation wavelength of 500 nm. Therefore, the intensity of the excitation was adjusted to be below the detector limit, and emission spectra were measured over the range of 300–800 nm for an empty integration sphere and again with the sample. The difference between the integrated area under the excitation peak in these two measurements is equivalent to the total number of photons absorbed, while the difference in the integrated area under the emission peak is equivalent to the

number of photons emitted. By forming the quotient of these areas, the quantum yield was calculated. The error of the quantum yield measurement was estimated by multiple measurements of rhodamine 6G over 14 days to be about absolute 5%. Temperature dependent-fluorescence measurements were carried out using an Edinburgh FLS 1000 spectrometer equipped with an Oxford Instruments Optistat-CF cryostat cooled with liquid helium. For this measurement, the aerogel samples were put inside of an open quartz cuvette with a 2 mm path length, and the sample space was flushed with helium. For time-correlated measurements, the samples were excited by an Edinburgh EPL pulsed laser with a 445.1 nm wavelength.

**Electron Microscopy.** TEM samples of nanoparticles in solution were prepared by drop-casting diluted solutions in chloroform onto a carbon-coated copper grid (300 mesh) by Quantifoil. For sample preparation of aerogels, the mentioned grids were pulled along an aerogel sample, thereby keeping small parts of gel stuck to the grid. The measurements were carried out in an FEI Tecnai G2 F20 transmission electron microscope with a field emission gun operated at 200 kV.

SEM samples were prepared by dropping fragments of the gel onto an adhesive carbon film and shaking off loosely attached parts. A JEOL JSM 6700F field emission scanning electron microscope with a 2 kV acceleration voltage and a secondary electron detector at a working distance of 8 mm was used to measure the samples.

**Theoretical Calculations.** The simulations were done by self-consistently solving the Schrödinger equation for one electron and one hole on a three-dimensional spatial grid in a single-band effective mass approximation. The potential was composed of the external potential formed by the band alignments and the Coulomb potential generated for the electron by the hole and for the hole by the electron. Electron and hole wave functions and eigenenergies were calculated iteratively until convergence was achieved. The band gaps of CdS and CdSe were set to 2.41 and 1.74 eV, respectively, and the conduction band offset was set to 150 meV.

## ■ ASSOCIATED CONTENT

### Supporting Information

The Supporting Information is available free of charge at <https://pubs.acs.org/doi/10.1021/acs.jpcllett.9b02695>.

Additional characterization of the nanocrystal building blocks and networks, further fluorescence lifetime measurements and evaluation including temperature-dependent measurements, synthesis procedures, and the band structure of the discussed materials, and further results of theoretical calculations (PDF)

## ■ AUTHOR INFORMATION

### Corresponding Author

\*E-mail: [nadja.bigall@pci.uni-hannover.de](mailto:nadja.bigall@pci.uni-hannover.de). Address: Institute of Physical Chemistry and Electrochemistry, Callinstraße 3A, 30167 Hannover, Germany.

### ORCID

Alf Mews: 0000-0001-5739-8820

Dirk Dorfs: 0000-0001-6175-4891

Nadja C. Bigall: 0000-0003-0171-1106

### Notes

The authors declare no competing financial interest.

## ■ ACKNOWLEDGMENTS

The authors would like to thank the Laboratory of Nano and Quantum Engineering for the use of the TEM, as well as J. Caro and A. Feldhoff for SEM. The project leading to these results received funding from the European Research Council (ERC) under the European Union's Horizon 2020 research and innovation programme (Grant Agreement No. 714429). N.C.B. furthermore acknowledges funding from the German Federal Ministry of Education and Research (BMBF) within the framework of NanoMatFutur (Support Code 03X5525). D.D. acknowledges funding by the DFG (Research Grant 1580/S-1). The project has in part been funded by the Deutsche Forschungsgemeinschaft (DFG, German Research Foundation) under Germany's Excellence Strategy within the Cluster of Excellence PhoenixD (EXC 2122, Project ID 390833453).

## ■ REFERENCES

- (1) Mohanan, J. L.; Arachchige, I. U.; Brock, S. L. Porous Semiconductor Chalcogenide Aerogels. *Science* **2005**, *307*, 397–400.
- (2) Gacoin, T.; Malier, L.; Boilot, J. P. New Transparent Chalcogenide Materials Using a Sol-Gel Process. *Chem. Mater.* **1997**, *9* (7), 1502–1504.
- (3) Gacoin, T.; Lahlil, K.; Larregaray, P.; Boilot, J. P. Transformation of CdS Colloids: Sols, Gels, and Precipitates. *J. Phys. Chem. B* **2001**, *105* (42), 10228–10235.
- (4) Ganguly, S.; Brock, S. L. Toward Nanostructured Thermoelectrics: Synthesis and Characterization of Lead Telluride Gels and Aerogels. *J. Mater. Chem.* **2011**, *21* (24), 8800.
- (5) Hithami-Mudiyanselage, A.; Senevirathne, K.; Brock, S. L. Assembly of Phosphide Nanocrystals into Porous Networks: Formation of InP Gels and Aerogels. *ACS Nano* **2013**, *7* (2), 1163–1170.
- (6) Kalebaila, K. K.; Georgiev, D. G.; Brock, S. L. Synthesis and Characterization of Germanium Sulfide Aerogels. *J. Non-Cryst. Solids* **2006**, *352* (3), 232–240.
- (7) Bigall, N. C.; Herrmann, A.-K.; Vogel, M.; Rose, M.; Simon, P.; Carrillo-Cabrera, W.; Dorfs, D.; Kaskel, S.; Gaponik, N.; Eychmüller, A. Hydrogels and Aerogels from Noble Metal Nanoparticles. *Angew. Chem., Int. Ed.* **2009**, *48* (51), 9731–9734.
- (8) Gaponik, N.; Wolf, A.; Marx, R.; Lesnyak, V.; Schilling, K.; Eychmüller, A. Three-Dimensional Self-Assembly of Thiol-Capped CdTe Nanocrystals: Gels and Aerogels as Building Blocks for Nanotechnology. *Adv. Mater.* **2008**, *20* (22), 4257–4262.
- (9) Yao, Q.; Arachchige, I. U.; Brock, S. L. Expanding the Repertoire of Chalcogenide Nanocrystal Networks: Ag<sub>2</sub>Se Gels and Aerogels by Cation Exchange Reactions. *J. Am. Chem. Soc.* **2009**, *131* (8), 2800–2801.
- (10) Yu, H.; Brock, S. L. Effects of Nanoparticle Shape on the Morphology and Properties of Porous CdSe Assemblies (Aerogels). *ACS Nano* **2008**, *2* (8), 1563–1570.
- (11) Naskar, S.; Miethe, J. F.; Sanchez-Paradinas, S.; Schmidt, N.; Kanthasamy, K.; Behrens, P.; Pfnür, H.; Bigall, N. C. Photoluminescent Aerogels from Quantum Wells. *Chem. Mater.* **2016**, *28* (7), 2089–2099.
- (12) Naskar, S.; Freytag, A.; Deutsch, J.; Wendt, N.; Behrens, P.; Köckritz, A.; Bigall, N. C. Porous Aerogels from Shape-Controlled Metal Nanoparticles Directly from Nonpolar Colloidal Solution. *Chem. Mater.* **2017**, *29* (21), 9208–9217.
- (13) Sayevich, V.; Cai, B.; Benad, A.; Haubold, D.; Sonntag, L.; Gaponik, N.; Lesnyak, V.; Eychmüller, A. 3D Assembly of All-Inorganic Colloidal Nanocrystals into Gels and Aerogels. *Angew. Chem., Int. Ed.* **2016**, *55* (21), 6334–6338.
- (14) Freytag, A.; Sánchez-Paradinas, S.; Naskar, S.; Wendt, N.; Colombo, M.; Pugliese, G.; Poppe, J.; Demirci, C.; Kretschmer, I.; Bahnemann, D. W.; et al. Versatile Aerogel Fabrication by Freezing

and Subsequent Freeze-Drying of Colloidal Nanoparticle Solutions. *Angew. Chem., Int. Ed.* **2016**, *55* (3), 1200–1203.

(15) Ranmohotti, K. G. S.; Gao, X.; Arachchige, I. U. Salt-Mediated Self-Assembly of Metal Nanoshells into Monolithic Aerogel Frameworks. *Chem. Mater.* **2013**, *25* (17), 3528–3534.

(16) Arachchige, I. U.; Brock, S. L. Highly Luminescent Quantum-Dot Monoliths. *J. Am. Chem. Soc.* **2007**, *129* (7), 1840–1841.

(17) Steiner, D.; Dorfs, D.; Banin, U.; Della Sala, F.; Manna, L.; Millo, O. Determination of Band Offsets in Heterostructured Colloidal Nanorods Using Scanning Tunneling Spectroscopy. *Nano Lett.* **2008**, *8* (9), 2954–2958.

(18) Talapin, D. V.; Koeppel, R.; Götzinger, S.; Kornowski, A.; Lupton, J. M.; Rogach, A. L.; Benson, O.; Feldmann, J.; Weller, H. Highly Emissive Colloidal CdSe/CdS Heterostructures of Mixed Dimensionality. *Nano Lett.* **2003**, *3* (12), 1677–1681.

(19) Kunneman, L. T.; Zanella, M.; Manna, L.; Siebbeles, L. D. A.; Schins, J. M. Mobility and Spatial Distribution of Photoexcited Electrons in CdSe/CdS Nanorods. *J. Phys. Chem. C* **2013**, *117* (6), 3146–3151.

(20) Saba, M.; Minniberger, S.; Quochi, F.; Roither, J.; Marceddu, M.; Gocalinska, A.; Kovalenko, M. V.; Talapin, D. V.; Heiss, W.; Mura, A.; et al. Exciton-Exciton Interaction and Optical Gain in Colloidal CdSe/CdS Dot/Rod Nanocrystals. *Adv. Mater.* **2009**, *21* (48), 4942–4946.

(21) Kraus, R. M.; Lagoudakis, P. G.; Rogach, A. L.; Talapin, D. V.; Weller, H.; Lupton, J. M.; Feldmann, J. Room-Temperature Exciton Storage in Elongated Semiconductor Nanocrystals. *Phys. Rev. Lett.* **2007**, *98* (1), 017401.

(22) Vezzoli, S.; Manceau, M.; Leménager, G.; Glorieux, Q.; Giacobino, E.; Carbone, L.; De Vittorio, M.; Bramati, A. Exciton Fine Structure of CdSe/CdS Nanocrystals Determined by Polarization Microscopy at Room Temperature. *ACS Nano* **2015**, *9* (8), 7992–8003.

(23) Persano, A.; De Giorgi, M.; Fiore, A.; Cingolani, R.; Manna, L.; Cola, A.; Krahn, R. Photoconduction Properties in Aligned Assemblies of Colloidal CdSe/CdS Nanorods. *ACS Nano* **2010**, *4* (3), 1646–1652.

(24) Sanchez-Paradinas, S.; Dorfs, D.; Friebe, S.; Freytag, A.; Wolf, A.; Bigall, N. C. Aerogels from CdSe/CdS Nanorods with Ultra-Long Exciton Lifetimes and High Fluorescence Quantum Yields. *Adv. Mater.* **2015**, *27* (40), 6152–6156.

(25) Geißler, D.; Würth, C.; Wolter, C.; Weller, H.; Resch-Genger, U. Excitation Wavelength Dependence of the Photoluminescence Quantum Yield and Decay Behavior of CdSe/CdS Quantum Dot/Quantum Rods with Different Aspect Ratios. *Phys. Chem. Chem. Phys.* **2017**, *19* (19), 12509–12516.

(26) Lübemann, F.; Miethe, J. F.; Steinbach, F.; Rusch, P.; Schlosser, A.; Zámbo, D.; Heinemeyer, T.; Natke, D.; Zok, D.; Dorfs, D.; et al. Patterning of Nanoparticle-Based Aerogels and Xerogels by Inkjet Printing. *Small* **2019**, *15*, 1902186.

(27) Schlosser, A.; Meyer, L. C.; Lübemann, F.; Miethe, J. F.; Bigall, N. C. Nanoplatelet Cryo-aerogels with Potential Application in Photoelectrochemical Sensing. *Phys. Chem. Chem. Phys.* **2019**, *21* (18), 9002–9012.

(28) Rusch, P.; Niemeyer, F.; Pluta, D.; Schremmer, B.; Lübemann, F.; Rosebrock, M.; Schäfer, M.; Jahns, M.; Behrens, P.; Bigall, N. C. Versatile Route to Core-shell Reinforced Network Nanostructures. *Nanoscale* **2019**, *11* (32), 15270–15278.

(29) Tang, X.; Kröger, E.; Nielsen, A.; Strelow, C.; Mews, A.; Kipp, T. Ultrathin and Highly Passivating Silica Shells for Luminescent and Water-Soluble CdSe/CdS Nanorods. *Langmuir* **2017**, *33* (21), 5253–5260.

(30) Carbone, L.; Nobile, C.; De Giorgi, M.; Sala, F. D.; Morello, G.; Pompa, P.; Hytch, M.; Snoeck, E.; Fiore, A.; Franchini, I. R.; et al. Synthesis and Micrometer-Scale Assembly of Colloidal CdSe/CdS Nanorods Prepared by a Seeded Growth Approach. *Nano Lett.* **2007**, *7* (10), 2942–2950.

(31) Kodanek, T.; Banbela, H. M.; Naskar, S.; Adel, P.; Bigall, N. C.; Dorfs, D. Phase Transfer of 1- and 2-Dimensional Cd-Based Nanocrystals. *Nanoscale* **2015**, *7* (45), 19300–19309.

(32) Bagaria, H. G.; Ada, E. T.; Shamsuzzoha, M.; Nikles, D. E.; Johnson, D. T. Understanding Mercapto Ligand Exchange on the Surface of FePt Nanoparticles. *Langmuir* **2006**, *22* (18), 7732–7737.

### **7.3 Influencing the Coupling Between Network Building Blocks in CdSe/CdS Dot/Rod Aerogels by Partial Cation Exchange**

Pascal Rusch, Franziska Lübke, Hadir Borg, J. Gerrit Eckert, Dirk Dorfs, Nadja C. Bigall

This paper and its revised version, which is shown here, has been submitted to *The Journal of Chemical Physics* and is currently under review.

## Influencing the Coupling Between Network Building Blocks in CdSe/CdS Dot/Rod Aerogels by Partial Cation Exchange

Pascal Rusch,<sup>a</sup> Franziska Lübke, <sup>a,b</sup> Hadir Borg,<sup>a,c</sup> J. Gerrit Eckert,<sup>a</sup> Dirk Dorfs,<sup>a,b,c</sup> Nadja C. Bigall<sup>\*a,b,c</sup>

<sup>a</sup> Institute of Physical Chemistry and Electrochemistry, Leibniz Universität Hannover, Callinstraße 3A, 30167 Hannover, Germany

<sup>b</sup> Cluster of Excellence PhoenixD (Photonics, Optics, Engineering – Innovation Across Disciplines), 30167 Hannover, Germany

<sup>c</sup> Laboratory of Nano and Quantum Engineering, Leibniz Universität Hannover, Schneiderberg 39, 30167 Hannover, Germany

\* Contact: Prof. Nadja C. Bigall, Institute of Physical Chemistry and Electrochemistry, Callinstraße 3A, 30167 Hannover, Germany, nadja.bigall@pci.uni-hannover.de

### Abstract

The assembly of CdSe/CdS dot/rod nanocrystals (NCs) with variable length of ZnS tip into aerogel networks is presented. To this end, a partial region selective cation exchange procedure is performed replacing Cd by Zn starting at the NC tip. The produced aerogel networks are investigated structurally and optically. The networks of tip-to-tip connected NCs have an intricate band structure with holes confined to the CdSe cores while electrons are delocalized within the CdS also within connected building blocks. However, the ZnS tips act as a barrier of variable length and strength between the NC building blocks partly confining the electrons. This results in NC based aerogel networks with tunable strength of coupling between building blocks.

The assembly of nanocrystal (NC) building blocks into porous network structures<sup>1-3</sup> (usually referred to as aerogels) has garnered interest due to the possibility of generating macroscopic materials while preserving nanoscopic properties of the building blocks. To this end, a plethora of materials ranging from metal chalcogenides<sup>4-8</sup>, metal phosphides<sup>9,10</sup>, metal nitrides<sup>11</sup> metal oxides<sup>12-14</sup> to metals<sup>15-17</sup> have been converted to aerogels. Likewise, different methods,<sup>18</sup> e.g. chemical ligand removal,<sup>4,6,17</sup> ligand removal by three-valent cations,<sup>19</sup> photochemical ligand removal,<sup>20</sup> electrochemical methods,<sup>21</sup> ice-templating<sup>22</sup> or ligand bridging,<sup>23</sup> have been developed to facilitate this aerogel assembly. As the nanoscopic properties of the building blocks, like size-dependent bandgap and high surface-to-volume ratio, are retained from building blocks to aerogel networks, these structures are promising for applications in sensing<sup>24,25</sup> and electro-<sup>26-30</sup> or photocatalysis.<sup>31,32</sup> Apart from their potential for these applications, NC-based aerogels also show unique and fascinating optical properties. By bandgap engineering of the NC building blocks, here CdSe/CdS dot/rod NCs, a network structure can be generated in which the hole are highly confined to the CdSe quantum dot cores, the electrons, however, are delocalized over a larger part of the interconnected network due to the very small conduction band offset in a CdSe/CdS structure.<sup>6</sup> This was first shown by the photoluminescence (PL) lifetime increasing drastically between the individual building blocks and the connected network structure.<sup>6</sup> More recently, these properties could be further investigated, for one by the introduction of PL quenching gold NCs into the network structures which could be shown to quench the PL over an area of the network and not only the directly adjacent building blocks. This in turn allows for an

estimation of the spatial extent of the electron delocalization.<sup>33</sup> Additionally, the selective coupling and decoupling of NC building blocks inside such network structures could be achieved by switching the synthesis sequence from either embedding the NC building blocks inside a silica aerogel or first connecting the NC building blocks to a network which is then surrounded by a silica shell. This procedure is able to generate two aerogel structures made up from similar materials, one, in which the semiconducting NC building blocks are isolated (decoupled) and one, in which they are connected (coupled). This can also be seen in the optical properties of these structures.<sup>34</sup> This emphasizes that the structure and properties of such NC-based aerogel networks can be influenced not only at the stage of building block synthesis but also further down the process at the stage of the network structure.<sup>35</sup>

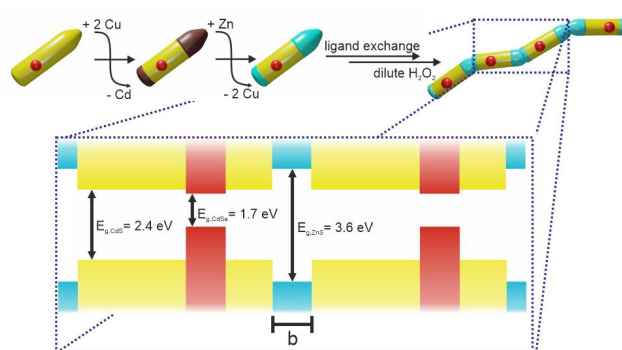


**Figure 1.** Schematic sequence of the synthesis (first cation exchange with copper then with zinc followed by gelation) leading to a network of ZnS tipped CdSe/CdS dot/rod nanocrystals exhibiting the band structure shown below with a variable length barrier ( $b$ ) introduced by the ZnS tips. Band gaps of the bulk materials given for illustration.

Building on these examples and the CdSe/CdS dot/rod-based network structure, the aim of this work is to carefully modify the individual building blocks to control the coupling between them. Thereby allowing further intermediate conditions between the aforementioned digital conditions, decoupled and coupled. To this end CdSe/CdS dot/rod building blocks are modified by partial cation exchange leading to ZnS tipped CdSe/CdS nanocrystals. These nanocrystal building blocks are then assembled into networks by the means of oxidative ligand removal with a dilute hydrogen peroxide solution and finally supercritically dried to yield NC-based aerogels. These aerogels exhibit a band structure as schematically shown in Figure 1 whereby the length of the barrier, i.e. the ZnS, between the CdSe/CdS units is variable through the amount of Zn ions exchanged in the building blocks.

The reference system in this investigation are CdSe/CdS dot/rod NC-based aerogels. Therefore, the starting point is the well-established hot-injection synthesis of CdSe quantum dots (QDs) which are then used as seeds in the seeded-growth of elongated CdS shells.<sup>6,36</sup> The result is a CdSe/CdS dot/rod NC of 15.9 nm length and 4.4 nm width grown onto 3.4 nm CdSe QDs, as shown in Figure 2A (size distribution of the dot/rods is shown in the supplementary material). The absorption spectra of these dot/rods show the absorption features of the CdSe QDs around 600 nm and the band edge of the CdS shell around 450 nm. The recombination of excited charge carriers results in an emission at 610 nm. This emission solely takes place in the CdSe QD cores due to the strong confinement of the holes to the CdSe.

These dot/rod building blocks are then phase transferred into aqueous solution by ligand exchange with 3-mercaptopropionic acid.<sup>37,38</sup> As seen in Figure 2C, the optical properties of these NCs only change minimally by this ligand exchange. However, when these NC building blocks are connected into aerogel networks, the optical properties change as described in previous works.<sup>6,34</sup> The structure of such networks is shown in transmission electron microscopy in Figure 2B and the intricate network of interconnected dot/rod building blocks can be seen. While the steady-state PL features are rather similar between NC building block dispersions and assembled aerogel, with minor changes most likely caused by the difference in surrounding (solvent or air), the time-resolved PL features change drastically. The CdSe/CdS dot/rod aerogels exhibit the characteristic ultralong PL lifetimes (see Figure 2D). As discussed in earlier works,<sup>6,34,39</sup> these are caused by the excited electrons delocalized over several connected building blocks resulting in a decreased overlap between electron and hole wavefunction (expressing as increase in PL lifetimes). In the absorption measurements a saturation of absorption can be seen at high energies (short wavelengths) for the aerogel. This can be attributed to the high concentration of NCs within an aerogel, which is orders of magnitude above the highly diluted samples usually employed in absorption spectroscopy. This leads to a harsh inner-filter effect preventing the measurement of the higher energy features of the absorption.

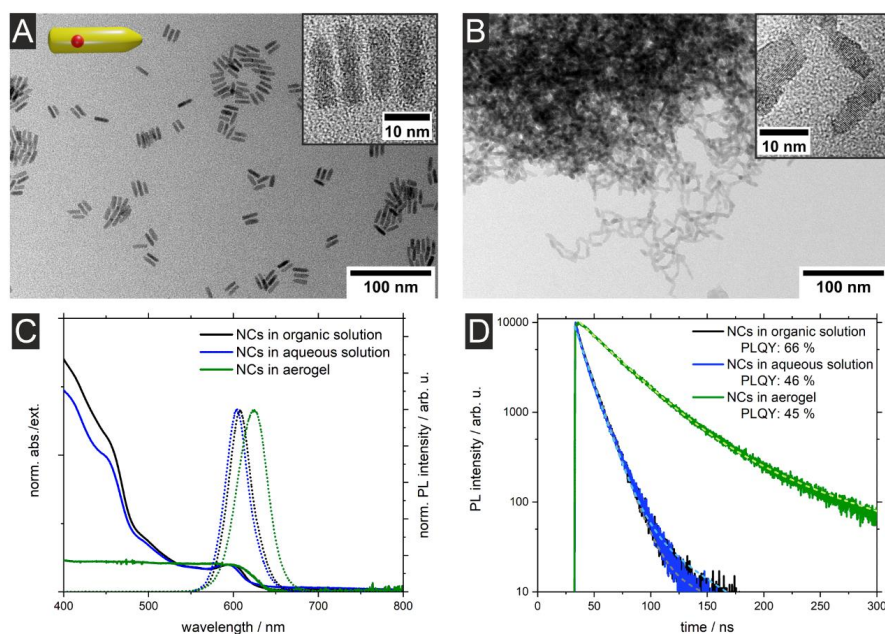


**Figure 2.** Aerogels based on CdSe/CdS dot/rod nanocrystals. TEM micrographs (A) of the individual CdSe/CdS dot/rods, inset showing higher magnification, (B) of the connected aerogel network of the dot/rods, inset showing higher magnification. Optical characterization of these structures, (C) absorption (solid line) and emission (dashed line) spectra and (D) photoluminescence decay (dashed lines show biexponential fit) of colloidal CdSe/CdS dot/rods in organic and aqueous solution and as connected aerogel network.

To study the influence of a controlled length of barrier between individual network building blocks, the CdSe/CdS dot/rod building blocks were modified by a partial ion exchange procedure, as described in literature.<sup>40</sup> This procedure allows the exchange of parts of the dot/rod structures starting at the tips of the NCs by first exchanging the desired amount of Cd with Cu (keeping a stoichiometry of 2 to 1 between Cu and Cd in mind) and then again exchanging Cu to Zn. This sequence is chosen due to the

ease with which Cu can be exchanged both into and out of chalcogenide NCs.<sup>41</sup> Varying the amount of Zn and Cu ions (to exchange between 0 and 40 % of the overall Cd content of the dot/rods) used in the procedure, enables control of the length of the ZnS tips on the CdSe/CdS dot/rods. The ZnS tipped CdSe/CdS NCs generated this way can be converted to aerogel networks using the same procedure as described for CdSe/CdS structures above. The complete procedure allows for the formation of aerogel networks made up from CdSe/CdS segments separated by a controllable ZnS barrier (see also schematic in Figure 1).

The successful modification of the dot/rod building blocks with ZnS tips was confirmed by scanning transmission electron microscopy (STEM) with energy dispersive x-ray spectroscopy (EDX), see Figure S4. In the measurements the Zinc is indeed located at the tips of the dot/rods. To further verify the position of the Zn in the structure, x-ray photoelectron spectroscopy (XPS) was performed on the samples. If the Zn would be incorporated evenly from all over the surface of the nanocrystal the amount of Zn measured by the surface sensitive XPS should be increased compared to the bulk measurement of the elemental composition which is performed by dissolving the whole nanocrystal. Since the elemental composition of XPS and bulk measurement are consistent, the incorporation of Zn starting only at the tip of the nanocrystal can be assumed. Bright field TEM micrographs of all dot/rods with varying Zn amounts and the resulting aerogel networks are also shown in the supplementary material.

As can be seen in the spectroscopic measurements of the ZnS-tipped dot/rods in Figure 3, the introduction of ZnS tips to the CdSe/CdS dot/rod structures leads to a slight hypsochromic shift in the emission. Likewise, in the absorption spectra (shown in Figure S6 in the supplementary material) of the dot/rods the first absorption band of the CdSe (at ca. 600 nm) is shifted to smaller wavelengths with increasing Zn content. Both changes indicate a change in the bandgap which can be caused by an increase in confinement in the nanocrystals. As a consequence of introducing a large bandgap material like ZnS to the tips of the dot/rods, this change is expected. Also, a change of the first excitonic transition in CdS around 480 nm can be seen. This transition becomes less intense and less defined with increasing amount of Cd exchanged as would be expectable. It can also be seen that the PL decay is faster than in the pristine dot/rod solution. However, as the primary decay component is very similar ( $\tau_1$  is ca. 7 ns) for all samples that underwent the cation exchange procedure, even the one in which no Cd was exchanged, this change in the time-resolved PL behavior can most likely be attributed to the change in surface ligands. During the cation exchange procedure, the dot/rods are introduced into a solution containing high amounts of oleylamine at elevated temperatures, therefore at least a partial exchange of surface ligands from phosphine-based to amine-based ligands has to be assumed. This difference in surrounding and protection can lead to a difference in PL decay. This can also be correlated to the measured quantum yields (Table S4 in the supplementary material). Comparing the pristine dot/rods to the sample without ZnS tips but after the exchanging procedure the quantum yield increases from 66% to 75 % indicating an increased ligand coverage or a thermal healing of crystal defects. In all partially exchanged samples the quantum yield decreases with the amount of Zn introduced into the structures (from 48 % PLQY for 20 % Zn content to 28 % PLQY for 40 % Zn content). This can be attributed to crystal defects caused by the stress of the cation exchange exerted on the structure which might facilitate a non-radiative recombination.

In the aqueous solutions a further change in PL decay and quantum yield of the dot/rods can be observed (see Table S1, S2 and S4 and Figure S7 in the supplementary material). The ligand exchange to mercaptopropionic acid (MPA) and the phase transfer to aqueous solution results in a drastic decrease in PL lifetime and PLQY for all particles that underwent the cation exchange procedure. Most prominently all dot/rods that contain Zn drop to ca. 1 % PLQY and a very short PL lifetime ( $\tau_1$  is ca. 1 ns). These effects are less pronounced in the reference sample that went through the cation

exchange procedure without introduction of Zn into the dot/rods, but similar in trend. This leads to two conclusions with regards to the ligand exchange on these dot/rods. Firstly, as a ligand MPA is less able to sufficiently shield a ZnS surface most likely caused by a different binding strength of MPA to the ZnS surface. A worse shielding might again allow for non-radiative recombination pathways. Secondly, as the sample without ZnS tips shows similar but less pronounced effects, the ligand exchange from oleylamine to MPA seems to be less favorable than an exchange from TOP/TOPO ligands to MPA as performed on the pristine dot/rods. This is most likely due to differences also in binding between the ligands and the CdS surface. In conjunction both the worse shielding of the ZnS surface by MPA and the differently effective ligand exchange are the most probable cause for the loss in quantum yield and PL lifetime comparing ZnS-tipped CdSe/CdS dot/rods in organic and aqueous solution. Importantly, the loss in PLQY is mostly recovered in the aerogel structures.

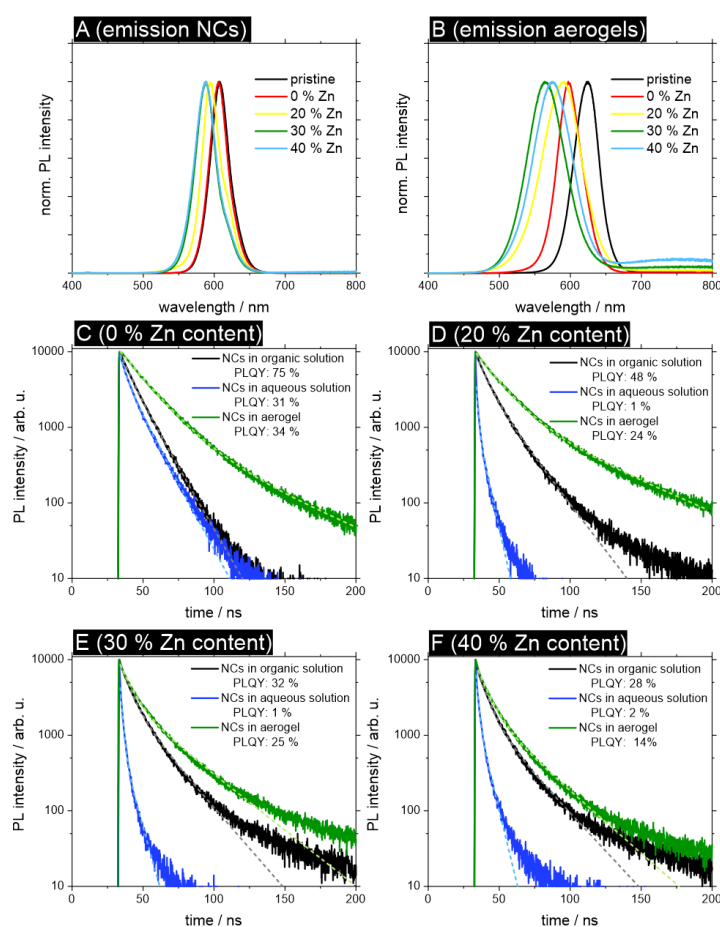


**Figure 3.** Photoluminescence properties of aerogel networks based on ZnS tipped CdSe/CdS dot/rod nanocrystals with different amounts of Zn exchanged into the structures (resulting in different ZnS tip lengths). Emission spectra of (A) colloidal dot/rod solutions in organic solvent and (B) the connected aerogel networks. Time-resolved photoluminescence of dot/rods in organic and aqueous solution and as aerogel networks for dot/rods with (C) 0 %, (D) 20 %, (E) 30 % and (F) 40 % of the initial Cd ions exchanged to Zn.

After conversion of CdSe/CdS dot/rods with and without ZnS tips to aerogel networks a broadening of the emission can be observed (see Figure 3B). Additionally, a drastic change in quantum yield is again

visible compared to the aqueous solutions with aerogels of ZnS-tipped dot/rods recovering quantum yields (from 24 % in 20 % Zn content sample to 14 % in 40 % Zn content sample, Table S4 in the supplementary material). The quantum yield recovering after removal of the solvent in the network also indicates the drastic drop in PLQY being caused by the aqueous surrounding and bad ligand shielding facilitating non-radiative recombination. With this study focused on the interaction between connected dot/rods in the aerogel networks, the most important optical property is the PL decay. The interaction between the building blocks is visible via the decay measurements as detailed earlier. Indeed, a significant influence of the Zn content and thereby the ZnS tip length on the PL decay of these dot/rod-based aerogel networks can be observed. The attachment of the particles is mostly tip-to-tip as described in earlier works<sup>6</sup> and visible in TEM (see supplementary material Figure S1, S2, S3 and S5). This is due to the higher probability of ligand removal at the tips during the network assembly. For similar reasons the cation exchange also takes place preferentially starting at the tip.<sup>40</sup> It has been shown that this process can be asymmetric with the exchange to progress faster on one of the tips than the other resulting in one longer ZnS segment and one shorter.<sup>40</sup> This leaves three orientations for the tip-to-tip connections, short ZnS segment to another short ZnS segment, short-to-long ZnS segments and long-to-long ZnS segments. This results in slight variations of the ZnS barrier length separating the CdSe/CdS units in the network. To similar effect, it is possible for building blocks to attach tip-to-side which also leaves a slight variability in the barrier length and might contribute to the fact that an increase in PL lifetime is still visible even in case of relatively large cation exchange ratios. The relation between the amount of ZnS introduced into the structures to their optical properties is nonetheless apparent. In the pristine dot/rods as mentioned earlier the characteristic long PL lifetimes in aerogels are found, likewise a distinct rise in PL lifetime is visible for the aerogel based on dot/rods which underwent the cation exchange procedure without replacing Cd compared to the respective dot/rods in organic solution (Figure 3C). In the aerogel based on dot/rods with 20 % of the Cd exchanged to form ZnS tips (with an average size of ZnS barriers of 3 nm) the increase in PL lifetime is similarly still visible (Figure 3D). When looking at higher Zn contents corresponding to 30 % of the Cd in the dot/rods (an average size of ZnS barrier of 4.5 nm) the increase in PL lifetime between aerogel and organic solution of the dot/rods is much less pronounced (Figure 3E). In the aerogel based on dot/rods with 40 % of Zn content (with an average of 6 nm ZnS barrier) an increase in PL lifetimes between aerogel and particles in organic solution is only minimally visible (Figure 3F). To confirm this PL decay behavior is caused by interaction through the NC contact in the aerogel and not through the spatial proximity of the NCs – as mentioned the aerogels are comparable to highly concentrated dispersions – decay measurements at various NC concentrations have likewise been performed (Figure S9). In these measurements an elongation of the PL lifetime with higher concentration can be observed. The negative curvature of the decay suggests a delayed filling and therefore emission-reabsorption processes as the cause of this observation. This trend is similar for all NCs regardless of the cation exchange. If a similar process based on proximity of the NCs would influence the decay behavior of the aerogels, it would be expected that the decay behavior of all aerogels is similar unlike the observed strong dependency between the amount of cations exchanged in the NC building blocks and the decay of the resulting aerogels.

The correlation between PL lifetime (as indicator of coupling between the building blocks) and length of ZnS barrier between them is apparent, i.e. the longer the ZnS tip section of the dot/rod is the higher the barrier and the PL decay becomes faster. Therefore, these PL lifetime measurements match well to the proposed electronic structure of aerogel networks of ZnS-tipped CdSe/CdS dot/rod and its consequences for charge carrier recombination.

In the emission spectra of the aerogels a broad, low intensity emission is visible at longer wavelengths (ca. 700 – 800 nm) compared to the main emission which can be attributed to trap state emission. A

time-resolved measurement in this wavelength range is shown in Figure S10. The extracted decay lifetime corresponds with the low intensity (ca. 5 %), long component which can be extracted from the decay of the most prominent emission (see Table S3). This suggests that this low intensity, long component is caused by contribution of the trap state emission to the decay profile.

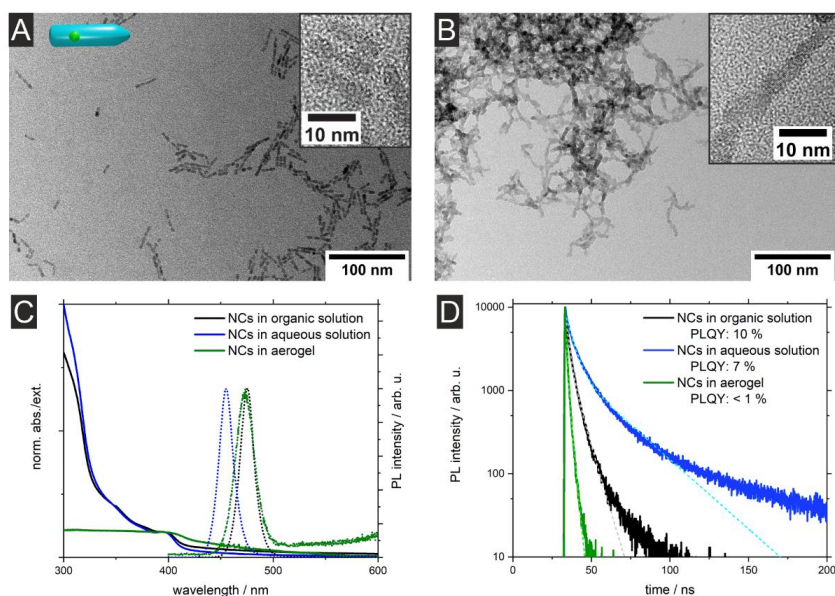


**Figure 4.** Aerogels based on ZnSe/ZnS dot/rod nanocrystals (synthesized by complete cation exchange of Cd to Zn in CdSe/CdS dot/rods). TEM micrographs of (A) the individual dot/rods and (B) the interconnected aerogel network with insets showing higher magnifications. Optical properties of ZnSe/ZnS dot/rod networks, (A) absorption (solid line) and emission (dashed line) and (D) time-resolved photoluminescence (dashed lines show biexponential fit) of ZnSe/ZnS dot/rods in organic and aqueous solution and as connected aerogel network.

Additionally, the complete cation exchange of the building blocks was also performed by carrying out the procedure with a generating ZnSe/ZnS dot/rod NCs. Contrary to their original CdSe/CdS counterparts, ZnSe/ZnS exhibits a highly confined bandstructure for both charge carriers. In CdSe/CdS the hole is confined to the CdSe core due to a large offset in the valence bands. The conduction band offset in CdSe/CdS on the other hand is small, with the exact value still subject to discussion in the literature. This leads to CdSe/CdS NCs being referred to as quasi type-II structures, where only one charge carrier is confined and the second one delocalized. In ZnSe/ZnS both conduction and valence band have a large offset leading to a strong localization of both hole and electron in the ZnSe core. This, naturally, has consequences for their optical properties. As displayed in Figure 4C and S6, the ZnSe/ZnS dot/rod NCs produced by complete cation exchange (measurements of the atomic composition only show minute amounts of remaining Cd<sup>2+</sup>, see Table S5) show the expected behavior, i.e. the absorption features of CdSe (at 590 nm) and CdS (at 450 nm) disappear and a new feature at 400 nm appears which can be attributed to ZnSe. The emission likewise shifts to 420 nm from 600 nm in the CdSe/CdS. As the emission will take part in the core of the structures this is a good indication of complete cation exchange. The time-resolved PL also shows a key difference between the two structures with considerably faster PL decays in the ZnSe/ZnS dot/rods due to the strong confinement of both charge carriers and therefore large overlap between the two wavefunctions. The PLQY of the ZnSe/ZnS structures drops significantly to 10% compared to the original CdSe/CdS (with a PLQY of

56 %). While this is counterintuitive for a structure with larger wavefunction overlap, it is most likely caused by the stress of the cation exchange generating additional crystal defects in the structures. Looking at the phase-transfer and ligand exchange of the ZnSe/ZnS dot/rods, a similar behavior as the partially exchanged CdSe/CdS/ZnS NCs described above is visible, i.e. the spectral features remain similar, while a loss in quantum yield can be observed (here from 10 % to 7 %). Interestingly, after the conversion of these ZnSe/ZnS dot/rods to aerogel networks their optical features show a different trend compared to CdSe/CdS dot/rod aerogels. As detailed earlier, the assembly of CdSe/CdS dot/rods to networks and their drying to aerogels results in a characteristic increase in PL lifetime caused by their quasi type-II electronic structure. Contrary, the aerogel built up from this strongly confined type-I building blocks (ZnSe/ZnS dot/rods, schematic band structure is shown in Figure S7) does not show an increase in PL lifetime but rather a faster PL decay compared to the building blocks in colloidal solution. Similarly, the behavior towards the atmosphere in the aerogel differs between the Cd-containing pristine or partially exchanged samples and the completely exchanged ZnSe/ZnS dot/rod aerogels. Aerogels build up from pristine CdSe/CdS and partially exchange CdSe/CdS/ZnS dot/rods show no difference in decay behavior when measured in air or in inert atmosphere. The completely exchanged ZnSe/ZnS dot/rod aerogels show a faster decay in inert atmosphere compared to air (see Figure S11). This hints at the aerogel surface and surrounding, e.g. through atmospheric oxygen, influencing the decay behavior for ZnSe/ZnS aerogels.

In conclusion, in this work the synthesis of ZnS-tipped CdSe/CdS dot/rod nanocrystals was performed and the length of the ZnS tips was varied between 0 and 3 nm by control of the reaction parameters. For the first time the phase-transfer and assembly of the NC as well as generation of aerogels based on these intricately designed ZnS-tipped CdSe/CdS building blocks was described. By investigation of the optical properties of the nanocrystals in solution and the assembled aerogel networks conclusions on the interactions between the nanocrystals and ligands could be drawn. Most importantly, it could be shown that via the introduction of ZnS barriers of controllable length between the NC building blocks in the network it is possible to tune the bandstructure of the connected network and control the interaction between the individual building blocks.

#### Data Availability Statement

The data that support the findings of this study are available from the corresponding author upon reasonable request.

#### Supplementary Materials

Additional details on synthetic procedures and characterization methods, as well as additional spectroscopic and electron microscopic characterization can be found in the supplementary material.

#### Author Declarations

The authors have no conflict of interest to disclose.

#### Acknowledgements

The project leading to these results was funded by the European Research Council (ERC) under the European Union's Horizon 2020 research and innovation program (grant agreement 714429). N. C. B. and D. D. would like to thank the German Research Foundation (DFG) for Funding under Germany's excellence strategy within the cluster of excellence PhoenixD (EXC 2122, project ID 390833453). J. G. E. is thankful for funding by the Ministry for Science and Culture of Lower Saxony (MWK) – School for Additive Manufacturing SAM The authors thank the Laboratory of Nano and Quantum Engineering (LNQE) for providing the TEM facility and Prof. Feldhoff of the Leibniz Universität Hannover for

providing the SEM facility. The authors also would like to thank Dr. Sara Sanchez-Paradinas and Patrick Adel for assistance.

#### References

- <sup>1</sup> T. Gacoin, L. Malier, and J.P. Boilot, *Chem. Mater.* **9**, 1502 (1997).
- <sup>2</sup> J.L. Mohanan, I.U. Arachchige, and S.L. Brock, *Science* **307**, 397 (2005).
- <sup>3</sup> C. Ziegler, A. Wolf, W. Liu, A.K. Herrmann, N. Gaponik, and A. Eychmüller, *Angew. Chemie - Int. Ed.* **56**, 13200 (2017).
- <sup>4</sup> I.U. Arachchige, J.L. Mohanan, and S.L. Brock, *Chem. Mater.* **17**, 6644 (2005).
- <sup>5</sup> N. Gaponik, A. Wolf, R. Marx, V. Lesnyak, K. Schilling, and A. Eychmüller, *Adv. Mater.* **20**, 4257 (2008).
- <sup>6</sup> S. Sanchez-Paradinas, D. Dorfs, S. Friebe, A. Freytag, A. Wolf, and N.C. Bigall, *Adv. Mater.* **27**, 6152 (2015).
- <sup>7</sup> S. Naskar, J.F. Miethe, S. Sánchez-Paradinas, N. Schmidt, K. Kanthasamy, P. Behrens, H. Pfnür, and N.C. Bigall, *Chem. Mater.* **28**, 2089 (2016).
- <sup>8</sup> K.K. Kalebaila and S.L. Brock, *Zeitschrift Fur Anorg. Und Allg. Chemie* **638**, 2598 (2012).
- <sup>9</sup> A. Hitihami-Mudiyanselage, K. Senevirathne, and S.L. Brock, *ACS Nano* **7**, 1163 (2013).
- <sup>10</sup> A. Hitihami-Mudiyanselage, K. Senevirathne, and S.L. Brock, *Chem. Mater.* **26**, 6251 (2014).
- <sup>11</sup> R. Deshmukh, E. Tervoort, J. Käch, F. Rechberger, and M. Niederberger, *Dalt. Trans.* **45**, 11616 (2016).
- <sup>12</sup> W. Cheng, F. Rechberger, and M. Niederberger, *ACS Nano* **10**, 2467 (2016).
- <sup>13</sup> F. Rechberger, G. Ilari, and M. Niederberger, *Chem. Commun.* **50**, 13138 (2014).
- <sup>14</sup> F. Rechberger, E. Tervoort, and M. Niederberger, *J. Am. Ceram. Soc.* **100**, 4483 (2017).
- <sup>15</sup> N.C. Bigall, A.-K. Herrmann, M. Vogel, M. Rose, P. Simon, W. Carrillo-Cabrera, D. Dorfs, S. Kaskel, N. Gaponik, and A. Eychmüller, *Angew. Chemie Int. Ed.* **48**, 9731 (2009).
- <sup>16</sup> A.K. Herrmann, P. Formanek, L. Borchardt, M. Klose, L. Giebeler, J. Eckert, S. Kaskel, N. Gaponik, and A. Eychmüller, *Chem. Mater.* **26**, 1074 (2014).
- <sup>17</sup> S. Naskar, A. Freytag, J. Deutsch, N. Wendt, P. Behrens, A. Köckritz, and N.C. Bigall, *Chem. Mater.* **29**, 9208 (2017).
- <sup>18</sup> F. Matter, A.L. Luna, and M. Niederberger, *Nano Today* **30**, 100827 (2020).
- <sup>19</sup> D. Zámbo, A. Schlosser, P. Rusch, F. Lübke, J. Koch, H. Pfnür, and N.C. Bigall, *Small* **1906934** (2020).
- <sup>20</sup> T. Hendel, V. Lesnyak, L. Kühn, A.K. Herrmann, N.C. Bigall, L. Borchardt, S. Kaskel, N. Gaponik, and A. Eychmüller, *Adv. Funct. Mater.* **23**, 1903 (2013).
- <sup>21</sup> C.C. Hewa-Rahinduwage, K.L. Silva, S.L. Brock, and L. Luo, *Chem. Mater.* **33**, 4522 (2021).
- <sup>22</sup> A. Freytag, S. Sánchez-Paradinas, S. Naskar, N. Wendt, M. Colombo, G. Pugliese, J. Poppe, C. Demirci, I. Kretschmer, D.W. Bahnemann, P. Behrens, and N.C. Bigall, *Angew. Chemie Int. Ed.* **55**, 1200 (2016).
- <sup>23</sup> A. Wolf, V. Lesnyak, N. Gaponik, and A. Eychmüller, *J. Phys. Chem. Lett.* **3**, 2188 (2012).

- <sup>24</sup> Q. Yao and S.L. Brock, *Nanotechnology* **21**, (2010).
- <sup>25</sup> A. Schlosser, L.C. Meyer, F. Lübkeemann, J.F. Miethe, and N.C. Bigall, *Phys. Chem. Chem. Phys.* **21**, 9002 (2019).
- <sup>26</sup> W. Liu, A.-K. Herrmann, D. Geiger, L. Borchardt, F. Simon, S. Kaskel, N. Gaponik, and A. Eychmüller, *Angew. Chemie Int. Ed.* **51**, 5743 (2012).
- <sup>27</sup> B. Cai, A. Dianat, R. Hübner, W. Liu, D. Wen, A. Benad, L. Sonntag, T. Gemming, G. Cuniberti, and A. Eychmüller, *Adv. Mater.* **29**, (2017).
- <sup>28</sup> B. Cai, R. Hübner, K. Sasaki, Y. Zhang, D. Su, C. Ziegler, M.B. Vukmirovic, B. Rellinghaus, R.R. Adzic, and A. Eychmüller, *Angew. Chemie Int. Ed.* **57**, 2963 (2018).
- <sup>29</sup> S. Henning, H. Ishikawa, L. Kühn, J. Herranz, E. Müller, A. Eychmüller, and T.J. Schmidt, *Angew. Chemie Int. Ed.* **56**, 10707 (2017).
- <sup>30</sup> D. Müller, D. Zámbo, D. Dorfs, and N.C. Bigall, *Small* **17**, (2021).
- <sup>31</sup> F. Rechberger and M. Niederberger, *Mater. Horizons* **4**, 1115 (2017).
- <sup>32</sup> L. Korala, J.R. Germain, E. Chen, I.R. Pala, D. Li, and S.L. Brock, *Inorg. Chem. Front.* **4**, 1451 (2017).
- <sup>33</sup> M. Rosebrock, D. Zámbo, P. Rusch, D. Pluta, F. Steinbach, P. Bessel, A. Schlosser, A. Feldhoff, K.D.J. Hindricks, P. Behrens, D. Dorfs, and N.C. Bigall, *Adv. Funct. Mater.* 2101628 (2021).
- <sup>34</sup> P. Rusch, B. Schremmer, C. Strelow, A. Mews, D. Dorfs, and N.C. Bigall, *J. Phys. Chem. Lett.* **10**, 7804 (2019).
- <sup>35</sup> P. Rusch, D. Zámbo, and N.C. Bigall, *Acc. Chem. Res.* **53**, 2414 (2020).
- <sup>36</sup> L. Carbone, C. Nobile, M. De Giorgi, F. Della Sala, G. Morello, P. Pompa, M. Hytch, E. Snoeck, A. Fiore, I.R. Franchini, M. Nadasan, A.F. Silvestre, L. Chiodo, S. Kudera, R. Cingolani, R. Krahne, and L. Manna, *Nano Lett.* **7**, 2942 (2007).
- <sup>37</sup> H.G. Bagaria, E.T. Ada, M. Shamsuzzoha, D.E. Nikles, and D.T. Johnson, *Langmuir* **22**, 7732 (2006).
- <sup>38</sup> T. Kodanek, H.M. Banbela, S. Naskar, P. Adel, N.C. Bigall, and D. Dorfs, *Nanoscale* **7**, 19300 (2015).
- <sup>39</sup> P. Rusch, D. Pluta, F. Lübkeemann, D. Dorfs, D. Zámbo, and N.C. Bigall, *ChemPhysChem* **1** (2021).
- <sup>40</sup> P. Adel, A. Wolf, T. Kodanek, and D. Dorfs, *Chem. Mater.* **26**, 3121 (2014).
- <sup>41</sup> H. Li, M. Zanella, A. Genovese, M. Povia, A. Falqui, C. Giannini, and L. Manna, *Nano Lett.* **11**, 4964 (2011).



## 8 Summary

In this thesis advances in the area of porous aerogel networks build up from nanocrystal building blocks are presented in synthetic methodology as well as characterization of such networks and conclusions from these on the underlying processes in the networks.

Initially, in chapter 5 CdSe/CdS dot/rod building blocks based on different sizes of CdSe quantum dots are assembled into networks made up from these different building blocks as well as mixtures thereof. This results in functional aerogel networks with an emission color in the green to red color space. This emission is adjustable simply through the ratio of different color building blocks as there is no energy transfer between the building blocks. This is likely caused by the strong confinement of the hole to the CdSe quantum dots. These structures are additionally investigated by temperature-dependent spectroscopy in this section. In these measurements two distinct effects are observed. At intermediate temperatures between room temperature and 77 K a minor dependency of photoluminescence lifetime to temperature is observed with colder temperatures leading to faster decays most likely caused by the diminished influence of higher excited states with increased electron delocalization through thermal mixing. At even lower, cryogenic temperatures (below ca. 20 K) two decay processes can be observed caused by the processes within the CdSe quantum dot, one fast (spin allowed, *bright*) decay and one extremely long (spin forbidden, *dark*) process.

In chapter 6 synthetic methods traditionally employed on nanocrystals in solution, i.e. the modification with silica shells, are for the first time transferred onto nanocrystal-based networks as substrates. This results in networks consisting of the core network made up of connected nanocrystal building blocks and a shell network of a continuous shell surrounding the core network. The successful generation of the such core-shell structured networks is demon-

strated for different shell materials (silica and titania) as well as different core networks (based on semiconductor or noble metal nanocrystals). The core-shell structuring results in a considerable mechanical stabilization of the modified networks.

Finally, in chapter 7 in-depth optical characterization and aerogel network structuring methods are combined. In section 7.2 the synthesis sequence of core-shell structured aerogel networks is adapted to either modify networks of connected nanocrystal building blocks or to first modify these building blocks to then connect core-shell building blocks into a network. This approach generates structures that are similar in material but differ in one crucial aspect, the connection of the nanocrystal building blocks. Networks of connected CdSe/CdS nanocrystals which are surrounded by a shell after assembly are shown to present the characteristic optical properties of the connected networks. Assembling CdSe/CdS/SiO<sub>2</sub> core/shell/shell structured building blocks results in isolated CdSe/CdS nanocrystals within these networks and therefore the optical characteristics of such individual building blocks. Additionally, in section 7.3 the approach to influence the optical properties of nanocrystal-based aerogel networks is expanded upon. Therefore not only the two extreme states of coupled and decoupled building blocks are achieved but intermediate states of interaction are generated. This is done by introducing short (ca. 1 nm – 3 nm) sections of ZnS by cation-exchange at the tips of the building blocks. Due to the large bandgap of ZnS, these represent a tunable but surmountable barrier of tunable size which can be used to change the strength of interaction between the individual CdSe/CdS building blocks.

In summary, methods to structure NC-based aerogels via the modification of their nanoscale building blocks or the modification of their microstructure have been developed and the optical properties of NC-based aerogels as well as the consequences of such modifications regarding the optical properties and the extent of interparticle interactions have been investigated.

## 9 Outlook

While this thesis presents advances in the theoretical understanding of nanocrystal-based aerogel networks as well as synthetic pathways to new core/shell structured aerogels, the future challenge will be to transfer these to applications and extend the investigations further.

Through the optical measurements in conjunction with the targeted synthesis of engineered building blocks and networks conclusions to their electronic properties were possible and the model of electron delocalization in the networks was further explored. In the studies in this work different network structures based on *quasi-type-II* building blocks and through synthetic procedures gradually extended to *type-I* nanocrystal networks as well as intermediates. For a better understanding of electronic processes in nanocrystal network structures it would also be interesting to expand future investigations to *type-II* building blocks or building blocks with changed band structure, e.g. *quasi type-II* nanocrystals in which a hole delocalization would be expected instead of the electron delocalization observed here.

In the investigation of networks based on a mix of CdSe/CdS dot/rod with different sized CdSe cores a straightforward way to colour tune these aerogels in the green to red spectrum was laid down. White light emission can therefore be expected to be achievable with blue back illumination or by additional introduction of blue emitting NCs (e.g. based on ZnSe cores) into the network. The use of NC-based aerogel purposes can circumvent the need of colloidal solutions and serve as an immobilization technique. There are, however, other methods of NC deposition and immobilization like chemical bath deposition and spray- or dip coating which have been used for fabrication of NC-based illumination appliances. Further development and proof-of-concept on similar NC aerogel-based devices is the next step in this direction to evaluate their applicability in comparison to established methods.

In the context of illumination devices one key property of aerogel networks, i.e. their large surface area, is not essential. For applications relying on the surface, this large surface area of aerogel networks is on the other hand a considerable advantage. There have been early experiments into photo- and electrocatalysis using aerogels as well as their application in (photo-)electrochemical sensors. In these prospects an understanding of the charge carrier processes within the network is key to adjust the aerogel catalyst or sensor to the targeted system. The insights presented herein should serve to provide this understanding and the proposed processes in excited heterostructured NC aerogel networks might also be transferred to other materials of similar band structures.

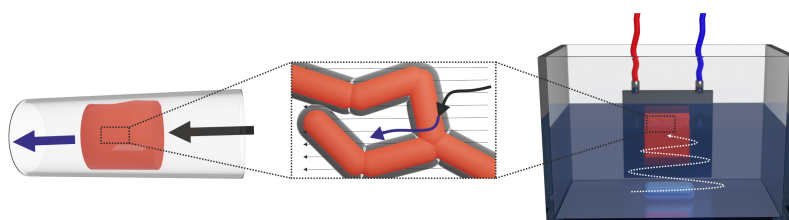


Figure 9.1: Two potential reactors with external forces for mixing to utilize a reinforced nanocrystal-based gel in, (left) tube reactor with reactand flowing through the gel and (right) stirred bath with the gel fixed to a side of the reactor

The more important advance in an endeavour to bring NC-based aerogels to applications, which is presented in this work, is the synthetic method of core/shell-structured aerogels. This technique opens several avenues to be further investigated and exploited. Firstly, the mechanical reinforcement of NC-based aerogels introduced by the core/shell-structuring enables the application of such gels in ways inaccessible beforehand. Early studies on NC aerogels in catalytic or sensory application often rely on powderized aerogel. With this mechanical reinforcement the monolith itself might be employed. Also due to the sensitivity to mechanical stress of NC aerogels stirring or other forms of mixing introduced not by diffusion but forcibly from outside can present problems. The mechanical stability of such core/shell-structured aerogels can allow for their application in reactors with outside mixing as schematically depicted in figure 9.1.

Secondly, even though the inner core network of nanocrystals is surrounded by a shell, ac-

---

According to initial experiments the surface is still accessible to cations or small molecules. The accessibility of the surface for reactants is important for surface active reactions which represent the most promising area of application of NC aerogels. In conjunction with the mechanical stability allowing outside mixing even with a slightly reduced surface accessibility core-shell structured NC aerogels might still prove to exhibit higher overall activity. On the other hand it could also be observed that larger objects are kept from the surface, e.g. 5 nm gold NCs could not quench the fluorescence of these core-shell networks. With an increased control over the shell porosity even a filter functionality of the shell might be possible, either shielding the core NC network from contaminants or introducing a selectivity into the catalyst/sensor.

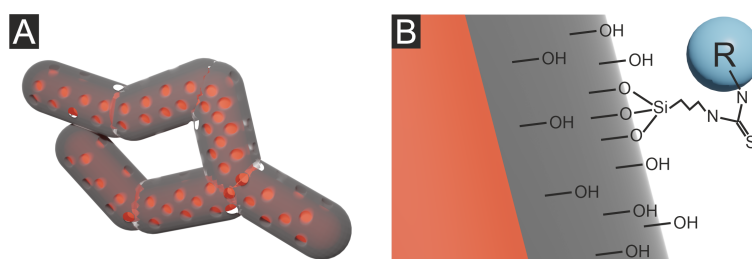


Figure 9.2: Schematic depiction of (A) a core/shell-structured aerogel with mesoporous shell and (B) an exemplary modification of a silica shell in core/shell-structured aerogels with a functional organic molecule R.

Thirdly, the most investigated shell system in this work is silica and access to other metal oxide through similar reactions might be possible. The exemplary system of titania shells was shown in this work. Titania and other metal oxides can themselves be optically active materials. With this the way to further functionalities apart from the mechanical reinforcement described herein introduced by the shell material itself are obtainable. Likewise, the subject of silica chemistry is staggeringly vast and need for further work within this system is self-explanatory. Silica can easily be modified by organic sections resulting in the area of silicones and organic-inorganic hybrid materials which have shown to be mechanically much stronger than silica. The porosity of silica can be directed by surface active ligands introduced into the synthesis to yield mesoporous silica, as schematically displayed in figure 9.2. Similar approaches might be applied to these core/shell-structured NC gels to either increase surface accessibility or intro-

duce a selectivity as mentioned above. Lastly, the modification of a silica surface with organic molecules is a common strategy to add further functionalities to NCs, see figure 9.2. This can equally be applied to the silica shell in these networks. This would allow for an aerogel containing an optically or catalytically active core NC network and a silica shell which is modified with organic molecules which could be catalytically, optically or even medically active.

The conclusions of this thesis provide a deeper understanding the (opto-)electronic properties of NC-based aerogels which can be aiding in their transformation into catalysts, sensors or optical materials. Especially the *post-gelation* core/shell-structuring of such networks opens up a multitude of pathways to produce new multifunctional NC-based aerogels or improve upon the existing ones.

# Appendix

## 9.1 List of Publications

### Publications included in this thesis

- **P. Rusch**, B. Schremmer, C. Strelow, A. Mews, D. Dorfs, N.C. Bigall (2019): "Nanocrystal Aerogels with Coupled or Decoupled Building Blocks",  
*J. Phys. Chem. Lett.*, 2019, DOI: 10.1021/acs.jpcclett.9b02695
- **P. Rusch**, F. Niemeyer, D. Pluta, B. Schremmer, F. Lübkeemann, M. Rosebrock, M. Schäfer, M. Jahns, P. Behrens, N.C. Bigall, "Versatile Route to Core-Shell Reinforced Network Nanostructures",  
*Nanoscale*, 2019, DOI: 10.1039/C9NR03645H
- **P. Rusch**, D. Pluta, F. Lübkeemann, D. Dorfs, D. Zámbo, N. C. Bigall: "Temperature and Composition Dependent Optical Properties of CdSe/CdS Dot/Rod-Based Aerogel Networks",  
*ChemPhysChem*, 2021, DOI: 10.1002/cphc.202100755
- **P. Rusch**, F. Lübkeemann, H. M. A. M. Borg, J. G. Eckert, D. Dorfs, N. C. Bigall: "Influencing the Coupling Between Network Building Blocks in CdSe/CdS Dot/Rod Aerogels by Partial Cation Exchange",  
*J. Chem. Phys.*, 2022, *under revision*

**Publications not included in this thesis**

- **P. Rusch**, D. Zámbo, N. C. Bigall: "Control over Structure and Properties in Nanocrystal Aerogels at the Nano-, Micro-, and Macroscale",  
*Acc. Chem. Res.*, 2020, DOI: 10.1021/acs.accounts.0c00463
- R. Himstedt\* , **P. Rusch\***, D. Hinrichs, T. Kodanek, J. Lauth, S. Kinge, L. D. A. Sibbeles, D. Dorfs: "Localized Surface Plasmon Resonances of Various Nickel Sulfide Nanostructures and Au-Ni<sub>3</sub>S<sub>2</sub> Core-Shell Nanoparticles",  
*Chem. Mater.*, 2017, DOI: 10.1021/acs.chemmater.7b02259
- D. Göbel\*, **P. Rusch\***, D. Duvinage, N. C. Bigall, B. J. Nachtsheim: "Emission color-tunable oxazol(in)yl-substituted excited-state intramolecular proton transfer (ESIPT)-based luminophores",  
*Chem. Comm.*, 2020, DOI: 10.1039/d0cc05780k
- I. Strauss, A. Mundstock, M. Treger, K. Lange, S. Hwang, C. Chmelik, **P. Rusch**, N.C. Bigall, T. Pichler, H. Shiozawa, J. Caro: "Metal–Organic Framework Co-MOF-74-Based Host–Guest Composites for Resistive Gas Sensing",  
*ACS Appl. Mater. Interfaces*, 2019, DOI: 10.1021/acsami.8b22002
- F. Lübke, J. F. Miethe, F. Steinbach, **P. Rusch**, A. Schlosser, D. Zámbo, T. Heinemeyer, D. Natke, D. Zok, D. Dorfs, N.C. Bigall: "Patterning of Nanoparticle-Based Aerogels and Xerogels by Inkjet Printing",  
*Small*, 2019, DOI: 10.1002/sml.201902186
- F. Rieck genannt Best, A. Mundstock, G. Dräger, **P. Rusch**, N. C. Bigall, H. Richter, J. Caro: "Methanol-to-Olefins in a Membrane Reactor with in situ Steam Removal – The Decisive Role of Coking",  
*ChemCatChem*, 2019, DOI: 10.1002/cctc.201901222
- F. Lübke, **P. Rusch**, S. Getschmann, B. Schremmer, M. Schäfer, M. Schulz, B. Hoppe, P. Behrens, N.C. Bigall, D. Dorfs: "Reversible Cation Exchange on Macroscopic CdSe/CdS

and CdS Nanorod Based Gel Networks",

*Nanoscale*, 2020, DOI: 10.1039/C9NR09875E

- D. Zámbo, A. Schlosser, **P. Rusch**, F. Lübke, J. Koch, H. Pfnür, N.C. Bigall: "A Versatile Route to Assemble Semiconductor Nanoparticles into Functional Aerogels by Means of Trivalent Cations",  
*Small*, 2020, DOI: 10.1002/smll.201906934
- Y. Appiarius, T. Stauch, E. Lork, **P. Rusch**, N. C. Bigall, A. Staubitz: "From a 1,2-azaborinine to large BN-PAHs via electrophilic cyclization: synthesis, characterization and promising optical properties",  
*Org. Chem. Front.*, 2021, DOI: 10.1039/d0qo00723d
- A. Alahmad, A. Feldhoff, N. C. Bigall, **P. Rusch**, T. Scheper, J.-G. Walter: "Hypericum perforatum L.-Mediated Green Synthesis of Silver Nanoparticles Exhibiting Antioxidant and Anticancer Activities",  
*Nanomaterials*, 2021, DOI: 10.3390/nano11020487
- I.-M. Ramirez y Medina, M. Rohdenburg, **P. Rusch**, D. Duvinage, N. C. Bigall, A. Staubitz: " $\pi$ -Conjugated stannole copolymers synthesised by a tin-selective Stille cross-coupling reaction",  
*Mater. Adv.*, 2021, DOI: 10.1039/d1ma00104c
- D. Zámbo, A. Schlosser, R. T. Graf, **P. Rusch**, P. A. Kißling, A. Feldhoff, N. C. Bigall: "One-Step Formation of Hybrid Nanocrystal Gels: Metal Domains on CdSe/CdS Nanorod and Nanoplatelet Networks",  
*Adv. Opt. Mater.*, 2021, DOI: 10.1002/adom.202100291
- Y. Liu, A. Chatterjee, **P. Rusch**, C. Wu, P. Nan, M. Peng, F. Bettels, T. Li, C. Ma, C. Zhang, B. Ge, N. C. Bigall, H. Pfnür, F. Ding, L. Zhang: "Monodisperse Molybdenum Nanoparticles as Highly Efficient Electrocatalysts for Li-S Batteries",  
*ACS Nano*, 2021, DOI: 10.1021/acsnano.1c05344

- D. Göbel, **P. Rusch**, D. Duvinage, T. Stauch, N. C. Bigall, B. J. Nachtsheim: "Substitution Effect on 2-(Oxazoliny)-phenols and 1,2,5-Chalcogenadiazole-Annulated Derivatives: Emission-Color-Tunable, Minimalistic Excited-State Intramolecular Proton Transfer (ESIPT)-Based Luminophores",  
*J. Org. Chem.*, 2021, DOI: 10.1021/acs.joc.1c00846
- M. Rosebrock, D. Zámbo, **P. Rusch**, D. Pluta, F. Steinbach, P. Bessel, A. Schlosser, A. Feldhoff, K. D. J. Hindricks, P. Behrens, D. Dorfs, N.C. Bigall: "Spatial Extent of Fluorescence Quenching in Mixed Semiconductor-Metal Nanoparticle Gel Networks",  
*Adv. Funct. Mater.*, 2021, DOI: 10.1002/adfm.202101628
- J. Schlenkrich, D. Zámbo, A. Schlosser, **P. Rusch**, N. C. Bigall: "Revealing the Effect of Nanoscopic Design on the Charge-Carrier Separation Processes in Semiconductor-Metal Nanoparticle Gel Networks",  
*Adv. Optical Mater.*, 2021, DOI: 10.1002/adom.202101712
- D. Zámbo, **P. Rusch**, F. Lübke, N. C. Bigall: "Noble Metal Nanorod Cryo-aerogels with Electrocatalytically Active Surface Sites",  
*ACS Appl. Mater. Interfaces*, 2021, DOI: 10.1021/acsami.1c16424
- A. M. Abdelmonem, D. Zámbo, **P. Rusch**, A. Schlosser, L. F. Klepzig, N. C. Bigall: "Versatile Route for Multifunctional Aerogels Including Flaxseed Mucilage and Nanocrystals",  
*Macromol. Rapid Commun.*, 2021, DOI: 10.1002/marc.202100794
- Y. Liu, S. Ma, M. Rosebrock, **P. Rusch**, Y. Barnscheidt, C. Wu, P. Nan, F. Bettels, Z. Lin, T. Li, B. Ge, N. C. Bigall, H. Pfnür, F. Ding, C. Zhang, L. Zhang: "Tungsten Nanoparticles Accelerate Polysulfides Conversion: A Viable Route toward Stable Room-Temperature Sodium-Sulfur Batteries",  
*Adv. Sci.*, 2022, DOI: 10.1002/advs.202105544
- Y. Appiaris, P. J. Gliese, S. A. W. Segler, **P. Rusch**, J. Zhang, P. J. Gates, R. Pal, L. A. Malaspina, K. Sugimoto, T. Neudecker, N. C. Bigall, S. Grabowsky, A. A. Bakulin, A. Staubitz: "BN-Substitution in Dithienylpyrenes Prevents Excimer Formation in Solution

and in the Solid State"

*J. Phys. Chem. C*, 2022, DOI: 10.1021/acs.jpcc.1c08812

- R. T. Graf, A. Schlosser, D. Zámbo, J. Schlenkrich, **P. Rusch**, A. Chatterjee, H. Pfnür, N. C. Bigall: "Interparticle Distance Variation in Semiconductor Nanoplatelet Stacks"  
*Adv. Funct. Mater.*, 2022, DOI: 10.1002/adfm.202112621 M. Niemeyer, P. Bessel, **P. Rusch**, R. Himstedt, D. Kranz, H. Borg, N. C. Bigall, D. Dorfs: "Nanosecond Pulsed Laser-Heated Nanocrystals Inside a Metal-Organic Framework Matrix"  
*ChemNanoMat*, 2022, DOI: 10.1002/cnma.202200169

## 9.2 Conference Contributions

### Oral Presentations

- **P. Rusch**, A. Schlosser, J. F. Miethe, N. C. Bigall: "Surrounding Nanoparticle Gels with Silica Shells", *117<sup>th</sup> General Assembly of the German Bunsen Society for Physical Chemistry - Bunsentagung*, 2018, Hannover, Germany
- **P. Rusch**, M. Rosebrock, N. C. Bigall: "Combining Nanoparticle and Silica Gels in a New Manner", *E-MRS 2018 Fall Meeting*, 2018, Warsaw, Poland
- **P. Rusch**, B. Schremmer, F. Lübke, N. C. Bigall: "Influencing Structure and Optical Properties of Core-Shell Network Structures", *1<sup>st</sup> Symposium on Aerogel Inspired Materials*, 2019, Newcastle Upon Tyne, United Kingdom
- **P. Rusch**, B. Schremmer, N. C. Bigall: "Controlling Properties of Nanoparticle-based Networks via Their Microstructure", *120<sup>th</sup> General Assembly of the German Bunsen Society for Physical Chemistry - Bunsentagung*, 2021, Regensburg, Germany

### Posters

- **P. Rusch**, N. C. Bigall: "Gelation of nanoparticles as bridge to the macroscopic", *WE-Heraeus summer school on "Exciting Nanostructures: Probing and tuning the electronic properties of confined systems"*, 2017, Bad Honnef, Germany

- **P. Rusch**, A. Schlosser, J. F. Miethe, N. C. Bigall:  
"Post-Gelation Modification by Stöber Synthesis",  
*Nanoday of the Laboratory of Nano and Quantum Engineering*, 2017, Hannover, Germany
- **P. Rusch**, M. Rosebrock, B. Schremmer, F. Lübke mann, N. C. Bigall:  
"Silica shell growth around CdSe/CdS nanorod aerogels", *International Workshop on "Single Nanostructures, Nanomaterials, Aerogels and Their Interactions: Combining Quantum Physics and Chemistry"*, 2018, Dresden, Germany
- **P. Rusch**, M. Rosebrock, B. Schremmer, F. Lübke mann, M. Jahns, P. Behrens, N. C. Bigall:  
"Modification of CdSe/CdS nanorod aerogels by silica coating", *4<sup>th</sup> International Seminar on Aerogels*, 2018, Hamburg, Germany
- **P. Rusch**, M. Rosebrock, B. Schremmer, F. Lübke mann, M. Jahns, P. Behrens, N. C. Bigall:  
"Modification of CdSe/CdS nanorod aerogels by silica coating", *Nanoday of the Laboratory of Nano and Quantum Engineering*, 2018, Hannover, Germany
- **P. Rusch**, M. Rosebrock, B. Schremmer, F. Lübke mann, M. Jahns, P. Behrens, N. C. Bigall:  
"Modification of CdSe/CdS nanorod aerogels by silica coating", *118<sup>th</sup> General Assembly of the German Bunsen Society for Physical Chemistry - Bunsentagung*, 2019, Jena, Germany
- **P. Rusch**, M. Rosebrock, B. Schremmer, F. Lübke mann, M. Jahns, P. Behrens, N. C. Bigall:  
"Coupling and Decoupling of building blocks in nanocrystal network structures",  
*20<sup>th</sup> International Sol-Gel Conference*, 2019, St. Petersburg, Russia
- **P. Rusch**, M. Rosebrock, B. Schremmer, F. Lübke mann, M. Schäfer, M. Jahns, P. Behrens, N. C. Bigall: "Influencing Structure and Optical Properties of Core-Shell Network Structures",  
*Nanoday of the Laboratory of Nano and Quantum Engineering*, 2019, Hannover, Germany

## 9.3 Curriculum Vitae

### Personal Information

date of birth	13.05.1993
place of birth	Hannover

### Education

03.2017 - 02.2022	<b>PhD student and scientific associate</b> under Supervision of Prof. N. C. Bigall, Institute of Physical Chemistry and Electrochemistry, Leibniz Universität Hannover
10.2014 - 02.2017	<b>M. Sc. Material- and Nanochemistry,</b> Leibniz Universität Hannover
10.2011 - 09.2014	<b>B. Sc. Chemistry,</b> Friedrich-Schiller-Universität Jena
08.2004 - 09.2011	<b>Abitur</b> (general higher education), Hölty-Gymnasium Wunstorf